Annu. Rev. Astro. Astrophys. 2012.50:251-304. Downloaded from www.annualreviews.org
by California Institute of Technology on 01/21/14. For personal use only.

ANNUAL REVIEWS **Further**
Click here for quick links to Annual Reviews content online, including:

- Other articles in this volume
- Top cited articles
- Top downloaded articles
- Our comprehensive search

# Galactic Stellar Populations in the Era of the Sloan Digital Sky Survey and Other Large Surveys

Željko Ivezić,[1] Timothy C. Beers,[2] and Mario Jurić[3]

[1] Department of Astronomy, University of Washington, Seattle, Washington 98195; email: ivezic@astro.washington.edu

[2] National Optical Astronomy Observatory, Tucson, Arizona 85719, and Department of Physics & Astronomy and the Joint Institute for Nuclear Astrophysics (JINA), Michigan State University, East Lansing, Michigan 48824; email: beers@noao.edu

[3] Harvard-Smithsonian Center for Astrophysics, Cambridge, Massachusetts 02138; email: mjuric@cfa.harvard.edu

Annu. Rev. Astron. Astrophys. 2012. 50:251–304

The *Annual Review of Astronomy and Astrophysics* is online at astro.annualreviews.org

This article's doi:
10.1146/annurev-astro-081811-125504

Copyright © 2012 by Annual Reviews.
All rights reserved

0066-4146/12/0922-0251$20.00

## Keywords

methods: data analysis; stars: statistics; Galaxy: disk, halo, stellar content, structure, interstellar medium

## Abstract

Studies of stellar populations, understood to mean collections of stars with common spatial, kinematic, chemical, and/or age distributions, have been reinvigorated during the past decade by the advent of large-area sky surveys such as the Sloan Digital Sky Survey, the Two-Micron All Sky Survey, the Radial Velocity Experiment, and others. We review recent analyses of these data that, together with theoretical and modeling advances, are revolutionizing our understanding of the nature of the Milky Way and galaxy formation and evolution in general. The formation of galaxies like the Milky Way was long thought to be a steady process leading to a smooth distribution of stars. However, the abundance of substructure in the multidimensional space of various observables, such as position, kinematics, and metallicity, is now proven beyond doubt and demonstrates the importance of mergers in the growth of galaxies. Unlike smooth models that involve simple components, the new data reviewed here clearly exhibit many irregular structures, such as the Sagittarius dwarf tidal stream and the Virgo and Pisces overdensities in the halo and the Monoceros stream closer to the Galactic plane. These recent developments have made it clear that the Milky Way is a complex and dynamic structure, one that is still being shaped by the merging of neighboring smaller galaxies. We also briefly discuss the next generation of wide-field sky surveys, such as SkyMapper, Panoramic Survey Telescope & Rapid Response System, *Global Astrometric Interferometer for Astrophysics*, and the Large Synoptic Survey Telescope, which will improve measurement precision manyfold and include billions of individual stars. The ultimate goal, development of a coherent and detailed story of the assembly and evolutionary history of the Milky Way and other large spirals like it, now appears well within reach.

Annu. Rev. Astro. Astrophys. 2012.50:251-304. Downloaded from www.annualreviews.org
by California Institute of Technology on 01/21/14. For personal use only.

# 1. INTRODUCTION

## 1.1. The Big Picture: Structure Formation and Near-Field Cosmology

The current cosmological paradigm states that the Universe had its beginning in the Big Bang. Galaxies, the fundamental (luminous) building blocks of the Universe, began forming relatively soon after this event (no more than a few gigayears). A major objective of modern astrophysics is to understand when and how galaxies formed, and how they have evolved since. Our own Galaxy, the Milky Way, provides a unique opportunity to study a galaxy in exquisite detail, by measuring and analyzing the properties of large samples of individual stars. Characterization of the stellar populations of the Milky Way provides clues about galaxy formation and evolution that cannot be extracted from observations of distant galaxies alone. Indeed, it is not possible to tell a coherent story of the formation of the first stars and galaxies without understanding the nature of the stellar populations of the Milky Way.

In the canonical model of Milky Way formation (Eggen, Lynden-Bell & Sandage 1962), the Galaxy began with a relatively rapid ($\sim 10^8$ years) radial collapse of the initial protogalactic cloud, followed by an equally rapid settling of gas into a rotating disk. The Eggen, Lynden-Bell & Sandage (ELS) scenario readily explained the origin and general structural, kinematic, and metallicity correlations of observationally identified populations of field stars and implied a smooth distribution of stars observable today. The predictions of the ELS scenario were quantified by the Bahcall & Soneira (1980) and Gilmore, Wyse & Kuijken (1989) models, and reviewed in detail by, e.g., Majewski (1993). In these smooth models, the Milky Way in the relatively nearby region (within $\sim$5 kpc) is usually modeled by three discrete components described by fairly simple analytic expressions: the thin disk, the thick disk, and the halo. The other known components, the bulge and the bar, are not expected to directly contribute to the stellar populations in this local region.

However, for some time, starting with the pioneering work of Searle & Zinn (1978), and culminating with recent discoveries of complex substructure in the distribution of the Milky Way's stars, this standard view has experienced difficulties. Unlike the smooth models with simple components that have been used on local scales, new data on larger scales indicate the presence of much more irregular structures, such as the Sagittarius (Sgr) dwarf tidal stream and the Virgo and Pisces overdensities in the halo, and the Monoceros stream closer to the Galactic plane. Recent observational developments, based on accurate large-area sky surveys, have made it abundantly clear that the Milky Way is a complex and dynamic structure that is still being shaped by the infall (merging) of neighboring smaller galaxies. Numerical simulations suggest that this merger process plays a crucial role in establishing the structure and motions of stars within galaxies and is a generic feature of current cosmological models (Steinmetz & Navarro 2002; Sommer-Larsen, Götz & Portinari 2003; Governato et al. 2004, 2007; Brook et al. 2005; Bullock & Johnston 2005; Johnston et al. 2008; Font et al. 2011).

The main purpose of this review is to summarize some of the recent observational progress in Milky Way studies and the paradigm shifts (this phrase implies a change in the basic assumptions about galaxy formation, from the smooth collapse model to the galaxy mergers scenario) in our understanding of galaxy formation and evolution resulting from this progress. This review is focused on only a few studies, based mostly on data collected by the Sloan Digital Sky Survey (SDSS; **http://www.sdss.org**) described by York et al. (2000) and does not represent an exhaustive overview of all the progress made during the past decade. One of our goals is to illustrate novel analysis methods enabled by new data sets. We begin with a brief overview of methodology and of a few major data sets, and then we describe the main observational results. We conclude by discussing some of the unanswered questions and observational prospects for the immediate future.

## 1.2. Stellar Populations: Definition and Role

In astronomy, the term stellar populations is often associated with Populations I, II, and III, although the precise meanings of these populations have changed over time. These stellar classes generally represent a sequence of decreasing metallicity and increasing age. Here, we use the term stellar population to mean any collection of stars with common spatial, kinematic, chemical, luminosity, and/or age distributions. For example, a sample of red-giant stars selected using appropriate observables and selection criteria is considered a population, although such a sample can include both Population I and Population II stars. Similarly, we often consider populations of disk and halo stars or samples selected from a narrow color range. In summary, any sample of stars that share some common property that is appropriate for mapping the Galaxy in the space of various observables is hereafter considered to be a population.

Most studies of the Milky Way can be described as investigations of the stellar distribution, or statistical behavior of various stellar populations, in the seven-dimensional (7D) phase space spanned by the three spatial coordinates, three velocity components, and metallicity (of course, the abundances of individual chemical elements can be treated as additional coordinates; this will be a key ingredient for progress in the next decade). Depending on the quality, quantity, and diversity of the data, such studies typically concentrate on only a limited region of this 7D space (e.g., the Solar Neighborhood, pencil beam surveys, or kinematically biased surveys) or consider only marginal distributions (e.g., the number density of stars irrespective of their metallicity or kinematics, or proper-motion surveys without metallicity or radial-velocity information). The primary driver of the substantial progress in our knowledge of the Milky Way over the past decade is the ability of modern sky surveys to deliver the data required for determining the phase-space coordinates for unprecedented numbers of faint stars over large areas of the sky. For example, in less than two decades the observational material for kinematic mapping has progressed from the first pioneering studies based on only a few hundred objects (Majewski 1992) to over a thousand objects (Chiba & Beers 2000), to the massive data sets including millions of stars reviewed here.

The availability of large stellar samples enables detailed studies of various distributions, including determination of the distributions' shape, rather than considering only low-order statistical measures, as is done for small samples. Deviations from Gaussian shapes often encode more information about the history of galaxy assembly than the distribution's mean and dispersion. The large samples are especially important for considering multivariate distributions (as opposed to one-dimensional marginal distributions), as the so-called curse of dimensionality (when the problem dimensionality is high, the probability for a data point to belong to a multidimensional bin becomes small, and the bins become sparsely populated if the sample is not sufficiently large) prevents their accurate determination with small samples.

In addition to increasing the sample size, the ability to detect faint stars is crucial for extending the sample distance limit. With SDSS, it has become possible to detect even main-sequence (dwarf) stars to a distance limit exceeding 10 kpc, and thus to probe both the disk and halo populations within the same data set. The advantage of carrying out analyses of multiple populations using stellar probes of similar intrinsic properties is difficult to overstate. By way of comparison, the main-sequence stars in the Hipparcos sample (Perryman et al. 1997) only explore the volume within ~100 pc of the Sun. The primary advantage of main-sequence stars over probes such as RR Lyrae stars, blue horizontal-branch (BHB) stars, and red-giant stars for studying Galactic populations is that they are much more numerous (on the order of a thousand times more than these other populations summed together), and thus enable a substantially higher spatial resolution of the resulting phase-space maps (assuming a fixed number of stars per multidimensional pixel in phase space, and neglecting the intrinsic limit on spatial resolution set by the distance precision).

Annu. Rev. Astro. Astrophys. 2012.50:251-304. Downloaded from www.annualreviews.org
by California Institute of Technology on 01/21/14. For personal use only.

Of course, these other probes are still valuable, because they can be used to explore the Galaxy to a larger distance limit than obtainable with main-sequence stars alone.

A theme common to most of the studies reviewed here is the use of photometric parallax relations to estimate stellar distances, followed by the subsequent direct mapping of various distributions using large samples of stars. This mapping approach does not require a priori model assumptions, but instead constructs multidimensional distribution maps first and only then looks for structure in the maps and compares them to Galactic models. A key observational breakthrough that made this approach possible was the availability of accurate multiband optical photometry to a faint flux limit over a large area of sky, delivered by SDSS, as discussed below.

Annu. Rev. Astro. Astrophys. 2012.50:251-304. Downloaded from www.annualreviews.org
by California Institute of Technology on 01/21/14. For personal use only.

## 1.3. Observations: Photometry, Spectroscopy, and Astrometry

In order to determine the coordinates of a star in 7D phase space, a variety of astronomical techniques must be used. As always, the most crucial quantity to measure is stellar distance. The largest sample of stars with trigonometric distances, obtained by the Hipparcos survey, is too shallow (and too small) to complement deep surveys such as SDSS and the Two-Micron All Sky Survey (2MASS) (see below for an overview of these surveys). Until the all-sky *Global Astrometric Interferometer for Astrophysics* (Gaia) survey measures trigonometric distances for about a billion stars brighter than $V = 20$ (see Section 8.4), various photometric methods need to be employed in order to estimate distances. A common aspect of these methods is that the luminosity (i.e., absolute magnitude) of a star is determined by constraints derived from its color measurements; then its distance is determined from the observed difference between its absolute and apparent magnitude. For certain populations, for example RR Lyrae stars, a good estimate of absolute magnitude is obtained as a simple constant (with some metallicity dependence); for other populations, such as main-sequence stars, the absolute magnitude depends on both effective temperature and metallicity, and sometimes on age (or surface gravity) as well. A photometric parallax method for main-sequence stars is described below.

The most accurate measurements of stellar metallicity are based on spectroscopic observations (but see below for a method of estimating metallicity using photometric data alone). Spectroscopic measurements are especially important when studying the extremely low end of the metallicity distribution function, where photometric methods become insensitive. In addition to measuring chemical composition, spectroscopic observations enable radial-velocity measurements. The two largest existing stellar spectroscopic surveys are SDSS and the Radial Velocity Experiment (RAVE) (see Section 1.3.1).

To measure all three components of the space-velocity vector, precise astrometric observations are also required. The projection of the space-velocity vector into the tangent plane (i.e., perpendicular to the radial-velocity component) is measured using proper motion (the astrometric position shift per unit time), which can be combined with the distance estimate to yield the space velocity. The proper-motion measurements place an additional constraint on observations; at least two (ideally, widely temporally separated) astrometric epochs must be available.

Therefore, multicolor imaging, multiepoch astrometry, and spectroscopy are required for measuring the coordinates of a star in the 7D position-velocity-metallicity phase space. It is the advent of massive and accurate imaging and spectroscopic surveys that delivered such measurements for large and relatively unbiased samples of stars, and thus enabled major progress in Milky Way phase-space mapping during the past decade.

**1.3.1. A photometric parallax method for main-sequence stars.** In order to estimate distances to main-sequence stars with an accuracy of 10–20% through the use of photometric parallax relations, multiband optical photometry accurate to several percent (i.e., to several hundredths of a magnitude) is required. This stringent requirement comes from the steepness of the color-luminosity relation (the derivative of the absolute magnitude in the SDSS $r$-band with respect to the $g-i$ color reaches ∼10 mag/mag at the blue end), and is the main reason why it was not possible to use this method with large sky surveys prior to SDSS.

Using globular cluster data obtained in the SDSS photometric system, Ivezić et al. (2008a) derived a polynomial expression for the absolute magnitude of main-sequence stars in the $r$-band as a function of their $g-i$ color and metallicity (see their equations A2 and A7). The accuracy of the resulting magnitudes is in the range of 0.1–0.2 mag (Ivezić et al. 2008a; Sesar, Ivezić & Jurić 2008), and the method enables studies of the ∼100 pc to ∼10 kpc distance range when used with SDSS data. The ability to estimate distances to main-sequence stars with sufficient accuracy using only SDSS photometry was crucial for wide-angle panoramic mapping of the Galaxy to a distance limit 100 times farther than possible with the Hipparcos data alone.

Annu. Rev. Astro. Astrophys. 2012.50:251-304. Downloaded from www.annualreviews.org
by California Institute of Technology on 01/21/14. For personal use only.

**1.3.2. A photometric metallicity method for main-sequence stars.** Stellar metallicity, together with effective temperature and surface gravity, is one of the three main parameters that affect the observed spectral energy distribution of most stars. In addition to being an informative observable for deciphering the Milky Way's chemical history (e.g., Majewski 1993, 2010, and references therein; Freeman & Bland-Hawthorn 2002; Helmi 2008), knowledge of stellar metallicity is crucial for accurate estimates of distances using photometric parallax relations.

The most accurate measurements of stellar metallicity are based on spectroscopic observations. However, despite recent progress in the availability of at least low-resolution digital stellar spectra (approaching a million!), the number of stars detected in imaging surveys is still vastly larger. In addition to generally providing better sky and depth coverage than spectroscopic surveys, imaging surveys obtain essentially complete flux-limited samples of stars. These simple selection criteria are advantageous when studying Galactic structure in comparison with the complex targeting criteria that are (by necessity) often used for spectroscopic samples.

As first suggested by Schwarzschild, Searle & Howard (1955), the depletion of metals in a stellar atmosphere has a detectable effect on the emergent flux, in particular in the blue spectral region where the density of metallic absorption lines is highest (Beers & Christlieb 2005, and references therein). Recent analysis of SDSS data by Ivezić et al. (2008a) demonstrated that for blue F- and G-type main-sequence stars, a metallicity estimate accurate to ∼0.2 dex can be derived from the $u-g$ color. They derived a polynomial expression that maps the measured $u-g$ versus $g-r$ color space to effective temperature and metallicity ($[Fe/H]$) (for updated coefficients see Bond et al. 2010). This transformation, applicable to stars with $0.2 < g-r < 0.6$, was calibrated using ∼100,000 stars with available spectroscopic metallicity determinations and has errors in the range of 0.2–0.3 dex when used with SDSS data [for stars in the metallicity range of $-2 < [Fe/H] < +0.3$, which includes ∼99% of all stars in the Milky Way; for more details, see Ivezić et al. 2008a, Bond et al. 2010]. Although applicable only within a restricted color range, this calibration has enabled the construction of metallicity maps using millions of stars, as discussed further below.

## 2. THE ADVENT OF LARGE-AREA DIGITAL SKY SURVEYS

Major advances in our understanding of the Milky Way have historically arisen from dramatic improvements in our ability to "see," as vividly exemplified by Galileo resolving the Milky Way disk into individual stars. Progressively larger telescopes have been developed over the past century, but until recently most astronomical investigations have focused on small samples of objects because the largest telescope facilities typically have rather small fields of view, and those with large fields of view could not detect very faint sources. Over the past two decades, however, astronomy moved beyond the traditional observational paradigm and undertook large-scale digital sky surveys, such as the SDSS and the Two Micron All Sky Survey (2MASS; **www.ipac.caltech.edu/2mass/**) (Skrutskie et al. 2006). This observational progress, based on advances in telescope construction, detectors, and above all, information technology, has had a dramatic impact on nearly all fields of astronomy, including studies of the structure of the Milky Way. Here we briefly overview the characteristics of the most massive recent data sets.

## 2.1. The Sloan Digital Sky Survey Imaging and Spectroscopic Surveys

The SDSS is a digital photometric and spectroscopic survey that covered over one quarter of the Celestial Sphere in the North Galactic cap (approximately, $|b| > 30°$) and produced a smaller area ($\sim$300 deg$^2$) but much deeper survey in the Southern Galactic hemisphere, along the Celestial Equator (Aihara et al. 2011, and references therein). The recent Data Release 8 has a sky coverage of about 14,600 deg$^2$ and includes photometric measurements for 469 million unique objects (approximately half are stars). The completeness of the SDSS catalogs for point sources is $\sim$99% at the bright end and drops to 95% at an $r$-band magnitude of $\sim$22. The wavelength coverage of the SDSS photometric system (*ugriz*, with effective wavelengths from 3,540 Å to 9,250 Å) and photometry accurate to $\sim$0.02 mag have enabled photometric parallax and metallicity estimates for many millions of stars. For comparison, the best large-area optical sky survey prior to SDSS, the photographic Palomar Observatory Sky Survey (POSS), had only two photometric bands and several times larger photometric errors, and it was limited by uncertain zero points that varied from plate to plate (Sesar et al. 2006).

In addition to its imaging survey data, the SDSS has obtained well over half a million stellar spectra, many as part of the Sloan Extension for Galactic Understanding and Exploration (SEGUE; Yanny et al. 2009) and its continuation the SEGUE-2, subsurveys carried out during the first (SDSS-II) and second (SDSS-III; Eisenstein et al. 2011) extensions of the SDSS project. These spectra have wavelength coverage over 3,800–9,200 Å and spectral resolving power $R \sim$ 2,000, with a typical signal-to-noise ratio per 150 km s$^{-1}$ resolution element of $>$30 at $r \sim 18.5$ and $\sim$3 at $r \sim 20$. SDSS stellar spectra are of sufficient quality to provide robust and accurate stellar parameters, such as effective temperature, surface gravity, and metallicity (parameterized as $[Fe/H]$). These publicly available parameters are estimated using a variety of methods implemented in an automated pipeline (the SEGUE Stellar Parameters Pipeline, SSPP) (Beers et al. 2006). A detailed discussion of these methods and their performance can be found in Papers I–V of the SSPP series (Allende Prieto et al. 2008; Lee et al. 2008a,b, 2011a; Smolinski et al. 2011). Based on a comparison with high-resolution abundance determinations, these researchers demonstrate that the combination of spectroscopy and photometry from the SDSS is capable of delivering estimates of $T_{\rm eff}$, log($g$), and $[Fe/H]$ accurate to 200 K (3%), 0.3 dex, and 0.2 dex, respectively. Random errors for the radial-velocity measurements are a function of spectral type, but are usually $<$5 km s$^{-1}$ for stars brighter than $r \sim 18$, rising to $\sim$20 km s$^{-1}$ for stars with $r \sim 20$ (Pourbaix et al. 2005, Yanny et al. 2009). Lee et al. (2011a) demonstrate that SDSS spectra are of sufficient quality to also determine $[\alpha/Fe]$ with errors below 0.1 dex (for stars with temperatures in the range of 4,500–7,000 K and sufficient signal-to-noise ratios). The distribution of SDSS stars with available spectroscopic estimates of atmospheric parameters in the log($g$) versus color plane is shown in **Figure 1**.

Annu. Rev. Astro. Astrophys. 2012.50:251-304. Downloaded from www.annualreviews.org
by California Institute of Technology on 01/21/14. For personal use only.

Annu. Rev. Astro. Astrophys. 2012.50:251-304. Downloaded from www.annualreviews.org
by California Institute of Technology on 01/21/14. For personal use only.

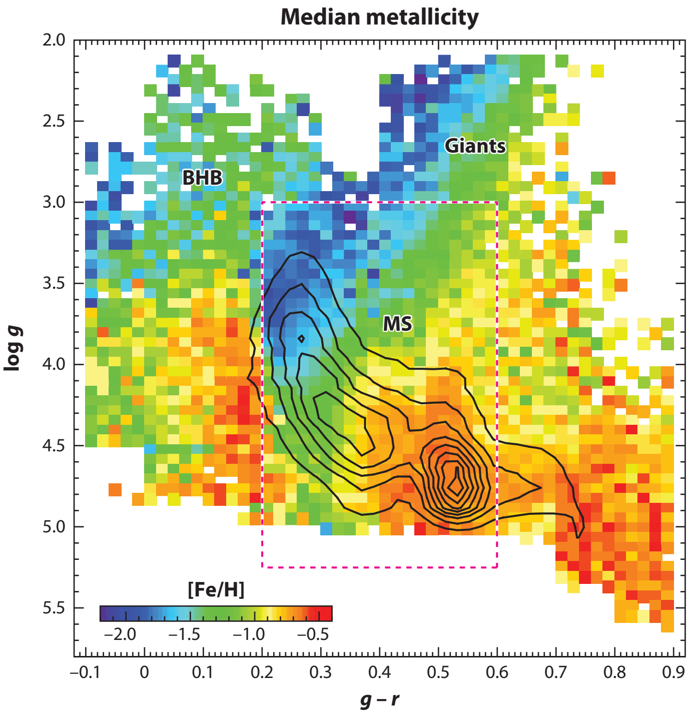

**Figure 1**

The stellar content of the Sloan Digital Sky Survey (SDSS) spectroscopic surveys through Data Release 6. Linearly spaced contours show the distribution of ~110,000 stars with $g < 19.5$ and $0.1 < g - r < 0.9$ (corresponding to effective temperatures in the range of 4,500 K $< T_{\mathrm{eff}} <$ 8,200 K) in the log($g$) versus $g - r$ plane ($g$ is the SDSS $g$-band magnitude, and log($g$) measures the surface gravity). The multimodal distribution is a result of the SDSS target-selection algorithm. The color scheme shows the median metallicity for all 0.02 mag by 0.06 dex pixels that contain at least 10 stars. The fraction of stars with $\log(g) < 3$ (giants) is 4%, and they are mostly found in two color regions: $-0.1 < g - r < 0.2$ [blue horizontal-branch (BHB) stars] and $0.4 < g - r < 0.65$ (red giants). They are dominated by low-metallicity stars ($[Fe/H] < -1$). The dashed lines outline the main-sequence (MS) region, where photometric metallicity methods can be applied. Reprinted from Ivezić et al. (2008a).

## 2.2. The Sloan Digital Sky Survey-Palomar Observatory Sky Survey Proper-Motion Survey

The time difference of about half a century between the POSS and SDSS imaging observations provides an excellent baseline to measure proper motions for tens of millions of stars to faint brightness levels. Munn et al. (2004) addressed the problem of large systematic astrometric errors in the POSS catalogs by recalibrating the USNO-B catalog (Monet et al. 2003), using the positions of galaxies measured by the SDSS. As a result of this calibration, the SDSS-POSS proper-motion measurements are now available for about 100 million unresolved sources, most of them stars. This catalog also includes about 70,000 spectroscopically confirmed SDSS quasars that were used to robustly estimate the proper-motion errors (Bond et al. 2010). The random errors increase from ~3 mas year$^{-1}$ at the bright end to ~6 mas year$^{-1}$ at $r \sim 20$ (the sample completeness limit), with systematic errors that are typically an order of magnitude smaller and with very small variation across the sky (for a discussion of deviations from Gaussian error behavior, see Dong et al. 2011). Even for stars at distances of 1 kpc, the implied tangential velocity errors are as small as 10–20 km s$^{-1}$, and well matched to the SDSS radial-velocity accuracy. This catalog represents a major improvement over previously available data sets both in size and accuracy.

## 2.3. The Two-Micron All Sky Survey Imaging Survey

The 2MASS databases are derived from an all-sky near-IR photometric survey with limiting (Vega-based, 10σ) magnitudes of $J = 15.8$, $H = 15.1$, and $K = 14.3$. The 2MASS point source catalog contains positional and photometric information for 471 million sources (mostly stars). The near-IR 2MASS colors are not as good as the optical SDSS colors for estimating photometric parallax and metallicity, because they only probe the Rayleigh-Jeans tail of the stellar spectral energy distribution. However, a major advantage of 2MASS over the SDSS is the full sky coverage and its ability to penetrate deeper through the interstellar dust in the Galactic plane. In addition, it is much easier to photometrically identify certain stellar populations using near-IR data than with optical data. For example, Majewski et al. (2003) have demonstrated that M-giant candidates, color-selected from the 2MASS database, are extremely powerful probes of halo substructure out to ∼100 kpc over the entire sky (these stars are practically impossible to robustly identify using SDSS photometry). For an analysis of the joint SDSS-2MASS stellar data set, we refer the reader to Covey et al. (2007).

Annu. Rev. Astro. Astrophys. 2012.50:251-304. Downloaded from www.annualreviews.org
by California Institute of Technology on 01/21/14. For personal use only.

## 2.4. The Radial Velocity Experiment Spectroscopic Survey

RAVE (**www.rave-survey.aip.de**) is a major new spectroscopic survey aiming to measure radial velocities and stellar atmosphere parameters (temperature, surface gravity, and metallicity) of up to one million stars using the Six Degree Field multi-object spectrograph on the 1.2-m UK Schmidt Telescope of the Anglo-Australian Observatory (Steinmetz et al. 2006). RAVE stars are selected from the magnitude range of $9 < I < 12$ and represent a bright complement to the SDSS spectroscopic sample (Siebert et al. 2011). The wavelength range for the RAVE spectra (8,410–8,795 Å, in the region of the Ca II Triplet, with a spectral resolving power of R ∼ 8,000) includes a number of lines in addition to calcium and should eventually provide reliable estimates of [α/*Fe*] for numerous stars in addition to overall metallicity ([*Fe/H*]). The RAVE catalog of stellar elemental abundances (Boeche et al. 2011) includes estimates of abundances for Mg, Al, Si, Ca, Ti, Fe, and Ni, with a mean error of ∼0.2 dex, for some 36,000 stars.

The third RAVE data release includes radial-velocity data for ∼77,000 stars and stellar parameters for ∼40,000 stars (Siebert et al. 2011), but spectra are already collected for over 300,000 stars (Zwitter et al. 2010). With a radial-velocity error of about 2 km s$^{-1}$, the RAVE velocities are more accurate than those delivered by the SDSS and are well suited for detailed kinematic studies of nearby disk stars (Ruchti et al. 2011). Proper motions (of varying accuracy) are available for most of the RAVE stars from other surveys, and model-based distance determinations accurate to ∼20% are also available (Zwitter et al. 2010, Burnett et al. 2011).

The distances probed by RAVE stars range from ∼300 pc (dwarfs) to ∼1–2 kpc (giants), and thus the RAVE data set connects the nearby Hipparcos sample and the more distant SDSS sample. Owing to these distance limits, RAVE data are more relevant for disk than for halo investigations. However, the RAVE survey has demonstrated the ability to identify at least a limited number (hundreds in the present sample, eventually several thousand) of bright, very low-metallicity stars with $[Fe/H] < -2.0$, including a handful with metallicity as low as $[Fe/H] < -4.0$ (Fulbright et al. 2010). Bright, very metal-poor stars are of particular interest, because follow-up high-resolution spectroscopy can be obtained with relatively short integration times on 4-m- to

Annu. Rev. Astro. Astrophys. 2012.50:251-304. Downloaded from www.annualreviews.org by California Institute of Technology on 01/21/14. For personal use only.

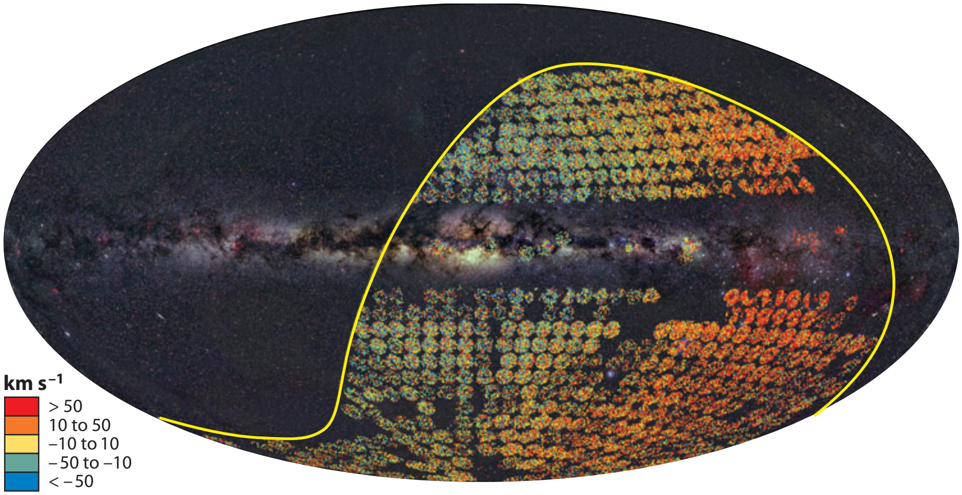

**Figure 2**

The sky coverage of the Radial Velocity Experiment (RAVE) DR3, shown as an Aitoff projection in Galactic coordinates and color-coded by the mean radial velocity. The nearly contiguous coverage over a wide solid angle, with detailed data for (eventually) up to a million stars, is representative of modern Milky Way surveys and enables new approaches to studying the Galaxy. The stars distances probed by the RAVE survey range up to ~1 kpc, thus the RAVE data set provides a valuable link between the nearby Hipparcos sample (<100 pc) and the more distant SDSS sample. Reprinted from Siebert et al. (2011).

8-m-class telescopes. In addition, the large-area, nearly contiguous coverage of the RAVE survey (see **Figure 2**) is very useful for panoramic Galactic mapping.

## 3. OVERVIEW OF THE STATE OF THE ART A DECADE AGO

Before discussing results concerning the nature of Galactic structure and stellar populations obtained during the past decade, we briefly review the state of related knowledge to a decade ago. We concentrate on the spectroscopic surveys in existence at that time and the questions they sought to address.

Circa 2000, there were two primary approaches in common use for the detection and analysis of significant numbers of stars with membership in the thick-disk and halo populations of the Galaxy. The first approach, essentially a continuation of the high-proper-motion-based surveys pioneered by Sandage and colleagues, is exemplified by the work of Ryan & Norris (1991) and that of Carney et al. (1996), and references therein. Their work concentrated on members of the halo population, although stars from the disk system were certainly present in their samples as well. The second approach, which followed on the efforts of Norris (1986), was the assemblage (Beers et al. 2000) and analysis (Chiba & Beers 2000) of a large sample of nonkinematically selected stars with $[Fe/H] < -0.6$ (this metallicity limit was chosen to minimize the contribution of disk-system stars). It was considered of central importance (as it remains now) to contrast the derived properties of samples chosen with differing biases—the former on kinematics and the latter on metallicity. For this reason, papers that followed commonly adopted the halo metallicity distribution functions (MDFs) as derived from the kinematically selected samples and the kinematics of the thick-disk and halo populations based on the nonkinematically selected samples. It is worth noting that, even prior to the results obtained by these two surveys, Freeman (1987) called attention to the

Annu. Rev. Astro. Astrophys. 2012.50:251-304. Downloaded from www.annualreviews.org
by California Institute of Technology on 01/21/14. For personal use only.

puzzling differences in the trends of the derived halo rotation velocities and velocity dispersions as a function of declining metallicity for the extant kinematically versus nonkinematically selected stars. Today, it seems likely that this puzzle may be resolved by the recognition that, even within the halo component, there exists a strong coupling between kinematics and metallicity that was not previously apparent.

The most pressing questions from a decade ago included the following, asked and answered (even if only partially) below. Answers to the above questions were essentially all limited by the relatively small numbers of stars with 7D phase-space information then available, as well as by the troublesome selection biases that were known to exist in the tracer samples. Even so, some progress toward resolution of these issues was being made at the time.

### 3.1. What Is the Nature of the Halo Metallicity Distribution Function?

What is the nature of the MDF for the halo population, and does it include significant numbers of stars with metallicities below $[Fe/H] \sim -3.0$?

Although the proper-motion-selected samples included only a handful of stars with $[Fe/H] < -3.0$, the objective-prism surveys that were the source of the lowest metallicity stars known at that time (e.g., Beers, Preston & Shectman 1992) included tens of stars below this metallicity. The inference could be made that, although stars of such low metallicity were rare compared to the more metal-rich halo stars with $[Fe/H] < -1.5$, they did in fact exist in substantial numbers.

### 3.2. The Eggen, Lynden-Bell & Sandage versus Searle-Zinn Model of Halo Formation

Can the kinematics of the halo of the Galaxy be adequately described by the rapid-collapse model of ELS (Eggen, Lynden-Bell & Sandage 1962), or did the observations require the more extended, chaotic assembly picture of Searle & Zinn (1978)?

One of the primary discriminants between the suggested galaxy formation models is the presence (or not) of halo stars with low orbital eccentricities, which might not be expected to be found in significant number if the ELS model was the correct interpretation. Papers published prior to work by Chiba & Beers (2000) did in fact identify such stars (e.g., Norris, Bessell & Pickles 1985), but only relatively few. The question was essentially resolved by the substantially larger numbers of low-metallicity, low-eccentricity halo stars discussed by Chiba & Beers (2000).

### 3.3. What Is the Shape of the Halo?

What is the shape of the density profile of the stellar halo, and does it remain constant with increasing distance (and/or declining metallicity)?

A number of papers prior to 2000 (e.g., Hartwick 1987; Preston, Shectman & Beers 1991) pointed out that the shape of the stellar halo density profile changes with Galactocentric distance, in the sense that it is relatively flattened in the inner region and becomes substantially rounder in the outer region. This result was validated by inferences based on the kinematics of local halo stars carried out by Sommer-Larsen & Zhen (1990) and Chiba & Beers (2000).

### 3.4. Are the Thin and Thick Disks Distinct Entities?

Is the disk system adequately modeled by the superposition of a thin-disk and thick-disk population; that is, are these two components demonstrably distinct from one another?

Although Norris & Ryan (1991) made the argument that a continuous extended disk configuration could be supported by the existing data at that time, Chiba & Beers (2000) claimed that the kinematics and abundances of thick-disk stars indicated that a distinct thick-disk component was the more likely interpretation. However, the question remained basically open as of a decade ago.

### 3.5. Is the Metal-Weak Thick Disk Real?

Is there evidence for the additional presence of a metal-weak thick-disk (MWTD) population, rotationally supported, but extending to lower metallicity stars than the canonical thick disk?

Although the original suggestion that a MWTD component may exist (Norris, Bessell & Pickles 1985; Morrison, Flynn & Freeman 1990) was supported by the analysis of Chiba & Beers (2000), claims to the contrary based on revised photometric studies (Twarog & Anthony-Twarog 1994) and high-resolution spectroscopic studies of suggested MWTD stars (e.g., Ryan & Lambert 1995) (but see also Bonifacio, Centurion & Molaro 1999) called the reality of the MWTD into question, at least at that time.

Annu. Rev. Astro. Astrophys. 2012.50:251-304. Downloaded from www.annualreviews.org
by California Institute of Technology on 01/21/14. For personal use only.

### 3.6. Are There Stellar Streams Other than Sagittarius?

Can one identify other streams of stars, similar to the then-recognized Sgr stream, that might be associated with origin in stripped dwarf galaxies?

Helmi et al. (1999) presented the detection of a small number of halo stars that appeared as a statistically significant overdensity in an otherwise sparsely populated region of angular momentum phase space and argued that they may have originated from the stripping of a once-coherent structure such as a dwarf galaxy. This inference was supported by additional data from Chiba & Beers (2000), and others since, but of course it was only one such example.

So, in toto, among the issues mentioned above, the data available as of a decade ago could at best claim only one clear victory (Issue 2), three strong maybes (Issues 1, 3, and 6), and two yet to be decided (Issues 4 and 5). Larger samples with well-understood selection biases were clearly needed.

## 4. WHAT DID WE LEARN DURING THE PAST DECADE?

Until recently, our global view of the Milky Way was hampered by the fact that most detected stars had no reliable distance estimates. Those stars that had usable distances were either limited to the Solar Neighborhood (e.g., for main-sequence stars in the Hipparcos sample to within ~100 pc or only ~1% of our distance to the Galactic center) or to smaller pencil-beam surveys. Our knowledge of the basic structural components of the Milky Way was thus limited to indirect inferences based on stellar population models motivated by other spiral galaxies (e.g., Bahcall & Soneira 1980, Robin et al. 2003). This limitation was alleviated recently by the advent of the SDSS, which provided accurate digital multiband optical photometry across a quarter of the sky. The SDSS photometry enabled the development and application of photometric parallax methods, which in turn led to direct mapping of stellar distributions in the multidimensional space spanned by spatial coordinates, velocity components, and chemical abundance measurements. The resulting maps provided the quantitative basis for separating the main structural components of the Galaxy, obtaining information on their phenomenological description, and enabled efficient searches for substructure and a robust comparison with various model predictions.

We first describe how these new data clearly reveal the disk and halo as two distinct Galaxy components, and then describe each of them in more detail. We do not discuss in detail here the third major Galaxy component, the bulge. For a recent excellent review of the bulge, see Minniti & Zoccali (2008). It is expected that spectroscopic data being collected by the SDSS-III Apache Point Observatory Galaxy Evolution Experiment (APOGEE) will soon yield unprecedented insight into chemical and kinematic properties of the bulge (Eisenstein et al. 2011; see also Section 8.1). We do not discuss the properties of the Galactic bar here and refer the reader to recent studies by Rattenbury et al. (2007), Cabrera-Lavers et al. (2008), and Robin et al. (2011), which summarize the current state of the art and include relevant references.

## 4.1. Separation of the Main Structural Components

Before the disk and halo can be studied in detail, a robust and accurate scheme for classifying stars into these two components needs to be developed. Using photometric data for ∼50 million stars, Jurić et al. (2008) constructed 3D maps (data cubes) of the stellar number-density distribution for 19 narrow color bins that span spectral types from mid-F- to early M-type stars. When the bin color is varied from the reddest to the bluest one, the maps are zoomed out, with subsamples covering distances ranging from 100 pc to 15 kpc. The distance to each star was estimated using a maximum likelihood implementation of the photometric parallax method, and stars are binned and counted in small 3D pixels whose size depends on the dynamical range provided by each color bin and Poisson noise limits (typically there are 250,000 pixels per map). Examples of 2D projections of the resulting maps are shown in **Figure 3**.

These maps are a powerful tool for studying the Milky Way's stellar number-density distribution. Traditional methods for modeling stellar counts in the magnitude-color space need to adopt a large number of poorly known relations, such as the stellar initial mass function, stellar mass-luminosity relationship, and stellar luminosity function, and a geometric description of the postulated components such as the disks, bulge, and halo. Alternatively, with these number-density maps the Milky Way's structure can be examined without any a priori assumptions about its components: The analysis of the Milky Way's structure is then akin to studies of external galaxies.

The quantitative description of these maps is still a nontrivial task, owing to the presence of rich substructures within the components. Whereas halo substructure has been known for some time (Ivezić et al. 2000, Yanny et al. 2000, Majewski et al. 2003, Belokurov et al. 2006a, Vivas & Zinn 2006), these new maps demonstrate that disk substructure is also complex. Nevertheless, the gross behavior can be captured by assuming standard Galaxy models based on two exponential disks and a power-law halo. Jurić et al. (2008) determined the best-fit parameter values for full two-dimensional smooth models and further refined them using residual minimization algorithms (see **Table 1**).

A cross section of the maps from **Figure 3** in the direction perpendicular to the disk plane is shown in **Figure 4**. The data shown in the middle and bottom panels clearly confirm a change in the number-count behavior around $|Z| \sim 1$–$1.5$ kpc, interpreted as evidence for an extended thick disk component by Yoshii (1982) (who referred to it as a "halo" component, even though

→

**Figure 3**

The panels in the left column show the measured stellar number-density [ln($n$), where $n$ is the number of stars per unit volume with arbitrary normalization], as a function of Galactic cylindrical coordinates, for stars selected from narrow ranges of $r - i$ color ($0.35 < r - i < 0.40$ in the *top row* to $1.30 < r - i < 1.40$ in the *bottom row*). The panels in the middle column show the best-fit smooth models; panels in the right column show the normalized (data-model) difference map. Note the large overdensities visible in the top three panels in the right column. Reprinted from Jurić et al. (2008).

Annu. Rev. Astro. Astrophys. 2012.50:251-304. Downloaded from www.annualreviews.org
by California Institute of Technology on 01/21/14. For personal use only.

Annu. Rev. Astro. Astrophys. 2012.50:251-304. Downloaded from www.annualreviews.org
by California Institute of Technology on 01/21/14. For personal use only.

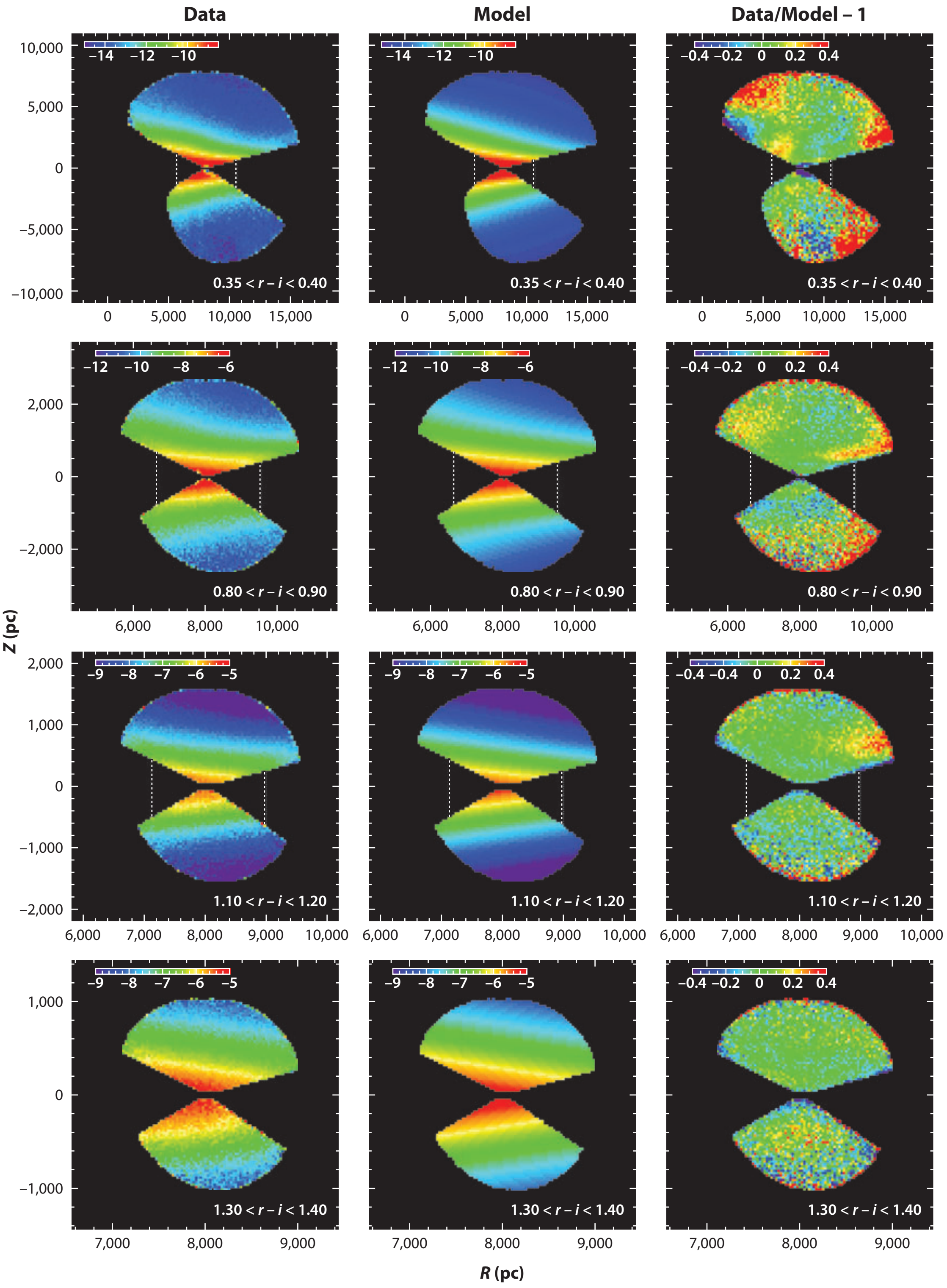

Annu. Rev. Astro. Astrophys. 2012.50:251-304. Downloaded from www.annualreviews.org
by California Institute of Technology on 01/21/14. For personal use only.

**Table 1 The best-fit parameters for the Jurić et al. (2008) Galactic model[a]**

| Parameter | Measured | Bias-corrected | Error estimate |
|---|---|---|---|
| $Z_0$ | 25 | | 20% |
| $L_1$ | 2,150 | 2,600 | 20% |
| $H_1$ | 245 | 300 | 20% |
| $f_d$ | 0.13 | 0.12 | 10% |
| $L_2$ | 3,261 | 3,600 | 20% |
| $H_2$ | 743 | 900 | 20% |
| $f_h$ | 0.0051 | . . . | 25% |
| $q$ | 0.64 | . . . | $\leq 0.1$ |
| $n$ | 2.77 | . . . | $\leq 0.2$ |

[a] Best-fit Galactic model parameters from Jurić et al. (2008), as directly measured from the apparent number-density distribution maps (second column) after correcting for a 35% assumed binary fraction and Malmquist bias due to photometric errors and dispersion around the mean of the photometric parallax relation (third column). $Z_\odot$ is the Solar offset from the Galactic plane (pc); $H_1$, $H_2$ and $L_1$, $L_2$ (pc) are the scale heights and lengths for the thin and thick disk, respectively; $f_d$ and $f_h$ are the thick disk and halo normalizations relative to the thin disk at ($R = R_\odot$, $Z = 0$), respectively; $q$ parameterizes the halo ellipticity (with the ellipsoid described by axes $a = b$ and $c = qa$; for $q < 1$ the halo is oblate, that is, "squashed" in the same sense as the disk); and $n$ is the power-law index for the halo number-density profile.

its inferred density was ten times that of the local halo and its scale height of ~2 kpc was commensurate with the values later determined by others) and Gilmore & Reid (1983). At the point where the additional, more-extended component becomes unable to explain the star counts, around $|Z| \sim 5$ kpc, another component—the stellar halo—is invoked to explain the data. Although these modern counts have exceedingly low statistical noise and fairly well-understood systematics, the three-component fit to the data shown in the bottom panel begs the question whether a single-component fit with some other function, parameterized with fewer free parameters, might suffice.

It turns out that the three additive components invoked to explain the counts exhibit distinctive chemical and kinematic behavior as well. **Figure 5** shows a panoramic view of the variation in the median [*Fe*/*H*] over an unprecedentedly large volume of the Galaxy. The map is based on photometric metallicity estimates for a sample of 2.5 million blue main-sequence stars (most of F spectral type) selected using very simple color and flux limits. It is easily discernible that the median metallicity farther than ~5 kpc from the Galactic plane is very uniform and about 1 dex lower than for stars within ~1 kpc from the plane.

The reason for the rapid decrease of median stellar metallicity with $|Z|$ for $|Z| < 5$ kpc, and very little variation farther from the plane, is illustrated in **Figure 6*a***. The two distinct distributions imply different Galaxy components, the halo and the disk, and are clearly evident. High-metallicity disk stars dominate close to the plane, whereas low-metallicity halo stars dominate beyond 3 kpc from the plane. The median metallicity for disk stars exhibits a vertical gradient, whereas the halo stars (at least in the relatively nearby volume) have a spatially invariant metallicity distribution. As $|Z|$ increases from $|Z| \sim 2$ kpc to $|Z| \sim 4$ kpc, halo stars become more numerous than disk stars, and the median metallicity drops by ~1.0 to 1.5 dex. A more detailed and quantitative discussion of these metallicity distributions is given by Ivezić et al. (2008a).

These two components, with distinct metallicity distributions, also have vastly different kinematic behavior, as shown in **Figure 6*b***. The high-metallicity disk stars exhibit large rotational velocity (about 220 km s$^{-1}$), whereas the low-metallicity halo stars display behavior consistent with no net rotation (to within 10–20 km s$^{-1}$). Similar to the behavior of their metallicity distributions, the rotational velocity for disk stars decreases with the distance from the Galactic plane, whereas it remains constant for nearby halo stars (see **Figure 7**).

Annu. Rev. Astro. Astrophys. 2012.50:251-304. Downloaded from www.annualreviews.org
by California Institute of Technology on 01/21/14. For personal use only.

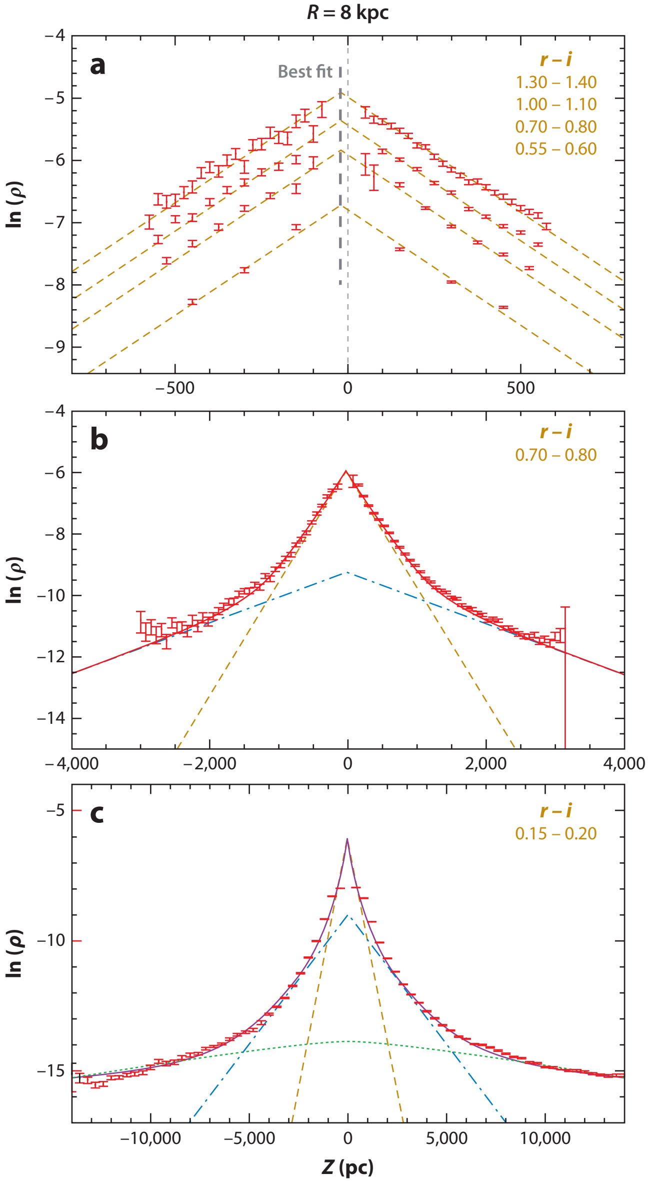

**Figure 4**

Cross sections through maps, similar to those shown in **Figure 3**, showing the vertical (|$Z$|) distribution at $R = 8$ kpc and for different $r - i$ color bins. The orange dashed lines are exponential models fitted to the red points (the sech$^2$ function is not a good fit; see footnote 28 of Jurić et al. 2008). The orange dashed lines in panel *a* correspond to a fit with a single, exponential disk. The vertical dashed line shows the best-fit position of the maximum density (not at 0 due to the Sun's offset from the disk midplane). The blue dot-dashed line in panel *b* corresponds to an additional disk component, and the data are fit with a sum of two disks with scale heights of 270 pc and 1,200 pc, respectively, and a relative normalization of 0.04 (the "thin" and the "thick" disks). The purple line in the bottom panel (closely following the data points) corresponds to a sum of two disks and a power-law spherical halo. The orange dashed line and the blue dot-dashed line are the disk contributions, and the halo contribution is shown by the green dotted line. For the best-fit parameters, see **Table 1**. Reprinted from Jurić et al. (2008).

Annu. Rev. Astro. Astrophys. 2012.50:251-304. Downloaded from www.annualreviews.org
by California Institute of Technology on 01/21/14. For personal use only.

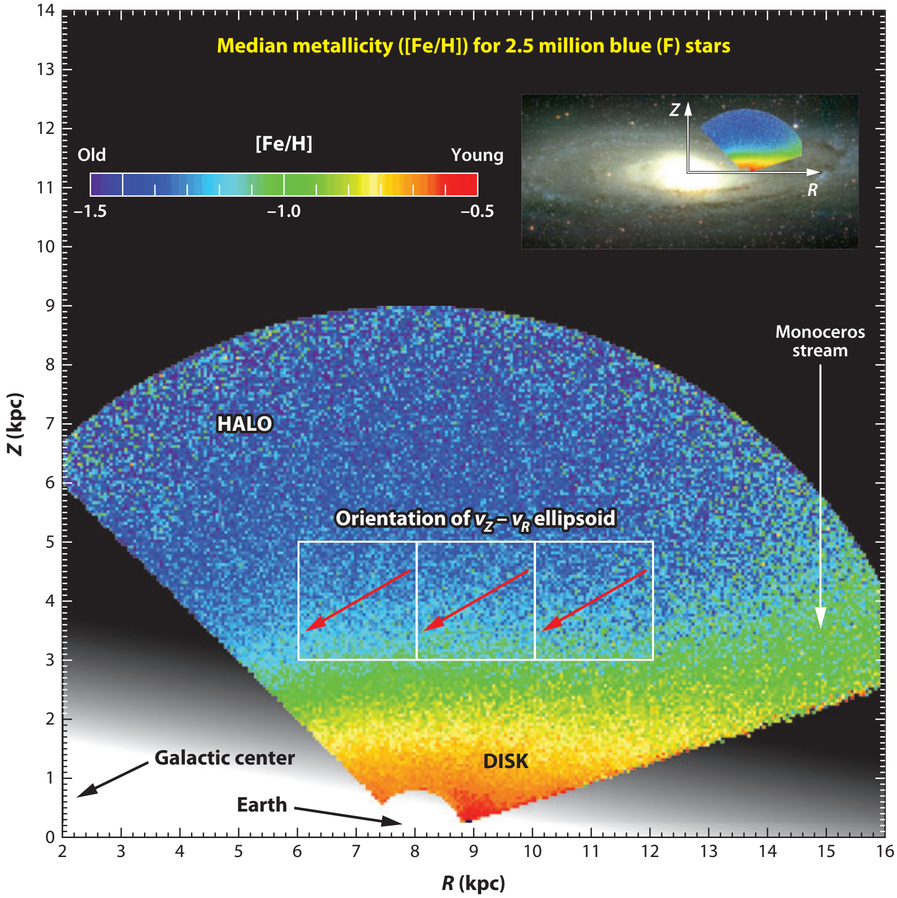

**Figure 5**

Variation of the median photometric stellar metallicity for ∼2.5 million stars from the Sloan Digital Sky Survey with $14.5 < r < 20$ and $0.2 < g - r < 0.4$, and photometric distance in the 0.8–9 kpc range expressed in cylindrical Galactic coordinates $R$ and $|Z|$. The ∼40,000 pixels (50 pc by 50 pc) contained in this map are colored according to the legend in the top left. Note that the gradient of the median metallicity is essentially parallel to the $|Z|$ axis, except in the region of the Monoceros stream, as marked. The gray-scale background is the best-fit model for the stellar number-density distribution from Jurić et al. (2008). The inset in the top right illustrates the extent of the data volume relative to the rest of the Galaxy; the background image is the Andromeda galaxy. The three squares outline the regions used to construct the $v_Z - v_R$ ellipsoids shown in **Figure 16**. The arrows illustrate the variation of the ellipsoid orientation, which always points toward the Galactic center. Adapted from Ivezić et al. (2008a).

Therefore, reasonably clean subsamples of halo and disk stars can be defined using a simple metallicity boundary $[Fe/H] = -1$. We proceed below with a more detailed discussion of each component.

## 5. THE MILKY WAY DISK

Recent massive data sets based on the SDSS have confirmed, with exceedingly high statistical signal-to-noise ratios, the abrupt change of slope in the log(counts) versus $|Z|$ plot around

Annu. Rev. Astro. Astrophys. 2012.50:251-304. Downloaded from www.annualreviews.org
by California Institute of Technology on 01/21/14. For personal use only.

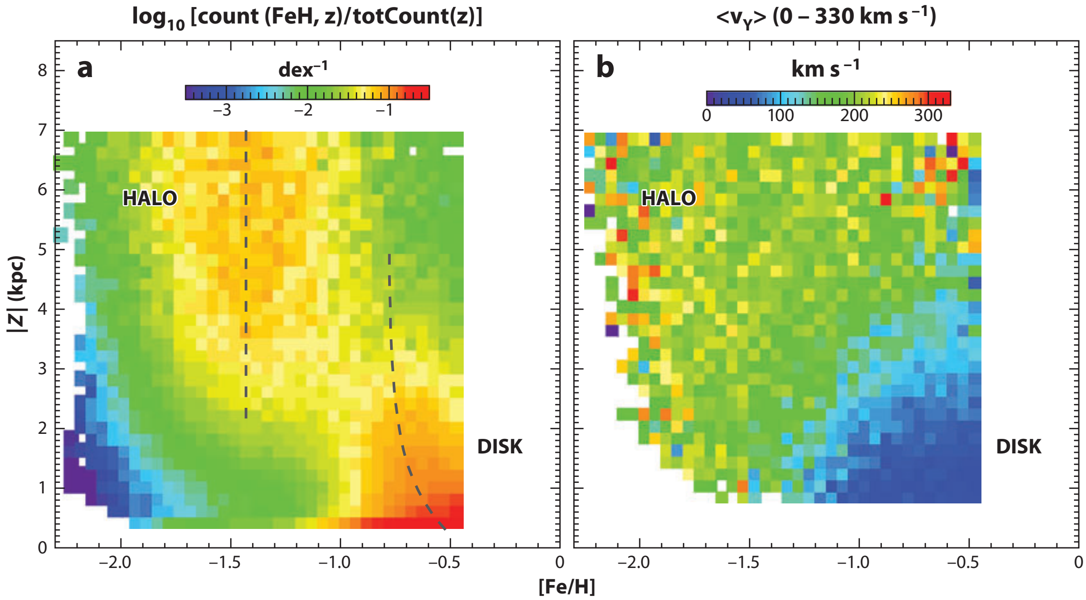

**Figure 6**

(*a*) The conditional metallicity probability distribution (each row of pixels integrates to unity) for ∼60,000 stars from a cylinder perpendicular to the Galactic plane, centered on the Sun, and with a radius of 1 kpc. The values are color-coded on a logarithmic scale according to the legend on top. The lack of stars with $[Fe/H] > -5.0$ is due to a bias in Sloan Digital Sky Survey Data Release 6 reductions, and an updated version of this map based on Data Release 7 is shown in figure A.3 of Bond et al. (2010). (*b*) The median heliocentric rotational velocity component (the value of ∼220 km s$^{-1}$ corresponds to no rotation), as a function of metallicity and distance from the Galactic plane, for the ∼40,000 stars from panel *a* that also satisfy $|b| > 80°$. Reprinted from Ivezić et al. (2008a).

$|Z| \sim 1$ kpc for disk stars (Jurić et al. 2008). This slope change was discovered almost three decades ago and interpreted as evidence for two disk components: the thin disk and the thick disk. Over a similar range in $|Z|$, there are clearly detected vertical gradients in the median stellar metallicity and rotational velocity (Ivezić et al. 2008a, and references therein). A key question now is whether the two disk components required to explain the counts can also be used to account for the chemical and kinematic measurements for the same stars. For example, are the metallicity and kinematic gradients due to the interplay of two additive components (with thick-disk stars dominating beyond $|Z| \sim 1$) or do they instead reveal a single disk with complex variations of basic properties (perhaps driven by a hidden variable, such as age)? In other words, do the new data require a disk decomposition into thin- and thick-disk components, and if so, what is an optimal way to define these components? It turns out that, even with the new data collected over the past decade, it is not easy to answer these questions.

The paper by Ivezić et al. (2008a) showed that the observed variations in the metallicity and velocity distributions of disk stars over the range $|Z| \sim 1$–3 kpc are only mildly inconsistent with the traditional simple decomposition into thin- and thick-disk components. However, they also found that the rotational velocity and metallicity at $|Z| \sim 1$ kpc, where the contributions of the two components are similar, are uncorrelated. This lack of correlation is in strong conflict with the traditional decomposition. Instead, Ivezić et al. (2008a) modeled the observed distributions using smooth shifts of the metallicity and velocity distributions that do not change their shape. They argued that their ability to describe the observations using functions with universal $|Z|$-independent shapes has fundamental implications for disk origin—instead of two distinct

Annu. Rev. Astro. Astrophys. 2012.50:251-304. Downloaded from www.annualreviews.org
by California Institute of Technology on 01/21/14. For personal use only.

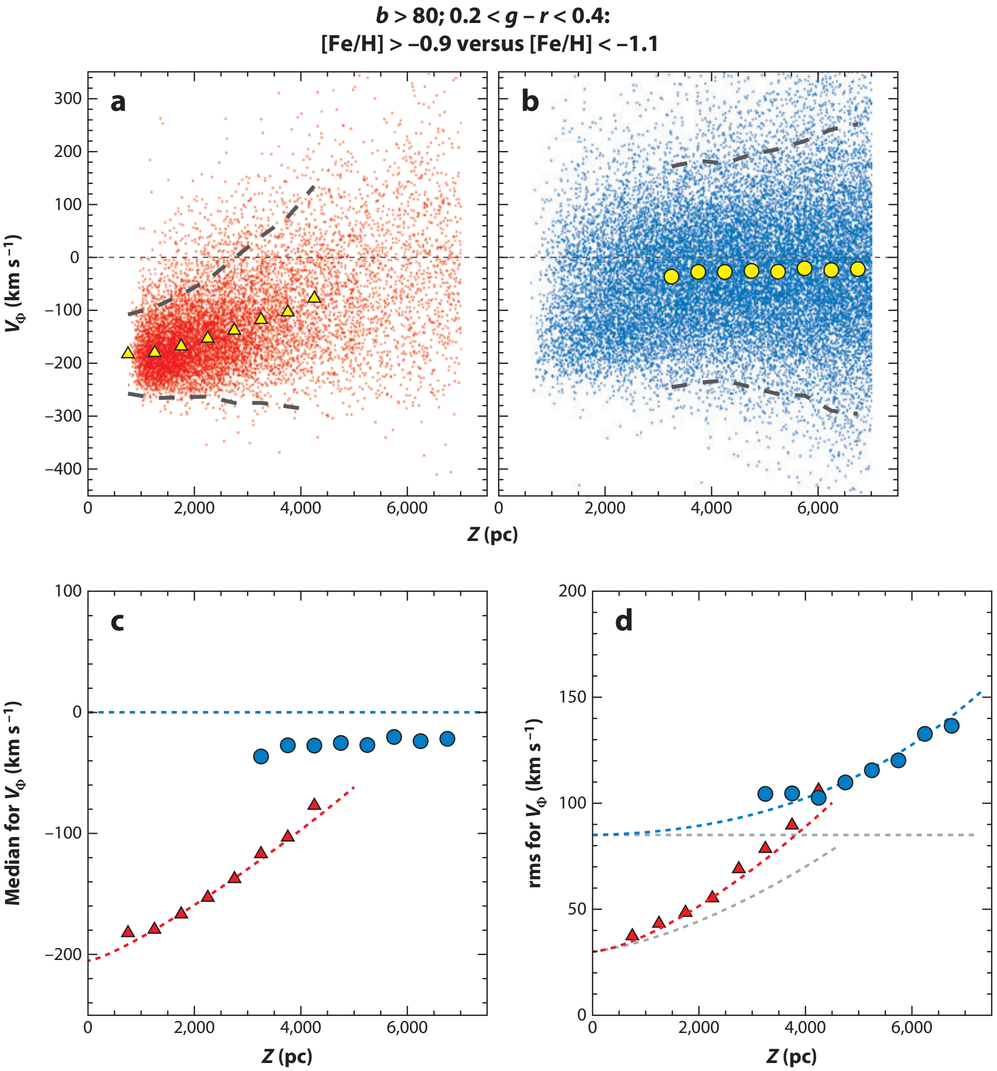

**Figure 7**

A comparison of the variation of rotational velocity (see equation 8 in Bond et al. 2010), $v_\Phi$, on distance from the Galactic plane, $|Z|$, for 14,000 high-metallicity ($[Fe/H] > -0.9$; panel *a*) and 23,000 low-metallicity ($[Fe/H] < -1.1$; panel *b*) stars with $|b| > 80°$. In panels *a* and *b*, individual stars are plotted as small dots, and the medians in bins of $|Z|$ are plotted as large symbols. The 2-$\sigma$ envelope around the medians is shown by heavy gray dashed lines. The bottom two panels compare the medians (*c*) and dispersions (*d*) for the two subsamples shown in the top panels, and the dashed lines in the bottom two panels show predictions of a kinematic model from Bond et al. (2010). The light gray dotted lines in panel *d* show model dispersions (without correction for measurement errors). Reprinted from Bond et al. (2010).

components with different formation and evolution histories, the data could be interpreted with a single, albeit complex, disk.

However, Ivezić et al. (2008a) also pointed out that stars from the Solar Neighborhood, kinematically selected as thick-disk stars, have larger $\alpha$-element abundances, at the same $[Fe/H]$, than do thin-disk stars (e.g., Bensby, Feltzing & Lundström 2004; Fuhrmann 2004; Feltzing 2006;

Reddy et al. 2006; Ramírez et al. 2007). In addition, the thick-disk stars, again selected kinematically, appear older than the thin-disk stars (e.g., Bensby, Feltzing & Lundström 2004; Fuhrmann 2004). Ivezić et al. (2008a) concluded that measurements of α-element abundances for samples of distant stars extending to several kiloparsecs from the midplane (as opposed to local samples) could resolve difficulties with traditional thin-thick disk decomposition when applied to their data. The means to obtain such a data set was recently produced by Lee et al. (2011a), who showed that the $[\alpha/Fe]$ ratio can be estimated using the comparatively low-resolution SDSS spectra—for stars with temperatures in the range of 4,500 K to 7,000 K and sufficient signal-to-noise, $[\alpha/Fe]$ estimates can be obtained with errors below 0.1 dex.

## 5.1. The Holy Grail for Thin-Thick Disk Decomposition: $[\alpha/Fe]$

Annu. Rev. Astro. Astrophys. 2012.50:251-304. Downloaded from www.annualreviews.org
by California Institute of Technology on 01/21/14. For personal use only.

Lee et al. (2011b) analyzed a sample of ∼17,000 G-type dwarfs with $[\alpha/Fe]$ measurements based on the techniques of Lee et al. (2011a). This data set is the first massive sample of stars at distances of several kiloparsecs with reasonably accurate distance estimates, measurements of all three velocity components, and measurements of both $[Fe/H]$ and $[\alpha/Fe]$, and the stars were selected using well-understood and simple color and flux selection criteria over a large area of sky. Thanks to these advantages, the Lee et al. (2011b) sample enabled a number of far-reaching observational breakthroughs:

1. The bimodal distribution of an unbiased sample of G-type dwarfs in the $[\alpha/Fe]$ versus $[Fe/H]$ diagram (see **Figure 8**) strongly motivates the separation of the sample by a simple $[\alpha/Fe]$ cut into two subsamples that closely resemble traditional thin and thick disks in their spatial distributions, $[Fe/H]$ distributions, and distributions of their rotational velocity (see figure 1 of Lee et al. 2011b).
2. The low-$[\alpha/Fe]$, thin-disk subsample has an $[Fe/H]$ distribution that does not strongly vary with position within the probed volume ($|Z| < 3$ kpc and $7 < R$ / kpc $< 10$), with a median value of $[Fe/H] \sim -0.2$. Similarly, the metallicity distribution for the high-$[\alpha/Fe]$, thick-disk subsample has a median value of $[Fe/H]$: $-0.6$ without a strong spatial variation (see figure 4 of Lee et al. 2011b).
3. The rotational velocity component, $v_\Phi$, decreases linearly with distance from the midplane, $|Z|$, with a gradient of $d|v_\Phi|/d|Z| = -10$ km s$^{-1}$ kpc$^{-1}$ for both the thin- and thick-disk subsamples (see figure 8 of Lee et al. 2011b). The difference between the mean values of $v_\Phi$ for the two subsamples of ∼30 km s$^{-1}$ (asymmetric drift) is independent of $|Z|$, and it explains the discrepancy between the $|Z|$ gradient of $-10$ km s$^{-1}$ kpc$^{-1}$ reported by Lee et al. (2011b) and gradients about 2–3 times steeper reported for the full disk by earlier studies (e.g., Ivezić et al. 2008a, Casetii-Dinescu et al. 2011): as $|Z|$ increases from the midplane to 2–3 kpc, the fraction of thick-disk stars increases from ∼10% to >90%; and the observed gradient when all stars are considered is affected by both the intrinsic gradient for each component and the velocity lag of thick-disk stars relative to thin-disk stars.
4. The rotational velocity component does not exhibit a gradient with respect to the radial coordinate, $R$, for thin-disk stars ($-0.1 \pm 0.6$ km s$^{-1}$ kpc$^{-1}$; a flat rotation curve), but only a small and marginally detected gradient for thick-disk stars ($-5.6 \pm 1.1$ km s$^{-1}$ kpc$^{-1}$).
5. The rotational velocity component and mean orbital radius are complex functions of the position in the $[\alpha/Fe]$ versus $[Fe/H]$ diagram (see **Figure 9**). The rotational velocity component shows a linear dependence on metallicity for both the thin- and thick-disk $[\alpha/Fe]$-selected subsamples (see **Figure 10**). The slopes of these $v_\Phi$ versus $[Fe/H]$ correlations have opposite signs, $d|v_\Phi|/d[Fe/H]$: $-25$ km s$^{-1}$ dex$^{-1}$ for the thin disk, and ∼45 km s$^{-1}$ dex$^{-1}$ for the thick disk, and they do not strongly vary with distance from the midplane. These

Annu. Rev. Astro. Astrophys. 2012.50:251-304. Downloaded from www.annualreviews.org
by California Institute of Technology on 01/21/14. For personal use only.

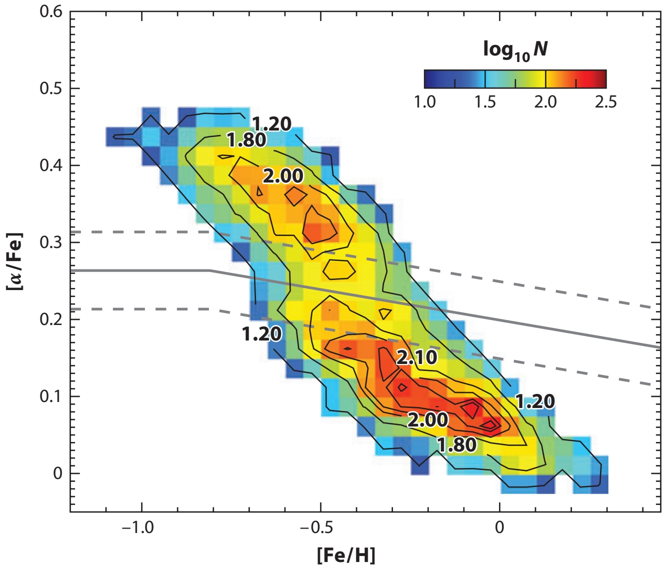

**Figure 8**

The $[\alpha/Fe]$ versus $[Fe/H]$ distribution of G-type dwarfs within a few kiloparsecs from the Sun. The number density (arbitrarily normalized) is shown on a logarithmic scale according to the legend and by isodensity contours. Each pixel (0.025 dex in the $[\alpha/Fe]$ direction and 0.05 dex in the $[Fe/H]$ direction) contains at least 20 stars (with a median occupancy of 70 stars). The distribution of disk stars in this diagram can be described by two components (thin disk and thick disk, respectively) centered on ($[Fe/H]$, $[\alpha/Fe]$) = (−0.2, +0.10) and (−0.6, +0.35). The solid gray line is the fiducial for division into likely thin- and thick-disk populations; note that a simple $[\alpha/Fe] = 0.24$ separation results in almost identical subsamples. The dashed gray lines show the selection boundaries adopted by Lee et al. (2011b), which exclude the central overlap region. Adapted from Lee et al. (2011b).

opposite gradients are partially responsible for the lack of correlation between $v_\Phi$ and $[Fe/H]$ at $|Z| \sim 1$ kpc as reported by Ivezić et al. (2008a) [for the full sample; the other reason for the lack of correlation is systematic errors in the photometric metallicity estimator (see the appendix in Lee et al. 2011b)].

6. Velocity dispersions for all three components of the local velocity ellipsoid increase with $[\alpha/Fe]$ as smooth functions and continuously across the adopted thin/thick disk boundary (see **Figure 11**). Approximate values for the velocity dispersions $\sigma_R$, $\sigma_Z$, $\sigma_\Phi$ are (40, 25, 25) km s$^{-1}$ for the thin-disk subsample and (60, 40, 40) km s$^{-1}$ for the thick-disk subsample, respectively (not corrected for bias due to measurement errors; on average, about 10–15 km s$^{-1}$ should be subtracted in quadrature).
7. Orbital eccentricity distributions (model-dependent and determined using an analytic Stäckel-type gravitational potential from Chiba & Beers 2000) are significantly different for the two $[\alpha/Fe]$-selected subsamples (see figure 10 of Lee et al. 2011b) and exhibit strong variations with position and metallicity (see figure 9 of Lee et al. 2011b). Notably, the shapes of the eccentricity distributions for the thin- and thick-disk populations are independent of distance from the plane and include only a minute fraction of stars with eccentricity above 0.6.

The behavior of the $[\alpha/Fe]$-selected subsamples of disk stars strongly argues in favor of the traditional decomposition into two (simpler) components. However, Lee et al. (2011b) did not explicitly test whether the counts of their two $[\alpha/Fe]$-selected subsamples are consistent with

Annu. Rev. Astro. Astrophys. 2012.50:251-304. Downloaded from www.annualreviews.org
by California Institute of Technology on 01/21/14. For personal use only.

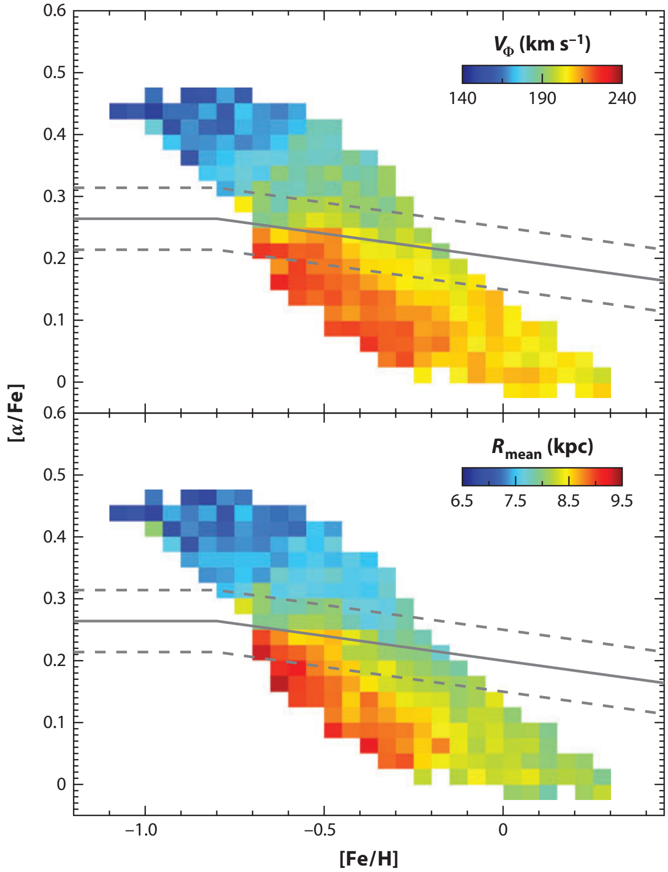

**Figure 9**

Distribution of mean rotational velocities ($v_\Phi$, panel *a*) and the orbital radii ($R_{\mathrm{mean}}$, panel *b*) for the G-dwarf sample from Lee et al. (2011b) in the [α/*Fe*] versus [*Fe/H*] diagram (3σ-clipped mean values). The orbital parameters are computed using an analytic Stäckel-type gravitational potential from Chiba & Beers (2000). The rotational velocity ($v_\Phi$) is defined in a left-handed coordinate system (the disk rotation is +220 km s$^{-1}$). Note the rich structure present in both panels. Adapted from Lee et al. (2011b).

the two best-fit additive exponential profiles obtained by Jurić et al. (2008), nor did they test in detail the hypothesis that the variation of the metallicity and rotational velocity distributions could be modeled using two simple components weighted by the counts ratio. We have used data from Lee et al. (2011b) (kindly provided by Young Sun Lee) to perform these tests here, as illustrated in **Figure 12**. We confirm that variations of the [α/*Fe*], [*Fe/H*], and rotational velocity distributions with $|Z|$ can indeed be interpreted as due to the interplay of two simple components, whose relative strength variation with $|Z|$ is consistent with the results of Jurić et al. (2008). In particular:

- The [α/*Fe*] distribution in the fiducial bin $|Z| = 400$–$600$ pc is bimodal. It can be explained as a linear combination of the slightly modified [α/*Fe*] distribution at $|Z| = 2$–$3$ kpc (non-Gaussian, and presumably dominated by the thick disk) and a Gaussian distribution with a mean of $\langle[\alpha/Fe]\rangle = +0.11$ and rms (root-mean-square) of 0.06 dex, and with weights of 0.43 and 0.57, respectively (see **Figure 12*a***). The only required modification of the

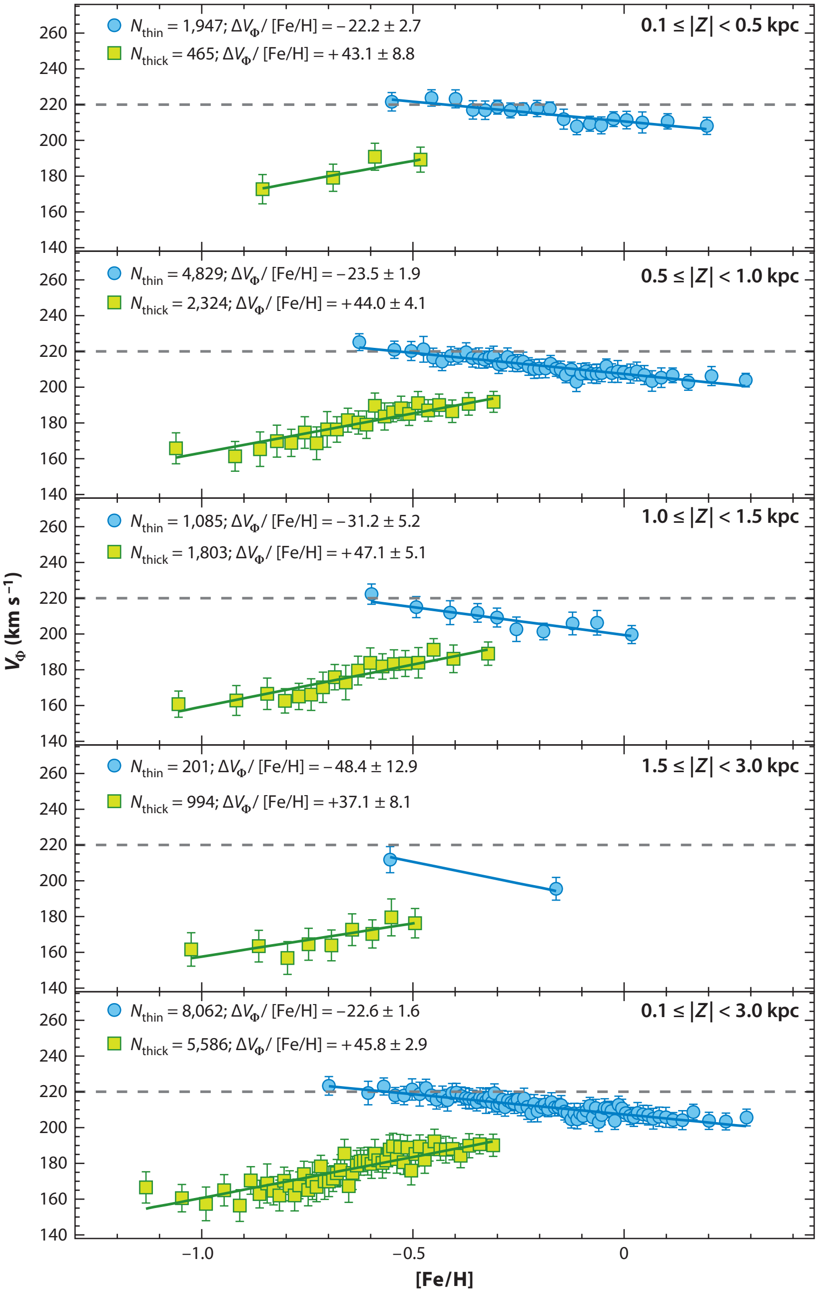

**Figure 10**

(*Top four panels*) Variation of the mean rotational velocity of G-dwarf stars with metallicity for different slices in distance from the Galactic plane, for stars separated using [$\alpha$/*Fe*]; thin-disk stars (*blue circles*) and thick-disk stars (*green squares*) are shown (adapted from Lee et al. 2011b). The rotational velocity ($v_\Phi$) is defined in a left-handed coordinate system (the disk rotation is +220 km s$^{-1}$, indicated by the gray dashed horizontal lines). Each dot represents a 3-σ-clipped average of 100 stars. (*Bottom panel*) The results for the full samples of stars considered. Estimates of the slopes and their errors listed in the panels are computed for unbinned data.

Annu. Rev. Astro. Astrophys. 2012.50:251-304. Downloaded from www.annualreviews.org
by California Institute of Technology on 01/21/14. For personal use only.

Annu. Rev. Astro. Astrophys. 2012.50:251-304. Downloaded from www.annualreviews.org
by California Institute of Technology on 01/21/14. For personal use only.

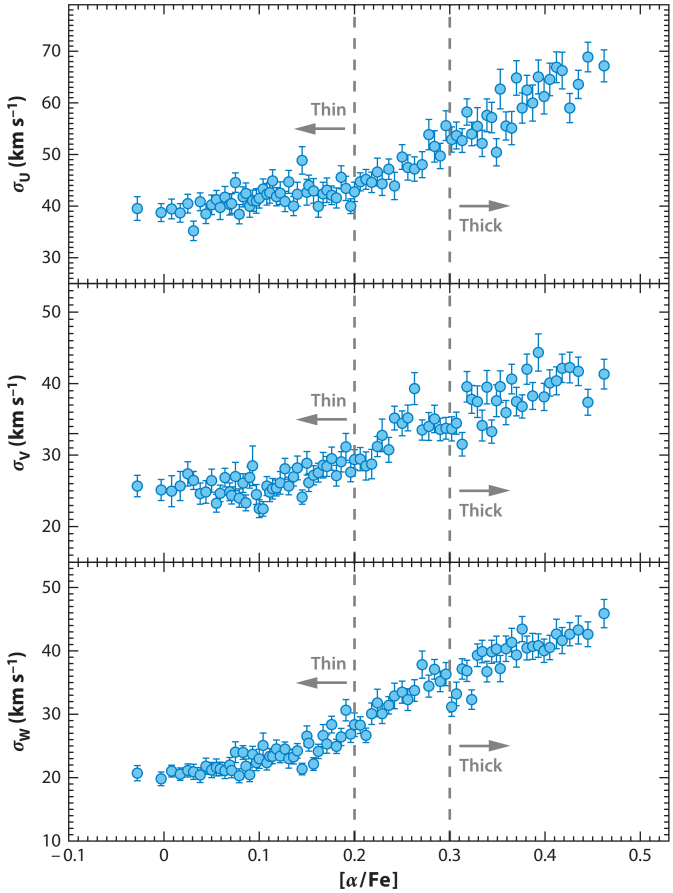

**Figure 11**

Variation of the three velocity dispersions with [α/*Fe*]. Each data point represents 200 stars, and the error bars are calculated by the bootstrap method. The gray vertical dashed lines at [α/*Fe*] = +0.2 and +0.3 are added to guide the eye and roughly correspond to thin/thick disk separation. The easily discernible increase of all three velocity dispersions with [α/*Fe*] provides kinematics-based support for the chemical [α/*Fe*]-based separation of the two dominant disk components. Reprinted from Lee et al. (2011b).

$|Z| = 2$–$3$ kpc [α/*Fe*] distribution is its shift toward lower [α/*Fe*] by 0.03 dex. The weights for the two components are consistent with a double-exponential fit to counts from Jurić et al. (2008), with the relative strength of the thick-disk component increased from Jurić et al. (2008)'s value of 0.13 to 0.16 here (a : 2σ change).

- The [*Fe*/*H*] distribution in the $|Z| = 400$–$600$ pc bin can be explained as a linear combination of the slightly modified [*Fe*/*H*] distribution at $|Z| = 2$–$3$ kpc (well described by a Gaussian) and a Gaussian distribution with a mean of $\langle [Fe/H] \rangle = -0.28$ and rms of 0.17 dex, and with the same weights as used for the [α/*Fe*] distribution (see **Figure 12*b***). The only required modification of the $|Z| = 2$–$3$ kpc [*Fe*/*H*] distribution is its shift toward higher [*Fe*/*H*] by 0.2 dex (uncertain to within 0.05–0.1 dex).
- The rotational velocity distribution in the $|Z| = 400$–$600$ pc bin can be explained as a linear combination of two Gaussian distributions (with $|v_\Phi|$ centered on 218 km s$^{-1}$ and 190 km s$^{-1}$, and with velocity dispersions of 22 km s$^{-1}$ and 40 km s$^{-1}$, respectively), again

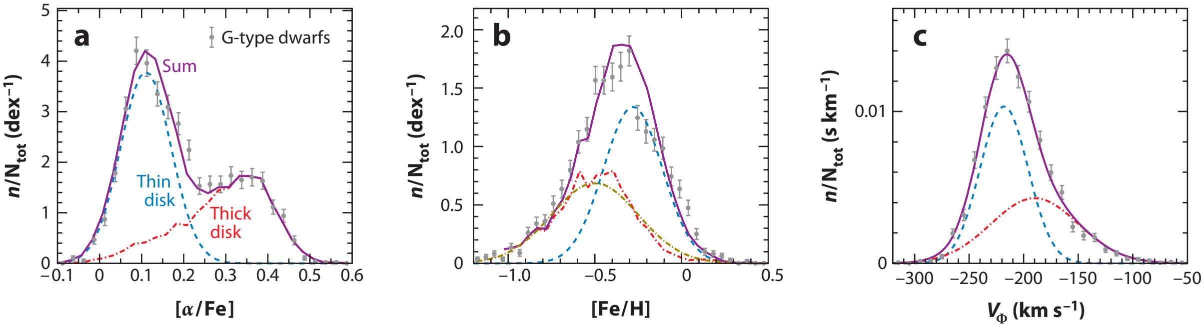

**Figure 12**

Tests of thin-/thick-disk decomposition using the sample of G-type dwarfs from Lee et al. (2011b). (*a*) The [α/*Fe*] distribution for ∼2,300 stars in the fiducial bin $|Z| = 400$–600 pc as gray circle symbols with (Poissonian) error bars. The bimodality is easily seen. The observed distribution can be modeled as the sum (shown by the *purple solid line*) of two components: the [α/*Fe*] distribution for ∼3,300 stars with $|Z| = 2$–3 kpc shifted to lower values by 0.03 dex (*red dot-dashed line*) and a Gaussian distribution, $N(0.11, 0.06)$ (*blue dashed line*). The weights for the two components (0.43 and 0.57 for the thick and thin components, respectively) are consistent with a double-exponential fit to star counts. (*b*) The [*Fe*/*H*] distribution for the same stars from the fiducial $Z = 400$–600 pc bin as symbols with error bars. Similar to the [α/*Fe*] distribution, it can be modeled as the sum (purple solid line) of two components: the [*Fe*/*H*] distribution for stars with $|Z| = 2$–3 kpc shifted to higher values by 0.2 dex (*jagged red dot-dashed line*) and $N(-0.28, 0.17)$ (*blue dashed line*). The weights for the two components (0.43 and 0.57) are the same as in panel *a*. The [*Fe*/*H*] distribution for stars with $|Z| =$ 2–3 kpc is well described by $N(-0.50, 0.25)$ (after application of a 0.2 dex offset), shown as the smooth dark yellow dot-dashed line. (*c*) The rotational velocity distribution for the same stars from the fiducial $|Z| = 400$–600 pc bin as symbols with error bars. It can be modeled as a linear combination of two Gaussian distributions, $N(-218, 22)$ and $N(-190, 40)$, again using the same relative weights (and line styles) as in panel *a*.

Annu. Rev. Astro. Astrophys. 2012.50:251-304. Downloaded from www.annualreviews.org
by California Institute of Technology on 01/21/14. For personal use only.

with the same weights as used for the [α/*Fe*] and [*Fe*/*H*] distributions (see **Figure 12*c***). When corrected for velocity measurement errors (dominated by proper-motion errors), these dispersions become 16 km s$^{-1}$ and 38 km s$^{-1}$, respectively.

The fact that all three distributions ([α/*Fe*], [*Fe*/*H*], and $v_\Phi$) in the $|Z| = 400$–600 pc bin can be described as linear combinations of the corresponding distributions in a distant bin dominated by the thick-disk component and a best-fit thin-disk Gaussian, with the same weights for all three cases that are consistent with the double-exponential fit to the star counts, strongly supports the hypothesis that the Milky Way disk comprises at least two distinct components. [Our analysis cannot exclude the possibility that the disk structure is more complex than implied by the sum of only two simple components. Indeed, **Figure 11** shows that all three velocity dispersions are smooth functions of the [α/*Fe*] ratio (and not step functions, for example). This smoothness implies that an [α/*Fe*]-based disk decomposition into only two components is at best a very good approximation, but definitely not the whole story. Most recently (after this review was submitted), Bovy, Rix & Hogg (2012) reanalyzed the same data set and concluded that evidence for the bimodal distribution of [α/*Fe*] all but disappears when selection effects are accounted for. The implication of their result is that a continuous distribution of scale heights is a more appropriate model than a simple two-component model for describing SDSS data from Lee et al. (2011b).] The required shifts of [α/*Fe*] and [*Fe*/*H*] distributions between the two *Z* bins imply vertical gradients of ∼0.015 dex kpc$^{-1}$ and ∼0.1 dex kpc$^{-1}$ for the thick-disk component (both with a relative uncertainty of about 30%). Together with the rotational velocity gradient of ∼10 km s$^{-1}$ kpc$^{-1}$ (for both the thin- and thick-disk components) from Lee et al. (2011b), these vertical gradients represent strong constraints on models for thick-disk formation.

Annu. Rev. Astro. Astrophys. 2012.50:251-304. Downloaded from www.annualreviews.org by California Institute of Technology on 01/21/14. For personal use only.

We note that, out of six distributions (three quantities for the two adopted disk components), the only strongly non-Gaussian distribution is the thick-disk [$\alpha/Fe$] distribution, that is, the [$\alpha/Fe$] distribution for stars in the $|Z| = 2$–3 kpc bin (**Figure 12*a***, *red dot-dashed line*). Its skewness is due to the presence of about 15% of the stars with [$\alpha/Fe$] $< +0.2$; their existence is puzzling. According to Lee et al. (2011b) and our own analysis of the kinematic and metallicity behavior of stars with [$\alpha/Fe$] $< +0.2$, they represent the thin-disk component. For example, in the $|Z| = 400$–600 pc bin, there are no stars with [$\alpha/Fe$] $< +0.2$ that also have [$Fe/H$] $< -0.5$ or $|v_\Phi| < 140$ km s$^{-1}$, and stars with [$Fe/H$] $< -0.5$ and $|v_\Phi| < 140$ km s$^{-1}$ have a median [$\alpha/Fe$] of $+0.40$, with an rms of only 0.05 dex. However, the puzzle is that, according to the double-exponential fit to star counts, the $|Z| = 2$–3 kpc bin should contain only ~1% of thin-disk stars, not 15%. In addition, for stars with $|Z| = 2$–3 kpc, the subsample with [$\alpha/Fe$] $< +0.2$ has the same [$Fe/H$] and $v_\Phi$ distributions as the subsample with [$\alpha/Fe$] $> +0.2$. Hence, it may be that the skewed [$\alpha/Fe$] distribution for stars in the $|Z| = 2$–3 kpc bin simply reflects a non-Gaussian measurement error distribution for the method described in Lee et al. (2011a). It is noteworthy that stars from the $|Z| = 2$–3 kpc bin are on average about 3 mag fainter than stars from the $|Z| = 400$–600 pc bin ($r \sim 18$ versus $r \sim 15$). Needless to say, independent measurements of [$\alpha/Fe$] for stars with $Z = 2$–3 kpc would provide valuable clues as to the proper interpretation.

In summary, when disk stars are separated by a simple, well-motivated [$\alpha/Fe$] cut, the resulting subsamples display remarkably simple spatial, kinematic, and metallicity distributions, which is consistent with the traditional decomposition into thin- and thick-disk components. It is likely that the differences in [$\alpha/Fe$] reflect different star-formation timescales [enrichment by Type Ia versus Type II supernovae for low and high [$\alpha/Fe$] values over long and short timescales, respectively; see Bensby, Feltzing & Lundström (2004), Johnston et al. (2008)]. Therefore, after detailed analysis of the full 7D phase space, SDSS data finally confirm that [$\alpha/Fe$] measurements provide the most robust decomposition of disk stars into thin-disk and thick-disk components.

However, a few words of caution are due here. The main results from Lee et al. (2011b) still need to be confirmed by independent data sets. It is somewhat worrisome that the RAVE-based results from Burnett et al. (2011) for the disk [$Fe/H$] distribution differ from the Lee et al. (2011b) results. At $|Z| \sim 0$, the RAVE results are about 0.2 dex more metal rich [although we note that the SDSS result for the median [$Fe/H$] $= -0.2$ at $|Z| = 0$ is consistent with the results from Nordström et al. (2004)], and the discrepancy increases to ~0.3 dex at $|Z| \sim 2.5$ kpc. It is not clear yet whether the discrepant results reported by the RAVE and SDSS surveys arise from differences in their adopted metallicity scales or are due to unaccounted for selection effects in the RAVE analysis (see section 6 of Burnett et al. 2011). Encouragingly, the spatial metallicity gradients at $|Z| \sim 1$ kpc, where thick-disk stars become more numerous than thin-disk stars, are robustly detected and similar in both studies, $d[Fe/H]/d|Z| : -0.2$ dex kpc$^{-1}$ (for stars from both components considered together). The median [$Fe/H$] at $|Z| \sim 1$ kpc reported by Lee et al. (2011b) is $-0.5$ dex, about 0.2 dex lower than reported by Burnett et al. (2011) using the RAVE data set, and about 0.2 dex higher than reported by Ivezić et al. (2008a) using photometric metallicities from the SDSS imaging survey. It remains to be seen how the [$\alpha/Fe$] measurements from the SDSS and RAVE surveys compare to each other; further study will presumably provide illumination.

The Burnett et al. (2011) study also reports age determination for RAVE stars (based on stellar models), with typical uncertainties of about a factor of two (see their figure 7). They detect a remarkable age gradient between the Galactic midplane and $|Z| \sim 2$ kpc (see figures 16 and 17 of Burnett et al. 2011), which is at least qualitatively consistent with the variation of the $g - r$ color of turnoff stars seen by the SDSS, and the velocity dispersion-age correlations for local disk stars from Nordström et al. (2004), Rocha-Pinto et al. (2004a), and West et al. (2008). They also detect a complex variation of metallicity distribution with stellar age (see figure 18 of Burnett et al. 2011).

In particular, the oldest stars (>8–9 Gyr) are predominantly low-metallicity ($[Fe/H] < -0.5$) stars. These age data represent a valuable addition to the Lee et al. (2011b) results. Nevertheless, determining age for individual stars is exceedingly difficult (Pont & Eyer 2004, Soderblom 2010), and one needs to consider all the caveats discussed by Burnett et al. at the end of their section 7. Given these difficulties, it seems best to proceed with caution. There would be clear advantage in, at the very least, obtaining age estimates for the SDSS sample (using different methodologies than used for the RAVE data) and making a more direct comparison based on this information.

Last but not least, we note that the observational material for studying the bulge of the Milky Way has also significantly improved during the past decade. Clarkson et al. (2008) used the *Hubble Space Telescope* to detect proper motions for over 15,000 bulge stars and "dissected" the kinematic properties of the bulge as a function of distance along the line of sight. A radial-velocity survey of bulge stars (BRAVA; Rich 2011) obtained data for 10,000 red giants in the Southern Galactic bulge and found clear departures from solid-body rotation that are consistent with an edge-on bar. Rangwala & Williams (2009) and Rangwala, Williams & Stanek (2009) reported radial-velocity and metallicity measurements for over 3,000 bulge stars, and now even $[\alpha/Fe]$ measurements are available for large samples of stars. For example, Gonzalez et al. (2011) determined $[\alpha/Fe]$ for 650 red-giant stars using $R \sim 22{,}000$ spectroscopy and found support for two bulge components in the observed metallicity and $[\alpha/Fe]$ distributions, which is reminiscent of the disk separation into thin- and thick-disk components. They argue that the chemical similarity of the low-metallicity bulge component and the thick disk hints for rapid, early formation for both structures. It is likely that such observational progress will lead to additional studies that simultaneously consider all of the major structural components of the Galaxy.

Annu. Rev. Astro. Astrophys. 2012.50:251-304. Downloaded from www.annualreviews.org
by California Institute of Technology on 01/21/14. For personal use only.

## 5.2. Comparisons of Observations with Disk Formation Models

Despite the past three decades of thick-disk studies, there is still no consensus on models for its formation and evolution (the thick disk is not unique to the Milky Way; for a review of thick disks in other galaxies, see van der Kruit & Freeman 2011). The proposed scenarios can be broadly divided into two groups: violent origin, such as heating of an existing thin disk due to mergers, and secular evolution, such as heating due to scattering off molecular clouds and spiral arms (see Lee et al. 2011b for a detailed discussion and references). In the first set of scenarios, the fraction of thick-disk stars accreted from merged galaxies remains an important and still unconstrained parameter, and further complexity arises from the possibility that some stars may have formed in situ, when star formation is triggered in mergers of gas-rich galaxies (Brook et al. 2007, and references therein). In the second set of scenarios, the main modeling difficulty is the lack of detailed knowledge about the relative importance of various scattering mechanisms. Over the past decade, the radial-migration mechanism (Sellwood & Binney 2002, Roškar et al. 2008b, Schönrich & Binney 2009b, Minchev & Famaey 2010) has been developed as an attractive secular scenario. Due to various computational and other difficulties, numerical models that combine the main features of the violent and secular scenarios are few.

The recent observational material contains rich information for model testing and is beginning to rule out some models. Modern data include simultaneous measurements of many observables for large numbers of stars and enable qualitatively new approaches to tests of disk-formation models. The more observables that are measured, the more powerful these tests become, because the data can be sliced along multiple axes in a variety of ways while maintaining small statistical errors due to the large sample sizes. For example, the two eccentricity distributions for $[\alpha/Fe]$-selected subsamples are much more powerful model discriminators than the eccentricity distribution for all stars lumped together. However, the complexity of such tests can be formidable—even a minimalistic selection of observables, such as coordinates $R$ and $|Z|$, chemical parameters [*Fe*/*H*] and [$\alpha$/*Fe*], and the essential kinematic parameters, rotational velocity and orbital eccentricity, span a 6D space. The basic model versus data comparisons for testing thick-disk formation and evolution scenarios include the following:

1. Comparison of the observed distribution of stars in the [$\alpha$/*Fe*] versus [*Fe*/*H*] diagram, as a function of the position in the Galaxy (e.g., can models reproduce the bimodal distribution seen in **Figure 8**? Does the fraction of the sample in the high-[$\alpha$/*Fe*] component increase with the distance from the midplane as observed?).
2. For subsamples defined using [$\alpha$/*Fe*], comparison of the shapes of their metallicity and kinematic distributions (e.g., can models reproduce the [*Fe*/*H*] distributions seen in figure 4 from Lee et al. 2011b and in **Figure 12**, or the eccentricity distributions seen in Lee et al.'s figure 10?).
3. For subsamples defined using [$\alpha$/*Fe*], comparison of the variations of their number density and low-order statistics for metallicity and kinematic distributions (e.g., $\langle v_\Phi \rangle$, velocity dispersions, mean/mode/median eccentricity) with position in the Galaxy (e.g., can models reproduce the spatial gradients of the $\langle v_\Phi \rangle$ seen in figure 8 from Lee et al. 2011b or the spatial gradients of the mean eccentricity from their figure 9?).
4. Comparison of high-order correlations between the observables, such as the complex variation of the mean rotational velocity with position in the [$\alpha$/*Fe*] versus [*Fe*/*H*] diagram (see **Figures 9** and **11**) or the variation of the orbital eccentricity with metallicity (see figure 9 in Lee et al. 2011b).

A few of the above tests have already been performed. In a strict statistical sense, all the proposed models can be outright rejected because the observed distributions of various parameters have very low statistical noise, and the models are not sufficiently fine-tuned (yet) to reproduce them (e.g., none of the model eccentricity distributions comes even close to passing the Kolmogorov-Smirnov test). For this reason, most of the model versus data comparisons are still qualitative, and only gross inconsistencies can be used to reject certain scenarios.

Beginning with Sales et al. (2009), a number of recent papers have used the shape of the derived orbital eccentricity distribution as a means to compare models to data from the SDSS and RAVE surveys (Dierickx et al. 2010, Casetti-Dinescu et al. 2011, Di Matteo et al. 2011, Lee et al. 2011b, Loebman et al. 2011, Wilson et al. 2011). We note that orbital eccentricity is derived from observations in a model-dependent way (a gravitational potential must be assumed), and different assumptions may lead to systematic differences between the observed and predicted distributions. Another detail to keep in mind is that stars with small rotational velocities are often excluded to minimize the contamination of disk samples by halo stars. However, disk stars with very high orbital eccentricity are also excluded by the same cut, and their exclusion may lead to unjustified model rejection. Although there are detailed differences in the eccentricity distributions derived from data, the mode of the distributions for stars at about 1–2 kpc from the midplane is typically in the range of 0.2–0.3, and the fraction of stars with eccentricities larger than 0.8 are below a percent or so (unfortunately, none of the recent papers listed above shows cumulative distributions, nor do they directly compare with various data-based distributions).

In most of the recent studies, four published simulations of thick disks formed by (*a*) accretion from disrupted satellites, (*b*) heating of a pre-existing thin disk by a minor merger, (*c*) radial migration, and (*d*) gas-rich mergers (see Sales et al. 2009 for references) are confronted with data. The model predictions for eccentricity distributions are nicely summarized in figure 3 from Wilson et al. (2011) and figure 17 from Casetti-Dinescu et al. (2011). Scenario *a* produces an

Annu. Rev. Astro. Astrophys. 2012.50:251-304. Downloaded from www.annualreviews.org
by California Institute of Technology on 01/21/14. For personal use only.

Annu. Rev. Astro. Astrophys. 2012.50:251-304. Downloaded from www.annualreviews.org
by California Institute of Technology on 01/21/14. For personal use only.

eccentricity distribution with a mode at ∼0.5, and scenario *b* predicts a bimodal eccentricity distribution that includes too many stars (∼10%) with eccentricities above 0.8 [see figure 3 in Sales et al. (2009) and figure 3 in Lee et al. (2011b), but note that stars with eccentricity larger than 0.8 exist in the sample from Casetti-Dinescu et al. (2011)]. In addition, scenario *b* does not exhibit the characteristic change of slope in the log(counts) versus $|Z|$ plot (see figure 1 in Sales et al. 2009). These discrepancies are the main reasons for the growing consensus that the gas-rich mergers and radial-migration scenarios are in best agreement (more precisely, least disagreement) with the present data.

Loebman et al. (2011) performed a number of the data versus model tests listed above in the limited context of the radial-migration models developed by Roškar et al. (2008a,b). They demonstrated that the overall features seen in the SDSS data, such as the gradients of metallicity and rotational velocity with distance from the midplane (see **Figure 13**), as well as the gradients of rotational velocity with metallicity (see figure 15 of Loebman et al. 2011), and the complex structure seen for the mean rotational velocity in the [α/*Fe*] versus [*Fe*/*H*] diagram (see figure 14 of Loebman et al. 2011) are qualitatively reproduced by the models (at a detailed quantitative level there is room for improvement). We note an important implication of those models—[α/*Fe*] should be an excellent proxy for age. Using a different numerical implementation of the radial-migration scenario, Schönrich and Binney (Schönrich & Binney 2009a,b; Schönrich 2011) demonstrated good agreement with the local Solar Neighborhood data from the Geneva-Copenhagen survey (Nordström et al. 2004).

These model successes hint that the thick disk may be a ubiquitous Galactic feature generated by stellar migration (though note that a similar analysis has not yet been carried out with the gas-rich merger models). However, although these models at least qualitatively reproduce much of the complex behavior seen in the data, radial migration cannot be the full story—there exist counter-rotating disks observed in some galaxies (Yoachim & Dalcanton 2008), thick disks are less prominent in high-mass galaxies (Yoachim & Dalcanton 2006), and remnants of merged galaxies are directly observed in the Milky Way (see the *right column* in **Figure 3** and the discussion in Section 6.4 below).

### 5.3. A Summary of Recent Disk Studies

To summarize, given the new SDSS and RAVE surveys, and other data, there is no doubt that the spatial and kinematic behavior of disk stars greatly varies as a function of their chemical composition, parameterized by the position in the [α/*Fe*] and [*Fe*/*H*] diagram. Whereas quantitative details still differ somewhat between different analysis methods and between the SDSS and RAVE data sets, robust conclusions are that the high-[α/*Fe*] subsample has all the characteristics traditionally assigned to the thick disk: larger scale height, lower [*Fe*/*H*], a rotational velocity lag, and larger dispersions for all three velocity components, when compared to the low-[α/*Fe*] subsample. There is mounting evidence that the ages of these stars are higher than those in the low-[α/*Fe*] subsample and similar to the age of our Galaxy, although the interpretation of age data is much more prone to systematics than chemical and kinematic data.

Despite this tremendous observational progress, there is still no consensus on theories for the origin of thick disk. The two main contenders remain gas-rich mergers and radial-migration scenarios, whereas the accretion and disk heating scenarios appear to be in conflict with the data. Nevertheless, no generic model/scenario should be fully rejected yet, because detailed comparisons with data have only begun and the input model parameter space has not been fully explored. Assuming that SDSS measurements reported by Lee et al. (2011b) survive further scrutiny (e.g., when compared to RAVE and other data sets), modelers will be kept busy for some time trying to explain the rich observational material collected over the past few years.

Annu. Rev. Astro. Astrophys. 2012.50:251-304. Downloaded from www.annualreviews.org
by California Institute of Technology on 01/21/14. For personal use only.

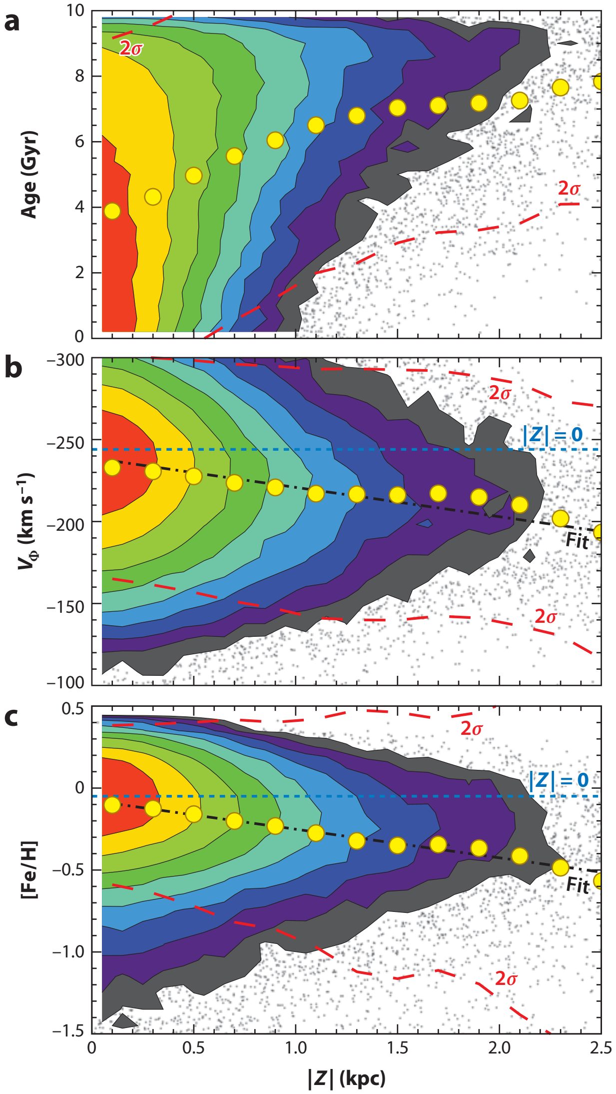

**Figure 13**

Predictions of the radial-migration model from Roškar et al. (2008b) for the variation of stellar age, rotational velocity, and metallicity with distance from the Galactic plane for stars in the solar cylinder. The simulated distributions are represented by color-coded contours (low, *dark gray*; to medium, *green*; to high, *red*) in the regions of high density, and as individual points otherwise. The large yellow symbols show the means for the $|Z|$ bins, and the red dashed lines show a 2-σ envelope. The dash-dotted lines are linear fits to the binned means, and the dashed horizontal lines show extrapolated values at $|Z| = 0$. The gradients seen in the bottom two panels are consistent with the SDSS-based results. Adapted from Loebman et al. (2011).

## 6. THE MILKY WAY HALO

Studies of the Galactic halo provide unique insights on the formation history of the Milky Way and for the galaxy formation process in general, because dynamical timescales are much longer than for disk stars and, thus, the "memory" of past events lasts longer (e.g., Johnston, Hernquist & Bolte 1996; Mayer et al. 2002). The past decade has seen tremendous progress in both observations and simulations of the Milky Way halo. For example, Wetterer & McGraw (1996) pointed out that there were only nine RR Lyrae stars discovered at Galactocentric distances larger than 30 kpc at that time. With the advent of the SDSS, 2MASS, QUEST, and other surveys, many hundreds of RR Lyrae stars (Vivas & Zinn 2006, Sesar et al. 2010a) and thousands of BHB stars (Sirko et al. 2004, Xue et al. 2008, Brown et al. 2010) have been detected all the way to ∼100 kpc. The 2MASS point source catalog has provided an all-sky view of the distribution of M giants beyond 30 kpc (Majewski et al. 2003), and a large sample of carbon-rich giants have been observed at similar distances (Ibata et al. 2001b). With SDSS data, it is now possible to study the halo within ∼10–20 kpc using tens of millions of main-sequence stars (Newberg et al. 2002, 2007; Belokurov et al. 2007b; Bell et al. 2008). Concurrently, models for the formation and evolution of stellar halos have grown increasingly more sophisticated and predictive (Ghigna et al. 2000; Bullock et al. 2001; Bullock & Johnston 2005; Law, Johnston & Majewski 2005; Helmi 2008; Johnston et al. 2008; Springel et al. 2008; Starkenburg et al. 2009; Font et al. 2011). For example, contemporary simulations of galaxy formation predict that stellar halos of Milky Way–type galaxies are assembled from inside out, with the majority of the mass (50–80%) coming from several massive ($10^8$–$10^{10}$ $M_\odot$) satellites that have merged more than 9 Gyr ago, whereas the remaining mass comes from lower mass satellites accreted in the past 5–9 Gyr (Bullock & Johnston 2005, De Lucia & Helmi 2008, Font et al. 2011).

The new data collected over the past decade led to significantly improved quantitative understanding of the spatial distribution, kinematics, and metallicity distribution of halo stars. We first review results for the relatively nearby halo within ∼20 kpc, probed in situ (hereafter, we use in situ to refer to measurements of stars located where their stellar population dominates, as opposed to extrapolated properties based on local samples) with main-sequence stars, then summarize observations out to ∼100 kpc with various other more luminous tracers, and finish with a discussion of stellar streams and other halo substructures.

Annu. Rev. Astro. Astrophys. 2012.50:251-304. Downloaded from www.annualreviews.org
by California Institute of Technology on 01/21/14. For personal use only.

## 6.1. The Smooth Halo Behavior as Probed by Main-Sequence Stars

Despite the presence of abundant halo substructure (see below), it is possible to describe the distribution of halo stars within $R \sim 20$ kpc at an impressive level of fidelity using a simple smooth, oblate, and cylindrically symmetric power-law model. The Jurić et al. (2008) study used SDSS data for ∼50 million stars, together with a photometric parallax method, to estimate their distances (see Section 1.3.1) and found that the local stellar halo can be modeled as

$$n(R, Z) = n_o f_H \left( \frac{R_e^2}{R^2 + (Z/q_H)^2} \right)^{\frac{n}{2}}, \tag{1}$$

where $n(R, Z)$ is the number of stars per unit volume (number density) as a function of the cylindrical coordinates $R$ and $Z$, $n_o$ is the local (at the solar position) number density of all stars, $f_H$ is the local fraction of halo stars, and $q_H$ parameterizes deviations from spherical symmetry ($q_H < 1$ for an oblate halo). After masking regions with obvious localized overdensities, Jurić et al. (2008) obtained the following best-fit parameters: $f_H = 0.005$, $q_H = 0.64$, and $n = 2.8$. Examples of the observed $n(R, Z)$, the best-fit model, and the fit residuals from the Jurić et al. (2008) study are shown in **Figure 3** (note that the disk component is also shown; see also the bottom panel in **Figure 4*c***). It is important to remember that the data set used by Jurić et al. (2008) does not extend beyond $R \sim 20$ kpc and $|Z| \sim 10$ kpc. Indeed, additional data suggest that the Jurić et al. (2008) single power-law halo cannot be extrapolated beyond 20 kpc (see below).

Recently, Bonaca et al. (2012) examined whether Equation 1 is an appropriate model for the distribution of main-sequence turn-off halo stars observed by Data Release 8 from the SDSS

(DR8; Aihara et al. 2011). DR8 covers almost a factor of two more area than analyzed by Jurić et al. (2008), including an order of magnitude greater coverage of the Southern Galactic hemisphere. After accounting for known overdensities and streams (Virgo, Hercules-Aquilae, Sagittarius; see Section 6.4), Bonaca et al. (2012) find no evidence for any residual triaxiality of the stellar halo. To the extent that can be probed with SDSS imaging data, the halo within 10–20 kpc from the Galactic center remains well described by an oblate ellipsoid (for a discussion of more distant parts of the halo, see Section 6.2).

Although the SDSS spectroscopic survey has provided metallicity measurements for a large number of stars, spectroscopic estimates of [*Fe/H*] are available for <1% of the stars used by Jurić et al. (2008). To provide a panoramic map of the [*Fe/H*] distribution for halo stars, Ivezić et al. (2008a) utilized a photometric metallicity method (see Section 1.3.2). Their [*Fe/H*] map, shown in **Figure 5**, demonstrates that the median metallicity of halo stars is essentially invariant within the probed volume; Ivezić et al. (2008a) determined an upper limit for its spatial gradient of 0.005 dex kpc$^{-1}$ within $|Z| < 10$ kpc. The local halo [*Fe/H*] distribution is well described by a Gaussian centered on $[Fe/H] = -1.46$, with an rms of 0.30 dex.

Annu. Rev. Astro. Astrophys. 2012.50:251-304. Downloaded from www.annualreviews.org
by California Institute of Technology on 01/21/14. For personal use only.

In the third paper of the Milky Way tomography series, Bond et al. (2010) used the large database of SDSS-POSS proper motions (see Section 2.2) and radial-velocity measurements from the SDSS spectroscopic survey (see Section 2.1) to quantify the kinematic behavior of halo stars. Similar to the behavior of counts and metallicity, Bond et al. (2010) found that halo kinematics also admit a simple model description. The very complex behavior of measured proper motions (see **Figure 14**) and radial velocities (see **Figure 15**) on the sky can be explained with a simple triaxial velocity ellipsoid that is invariant in spherical coordinates, with $\sigma_r = 141$ km s$^{-1}$, $\sigma_\Phi = 85$ km s$^{-1}$, and $\sigma_\theta = 75$ km s$^{-1}$, and their uncertainties of ~5 km s$^{-1}$. For example, the substantial variation in the dispersion of measured radial velocities across the sky seen in **Figure 15*c*** is due to the change of the orientation of velocity ellipsoid with respect to the line of sight (see **Figure 16**) rather than some localized substructure. A similar triaxial velocity ellipsoid was measured by Smith et al. (2009), using more robust proper motions based on only SDSS astrometry [as opposed to the SDSS-POSS data set used by Bond et al. (2010)], although in only a single direction on the sky. This remarkable alignment of the halo velocity ellipsoid with spherical coordinates (halo stars "know" where the Galactic center is—see **Figure 16**) is also supported by independent data from the RAVE survey (Siebert et al. 2008) and represents a strong constraint on the shape of gravitational potential—the potential must be close to spherically symmetric within ~20 kpc from the Galactic center (Smith, Wyn Evans & An 2009, and references therein). The spherical symmetry of the gravitational potential is also invoked as an explanation for the lack of precession of the orbital plane of debris of the Sgr dwarf spheroidal (see below) by Fellhauer et al. (2006), which is implied if the observed bifurcation in the distribution of debris is due to multiple (young and old) streams. However, Helmi (2004) concluded that the dark matter halo has a prolate shape, based on modeling the dynamics of the leading (old) stream.

It is noteworthy that the difference of 10 km s$^{-1}$ between $\sigma_\Phi$ and $\sigma_\theta$ measured by Bond et al. (2010) is only marginally detected [less than $2\sigma$ significance if the measurement errors are ~5 km s$^{-1}$, as claimed by Bond et al. (2010)]. An even smaller difference was measured by Smith et al. (2009) using proper motions based on only SDSS astrometry ($\sigma_\Phi = 82$ km s$^{-1}$ and $\sigma_\theta = 77$ km s$^{-1}$), with quoted errors of ~2 km s$^{-1}$ [which are likely to be underestimated because distance errors are not taken into account; both Bond et al. (2010) and Smith et al. (2009) used the photometric parallax relation from Ivezić et al. (2008a)]. The significance of the difference between $\sigma_\Phi$ and $\sigma_\theta$ is important, because if $\sigma_\Phi = \sigma_\theta$, then the halo stellar density distribution should not be oblate, as measured by Jurić et al. (2008), but spherical instead (Smith, Wyn Evans & An 2009). Indeed, using kinematic constraints based on their measurements of $\sigma_\Phi$ and $\sigma_\theta$, Smith et al. (2009)

Annu. Rev. Astro. Astrophys. 2012.50:251-304. Downloaded from www.annualreviews.org by California Institute of Technology on 01/21/14. For personal use only.

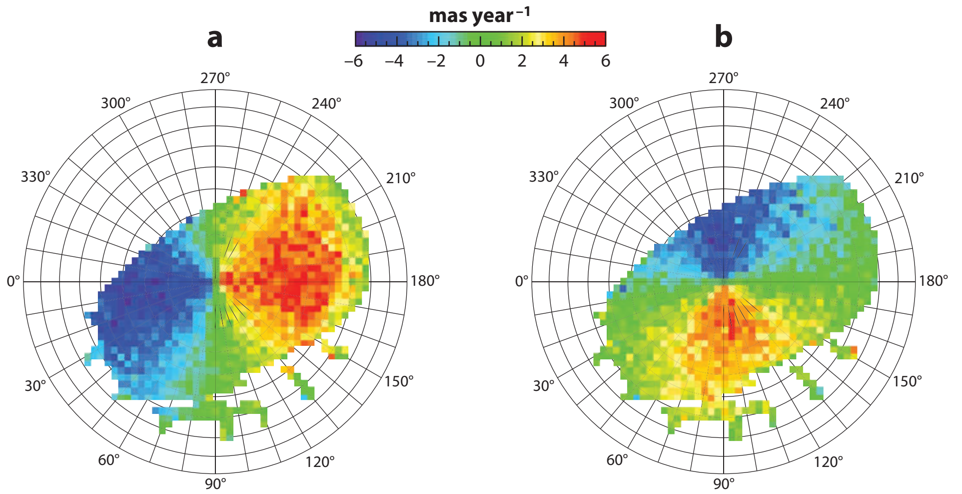

**Metal-poor, 8 < $D$/kpc < 10, <$\mu_L$>**

**Metal-poor, 8 < $D$/kpc < 10, <$\mu_B$>**

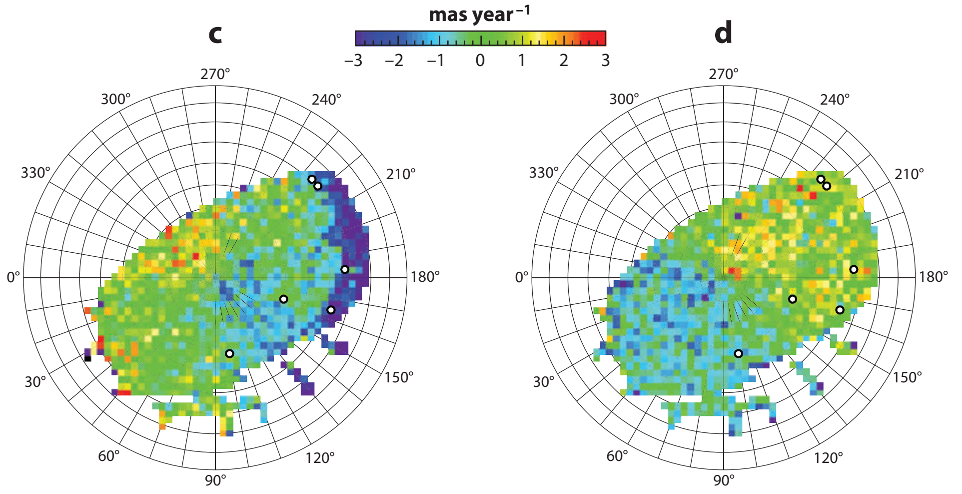

**Metal-poor, 8 < $D$/kpc < 10, $\mu_L$: <residuals>**

**Metal-poor, 8 < $D$/kpc < 10, $\mu_B$: <residuals>**

**Figure 14**

Distribution of the median longitudinal proper motion in a Lambert projection of the North Galactic cap for low-metallicity (spectroscopic $[Fe/H] < -1.1$), blue ($0.2 < g - r < 0.4$) stars with distances in the range of 8–10 kpc. The top two panels show the (*a*) median longitudinal and (*b*) latitudinal proper motions; (*c*,*d*) the median difference between the observed and model-predicted values. The maps are color-coded according to the legends in the middle (milliarcseconds per year); note that the bottom scale has a harder stretch to emphasize structure in the residual maps). In panels *c* and *d*, the white symbols show the positions of the six northern cold substructures (see Section 6.4) identified by Schlaufman et al. (2009). Adapted from Bond et al. (2010).

Annu. Rev. Astro. Astrophys. 2012.50:251-304. Downloaded from www.annualreviews.org
by California Institute of Technology on 01/21/14. For personal use only.

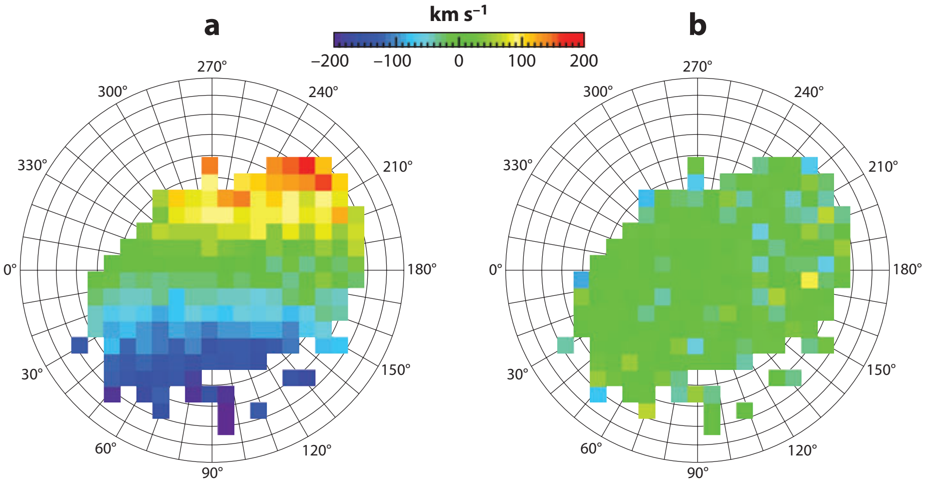

Metal-poor, 2 < $D$/kpc < 7, data < $V_{\rm rad}$ >

Metal-poor, 2 < $D$/kpc < 7, residual ($D$−$M$) for < $V_{\rm rad}$ >

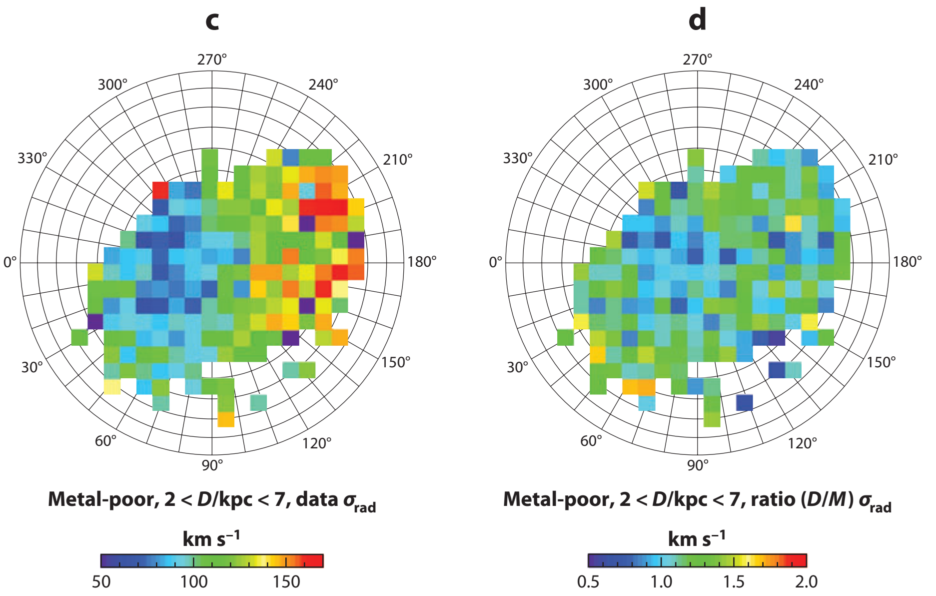

Metal-poor, 2 < $D$/kpc < 7, data $\sigma_{\rm rad}$

Metal-poor, 2 < $D$/kpc < 7, ratio ($D$/$M$) $\sigma_{\rm rad}$

**Figure 15**

Comparison of medians and dispersions for the measured and modeled radial velocities of 20,000 blue ($0.2 < g - r < 0.4$) halo stars (spectroscopic $[Fe/H] < -1.1$) at distances $D = 2$–7 kpc, and $b > 20°$. (*a*) The median measured radial velocity in each pixel, color-coded according to the legend shown at the top (units are in kilometers per second). (*b*) The difference between this map and an analogous, visually similar map based on model-generated values of radial velocity using the same scale as in panel *a*. (*c*) The dispersion of measured radial velocities, color-coded according to the legend. (*d*) The ratio of this map and an analogous, visually similar map based on model-generated values of radial velocity, color-coded according to the legend. Reprinted from Bond et al. (2010).

Annu. Rev. Astro. Astrophys. 2012.50:251-304. Downloaded from www.annualreviews.org by California Institute of Technology on 01/21/14. For personal use only.

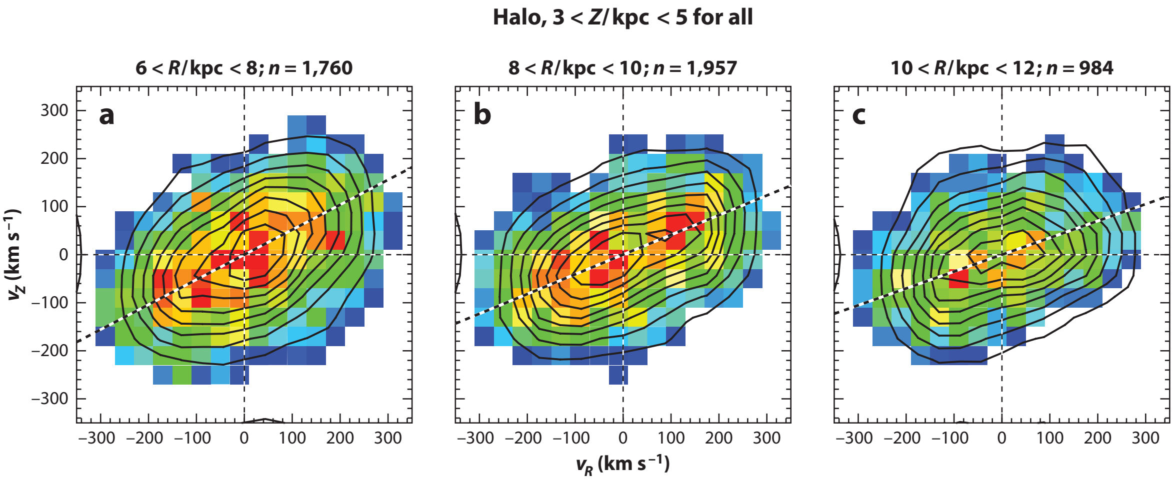

**Figure 16**

The two-dimensional $v_Z$ versus $v_R$ projections of the velocity distribution for three subsamples of candidate halo stars selected using spectroscopic metallicity ($-3 < [Fe/H] < -1.1$), with $3 < |Z|/\mathrm{kpc} < 5$, and (*a*) $6 < R/\mathrm{kpc} < 8$, (*b*) $8 < R/\mathrm{kpc} < 10$, and (*c*) $10 < R/\mathrm{kpc} < 12$. These $R - Z$ boundaries are illustrated in **Figure 5**. The distributions are shown using linearly spaced contours with a color-coded map showing smoothed counts in pixels (low, *blue*; to high, *red*). The measurement errors are typically 60 km s$^{-1}$, and the dashed black and white lines show the median direction toward the Galactic center. Note the strong evidence for a velocity-ellipsoid tilt and the variation of the tilt with $R$, so the ellipsoid always points toward the Galactic center. Reprinted from Bond et al. (2010).

obtained an implied stellar halo flattening parameter of $q_H = 0.98$, in puzzling disagreement with the value of $q_H = 0.64$ measured in situ by Jurić et al. (2008). Nevertheless, Smith et al. pointed out that their solution for the stellar halo density distribution is not unique, thus the resolution of this puzzle may be in multicomponent models, such as those discussed below.

Finally, we point out that although the model advocated by Bond et al. (2010) assumes no halo rotation, their data could not rule out net rotation at the level of up to ∼20 km s$^{-1}$. The key systematic errors limiting the precision are the distance scale errors, uncertain correction to the local standard of rest, and systematic errors in radial-velocity and proper-motion measurements [see section 5.3 of Bond et al. (2010)]. Nevertheless, Smith et al. (2009) did not detect halo rotation from their sample with more robust proper-motion measurements; similarly Allende Prieto et al. (2006) found no evidence for halo rotation using SDSS radial velocities.

## 6.2. Beyond a Simple Power Law: One Halo, Two Halos, Many Halos?

Due to the SDSS faint flux limit, the Jurić et al. (2008) results for the spatial distribution of main-sequence halo stars are limited to the volume within $R \sim 20$ kpc and $|Z| \sim 10$ kpc. Additional data suggest that the Jurić et al. (2008) single power-law halo model cannot be extrapolated beyond these limits. First, a kinematic analysis of halo stars, within the same distance limits by Carollo et al. (2007, 2010), suggests that the halo consists of two broadly overlapping structural components, an "inner halo" and an "outer halo" (see **Figure 17**). These labels are not merely descriptors for the regions studied, but rather they are labels for two individual stellar populations. These components exhibit different spatial density profiles, stellar orbits, and stellar metallicities, with the inner halo to outer halo transition occurring, according to these researchers, at Galactocentric distances of 15–20 kpc. This result follows from their kinematic analysis of SDSS calibration stars

Annu. Rev. Astro. Astrophys. 2012.50:251-304. Downloaded from www.annualreviews.org
by California Institute of Technology on 01/21/14. For personal use only.

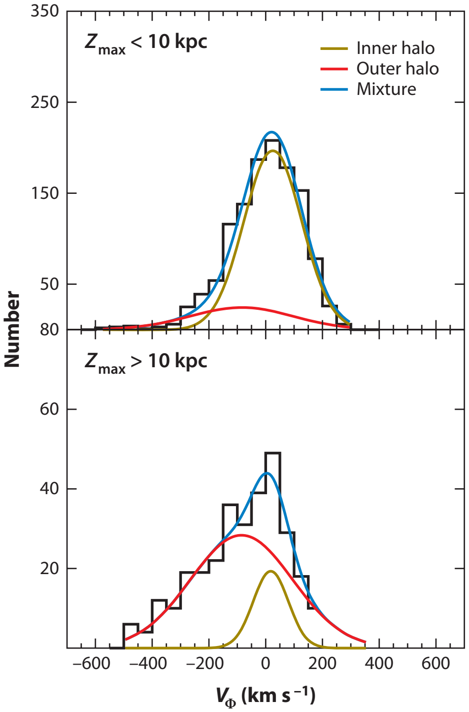

**Figure 17**

Rotational properties for the low-metallicity ($[Fe/H] < -2.0$) subsample of Sloan Digital Sky Survey calibration stars, divided into stars with maximum orbital distances from the plane ($Z_{max}$) above or below 10 kpc. The histograms show the observed distribution of rotational velocity ($v_\Phi$), and the smooth curves show models for the inner (*dark yellow*) and outer (*red*) halo components (the model sum is shown by the *blue curves*). Reprinted from Carollo et al. (2010).

within 4 kpc (including stars other than main-sequence dwarfs) and is not an in situ measurement. The inner halo was shown to comprise a population of stars exhibiting a flattened spatial density distribution, with an inferred axial ratio on the order of $q_H \sim 0.6$ and $n = 3.2 \pm 0.2$, no rotation at the level of $\sim$10 km s$^{-1}$, and a metallicity distribution peaked at $[Fe/H] \sim -1.6$. These properties of the inner halo are in very good agreement with the results of Jurić et al. (2008), Ivezić et al. (2008a), and Bond et al. (2010), based on direct mapping [as opposed to indirect inferences in the Carollo et al. (2007, 2010) analyses]. The outer halo comprises stars that exhibit a more spherical spatial density distribution, with an axial ratio $q_H \sim 0.9$ and $n = 1.8 \pm 0.3$, a clear retrograde net rotation ($\langle v_\Phi \rangle \sim -80$ km s$^{-1}$), and a metallicity distribution peaked at $[Fe/H] \sim -2.2$.

The Carollo et al. (2007, 2010) results were recently questioned by Schönrich, Asplund & Casagrande (2011), who argued that distance errors resulting from luminosity biases and/or improper accounting for measurement errors and the use of Gaussian fitting resulted in a distorted identification of the halo components. They re-evaluated the same data and failed to detect "any reliable evidence for a counter-rotating halo component" (Schönrich, Asplund & Casagrande 2011, p. 3807). In a rebuttal of these claims, Beers et al. (2012) reanalyzed their original data set (reclassifying the main-sequence turnoff stars that were the primary source of concern for Schönrich and colleagues), pointed out that Schönrich et al. had themselves adopted an incorrect main-sequence luminosity relationship from Ivezić et al. (2008a) (which significantly affected their

Annu. Rev. Astro. Astrophys. 2012.50:251-304. Downloaded from www.annualreviews.org
by California Institute of Technology on 01/21/14. For personal use only.

interpretation), and confirmed the presence of a lower metallicity counter-rotating halo (whether or not the turnoff stars in question were used in the analysis). The Beers et al. paper also provided additional evidence for the presence of an inner/outer halo dichotomy, based on other data sets and methods of analysis. They concluded that,

> Ultimately, geometric distances from Gaia for stars in the halo populations will eliminate any remaining questions concerning the impact of uncertain photometric parallaxes on these conclusions. However, our view is that presently available data already reject the single-halo interpretation beyond reasonable doubt.

Ideally, to resolve these ambiguities, the spatial distribution of halo stars and their kinematic and chemical behavior should be measured in situ using main-sequence stars. Unfortunately, even turnoff stars with $M_r = 5$ would be as faint as $r = 25$ at a distance of 100 kpc. Until the advent of the Large Synoptic Survey Telescope (LSST) and Gaia (for robust calibration of the photometric parallax relation) surveys (see Section 8), it will not be possible to perform such measurements over a large area of sky. Nevertheless, several studies over small sky areas, or using tracers more luminous (but less numerous!) than main-sequence stars, have provided further, and often intriguing, insights into the properties of the halo.

The analysis of de Jong et al. (2010), based on a color-magnitude diagram fitting approach using templates of old stellar populations with differing metallicities, produced a sparse 3D map of the stellar distribution of SDSS main-sequence turnoff stars within $r \sim 30$ kpc, derived from the ten vertical (in Galactic coordinates) photometric scans of width 2.5° obtained during the SEGUE subsurvey of SDSS-II. **Figure 6** of de Jong et al. (2010) provides clear in situ evidence for a shift in the mean metallicity of the Milky Way's stellar halo—within $r \sim 15$ kpc their derived stellar halo exhibits a mean metallicity of $\langle[Fe/H]\rangle \sim -1.6$, changing to $\langle[Fe/H]\rangle \sim -2.2$ at larger Galactocentric distances. In addition, inspection of the spatial density profiles of their template populations (figure 7 of de Jong et al. 2010) suggests rather different spatial behaviors for their "inner-halo like" template population and that of their "outer-halo like" template population. Their derived inner-halo density profile falls off rapidly with distance from the Galactic center to $r \sim 15$–20 kpc; beyond this region a substantially lower density, slowly varying, outer-halo density profile was found. Note that the de Jong et al. analysis was restricted to distances of $r < 30$ kpc. When they fit a single power-law to this entire region, they obtained an index of $n = 2.75 \pm 0.07$, in excellent agreement with the previous work of Bell et al. (2008) and Jurić et al. (2008).

Over most of the sky observed by the SDSS, the distribution of blue main-sequence stars can be mapped out to a distance limit of ∼20–30 kpc. However, in ∼300 deg$^2$ of sky from the so-called Stripe-82 area, coadded imaging based on multiple observations has a limiting magnitude about two magnitudes fainter ($r \sim 24$) than single-epoch SDSS data and can be used to map the number-density distribution of blue main-sequence stars out to ∼40 kpc. Sesar et al. (2010a) analyzed this data set and found that it agrees well with the extrapolations of the Jurić et al. (2008) model to Galactocentric distances less than ∼25 kpc. However, at larger distances the model overpredicts the observed counts by about a factor of two, strongly suggesting that the halo stellar number-density profile becomes much steeper. Although Sesar et al. could not derive precise quantitative adjustments to the Jurić et al. (2008) model parameters, they approximately estimated a change of the halo power-law index from $n \sim 3$ to about $n \sim 5$. They also detected a decrease in the median metallicity between Galactocentric radii of 10 kpc and 20 kpc of 0.02 dex kpc$^{-1}$, which is a factor of four larger than the upper limit of 0.005 dex kpc$^{-1}$ determined by Ivezić et al. (2008a) within 10 kpc. Extrapolation of this gradient to a Galactocentric radius of ∼50 kpc would result in a metallicity value similar to that determined for the outer halo by Carollo and colleagues. Note that, in the interpretation of Carollo et al. (2007, 2010), this "gradient" is actually the result of the lessening degree of importance of the inner halo, relative to the more metal-poor outer halo, as one moves outward. Once the outer-halo population dominates, there is no expected decline in metallicity.

Sesar, Jurić & Ivezić (2011) used the Canada-France-Hawaii Telescope Legacy Survey (CFHTLS) data, covering 170 deg$^2$, to study the distribution of near-turnoff main-sequence stars along four lines of sight to heliocentric distances of ∼35 kpc. They found that the halo stellar number-density profile becomes steeper at Galactocentric distances greater than ∼28 kpc, with the power-law index changing from $n = 2.62 \pm 0.04$ to $n = 3.8 \pm 0.1$. They measured the oblateness of the halo to be $q_H = 0.70 \pm 0.01$ (statistical error only), and they detected neither evidence of it changing across the range of probed distances nor any changes in the median metallicity.

Deason, Belokurov & Evans (2011) explored similar issues using a sample of ∼20,000 BHB and blue straggler stars detected by the SDSS over 14,000 deg$^2$ of sky, and they obtained almost identical results to those of Sesar, Jurić & Ivezić (2011), based on main-sequence stars. Their best fitting model has an inner power-law index of $n = 2.3$ and an outer index of $n = 4.6$, with the transition occurring at ∼27 kpc and a constant halo flattening of $q_H = 0.6$. They concluded that "the stellar halo is composed of a smooth underlying density, together with some additional substructures such as the Virgo Overdensity and the Sagittarius Stream" (Sesar, Jurić & Ivezić 2011, p. 2914). In addition, the distribution of RR Lyrae stars from the Southern Edgeworth-Kuiper Belt Object survey (Keller et al. 2008) and of RR Lyrae stars from SDSS Stripe 82 data (Watkins et al. 2009, Sesar et al. 2010a) indicates a steeper density profile beyond 30 kpc. Furthermore, using the Lowell Observatory Near-Earth Object Search sample of RR Lyrae stars, Miceli et al. (2008) argued for the presence of a dual halo in order to account for the apparently very different spatial profiles of Oosterhoff Type I and Oosterhoff Type II subsamples. Taken together, these studies provide strong in situ support for rejecting the single-halo hypothesis.

Annu. Rev. Astro. Astrophys. 2012.50:251-304. Downloaded from www.annualreviews.org
by California Institute of Technology on 01/21/14. For personal use only.

## 6.3. What Is the Nature of the Outer Halo?

Despite the growing evidence that stellar distribution in the Milky Way halo is more complex than a smooth single power law and may well comprise at least two primary stellar populations, quantitative knowledge about the most distant parts of the Milky Way is still limited. The smooth analytic descriptions of the stellar distribution discussed above begin to fail beyond 30 kpc from the Galactic center due to the presence of rich substructure, as discussed in the next section. Even when these deviations are ignored, only qualitative statements can be made about the spatial and metallicity distributions of halo stars—beyond 30 kpc, the spatial distribution is probably steeper than a $1/r^3$ power law, and the median metallicity is likely lower by 0.3–0.5 dex than the value of $[Fe/H] \sim -1.5$ representative for the inner halo (based on BHB stars; see Xue et al. 2008, Beers et al. 2012). Indirect evidence suggests that the outer halo possesses a retrograde net rotation; this result should be checked by further study.

More robust results exist for the behavior of the halo radial-velocity dispersion out to ∼100 kpc. Battaglia et al. (2005) used a heterogeneous sample of 240 objects (globular clusters, satellite galaxies, BHB stars, and red giants) and measured a decrease in radial-velocity dispersion from 120 km s$^{-1}$ at 30 kpc to about 80 km s$^{-1}$ at 100 kpc (these researchers also claim 50 km s$^{-1}$ at 120 kpc, but there are only four objects beyond 100 kpc in their sample). Using about 2,400 BHB stars detected by the SDSS out to 60 kpc, Xue et al. (2008) measured a slightly lower velocity dispersion than Battaglia et al. (e.g., ∼100 km s$^{-1}$ at 30 kpc versus 120 km s$^{-1}$) and a shallower gradient by about a factor of two (e.g., their best fit implies a drop of 18 km s$^{-1}$, or 18%, between 30 kpc and 100 kpc, compared to a drop of 40 km s$^{-1}$, or 33%, in Battaglia et al.). Brown et al. (2010)

Annu. Rev. Astro. Astrophys. 2012.50:251-304. Downloaded from www.annualreviews.org
by California Institute of Technology on 01/21/14. For personal use only.

used a mix of 910 BHB and blue straggler stars from the Hypervelocity Star survey to measure the halo radial-velocity dispersion out to 75 kpc. They obtained results in statistical agreement with Battaglia et al. (2005) and Xue et al. (2008), which they summarized as (see their **Figure 7** for a pictorial summary) "the Milky Way radial-velocity dispersion drops from $\sigma = 110$ km s$^{-1}$ at $R_{gc} = 15$ kpc to $\sigma = 85$ km s$^{-1}$ at $R_{gc} = 80$ kpc." ($R_{gc}$ is the Galactocentric radius).

In contrast, De Propris, Harrison & Mares (2010) used ~700 BHB stars from the 2Qz Redshift Survey, and found a very strong increase in the radial-velocity dispersion from 100 km s$^{-1}$ at 30 kpc to 200 km s$^{-1}$ at 80–100 kpc. Furthermore, their dispersion value of ~150 km s$^{-1}$ at 60 kpc is significantly different from the 94 km s$^{-1}$ obtained by Xue et al. (2008) using the same tracer population. The value of ~150 km s$^{-1}$ at 60 kpc seems completely ruled out by other studies (e.g., see figure 7 in Brown et al. 2010).

Currently, there are no in situ measurements of tangential velocity dispersion for stars from the outer halo. As discussed above, the difference between $\sigma_\Phi$ and $\sigma_\theta$ is an important measurement for understanding the gravitational potential and stellar distribution in the halo. It seems that such measurements will be possible for post-main-sequence stars with Gaia. For example, a star with $M_r = 1$ would have an SDSS $r$-band magnitude of 19 at a distance of 40 kpc. The expected proper-motion error from Gaia is ~0.1 mas year$^{-1}$ for such a star (see Section 8), and this corresponds to a velocity error of 20 km s$^{-1}$. Such an error is sufficiently small to enable detailed mapping of $\sigma_\Phi$ and $\sigma_\theta$, based on enormous numbers of distant BHB and red-giant stars.

The chemistry of the outer-halo population, and its differences with respect to the inner-halo population, has only begun to be explored. Present evidence indicates that the diversity of stellar abundance ratios is far greater for members of the outer halo than for the inner halo (see the introduction of Carollo et al. 2011). The most striking chemical differences between the inner- and outer-halo populations may be revealed by the recently recognized contrast in the frequency of so-called carbon-enhanced metal-poor (CEMP) stars by Carollo et al. (2011). These researchers have argued that the previously recognized increase in the frequency of CEMP stars with declining metallicity is due to the fact that the outer-halo component of the Galaxy possesses about twice the fraction of CEMP stars, relative to carbon-normal stars, at a given low metallicity, than the inner-halo component. In their view, the observed correlation is a manifestation of the lower metallicity of outer-halo stars, which begin to dominate halo samples at low abundance. This idea can also account for the observed increase in the fraction of CEMP stars, at a given metallicity, as a function of height above the Galactic plane (Frebel et al. 2006, Carollo et al. 2011), and this is a result that would be difficult to understand in the context of a single-halo population.

In summary, the outer parts of the halo, beyond ~30 kpc from the Galactic center, probably have a steeper density distribution ($n > 3$) and lower median metallicity ($[Fe/H] < -1.5$) than does the inner halo. The outer halo appears to be less "squashed" than the inner halo, likely exhibits a net retrograde rotation, and its radial-velocity dispersion probably decreases with Galactocentric distance. There appear to be clear differences in the chemistry of outer-halo stars relative to those of the inner halo. And, as discussed in the next section, both fine and coarse substructure in the outer halo appears much more prominent than in the inner halo.

### 6.4. Streams and Other Substructures

Was the Milky Way halo, or at least its outer parts, actually assembled from many merged satellite galaxies? Within the framework of hierarchical galaxy formation (Freeman & Bland-Hawthorn 2002), the spheroidal component of the luminous matter should reveal substructures, such as tidal tails and streams (Johnston, Hernquist & Bolte 1996; Helmi & White 1999; Bullock, Kravtsov

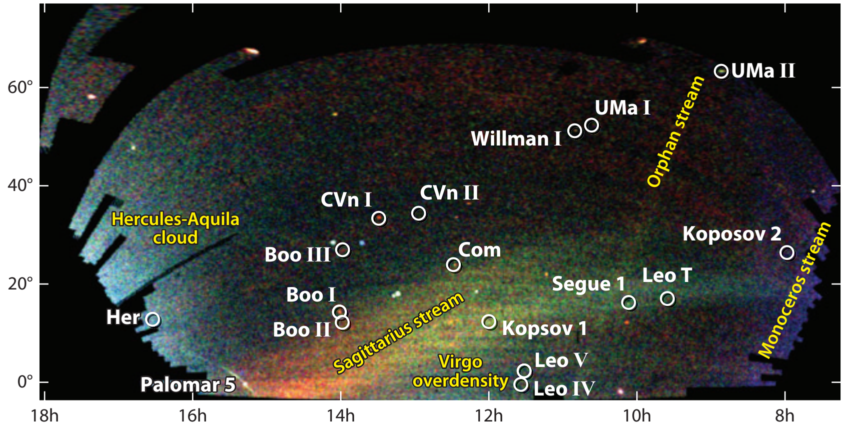

**Figure 18**

The "Field of Streams" map of blue stars in the outer regions of the Milky Way, derived from the Sloan Digital Sky Survey (SDSS) images of the northern sky, shown in a Mercator-like projection of equatorial coordinates. The color indicates the distance of the stars (of the order 10 kpc), with red being the most distant and blue being the closest, whereas the intensity indicates the density of stars on the sky. There are several structures visible in this map, as marked, that demonstrate the halo is not a smooth structure. Circles enclose new Milky Way companions discovered by the SDSS, as labeled; two of these are faint globular star clusters, whereas the others are faint dwarf galaxies. Adapted from Belokurov et al. (2006a); courtesy of V. Belokurov, Institute of Astronomy, Cambridge.

& Weinberg 2001; Harding et al. 2001). Substructures are expected to be ubiquitous in the outer halo (Galactocentric radii beyond 15–20 kpc), where the dynamical timescales are sufficiently long for them to remain spatially coherent (Johnston, Hernquist & Bolte 1996; Mayer et al. 2002), and indeed many have been discovered during the past decade; the famous "Field of Streams" (Belokurov et al. 2006a) is shown in **Figure 18**.

The tidal streams of the disrupting Sagittarius dwarf spheroidal galaxy (Ibata, Gilmore & Irwin 1994) were the first ones discovered (Ivezić et al. 2000, Yanny et al. 2000, Vivas et al. 2001, Newberg et al. 2003), and they are still the best examples of such substructures, with the streams wrapping around most of the sky (Ibata et al. 2001b, Majewski et al. 2003). [We note that no clear stellar component has been associated with the Magellanic Stream yet, despite searches for it (Westerlund 1990, Moore & Davis 1994, Saha et al. 2010, Cioni et al. 2011).] Other known substructures include the Virgo Stellar Stream (Duffau et al. 2006, Prior et al. 2009), and several other small and large structures associated with the Virgo overdensity (Newberg et al. 2007, Vivas et al. 2008), the Monoceros structure (Ibata et al. 2003, Rocha-Pinto et al. 2003, Yanny et al. 2003, Ivezić et al. 2008a), the Triangulum-Andromeda overdensity (Rocha-Pinto et al. 2004b), the Hercules-Aquila cloud (Belokurov et al. 2007a), the Pisces overdensity (Kollmeier et al. 2009; Sesar et al. 2007, 2010a,b; Watkins et al. 2009), the Orphan stream (Belokurov et al. 2007b), and other smaller overdensities (Newberg et al. 2002; Belokurov et al. 2006b,c; Clewley & Kinman 2006; Vivas & Zinn 2006; Starkenburg et al. 2009) and streams (Grillmair & Dionatos 2006, Grillmair 2009, Klement et al. 2009, Schlaufman et al. 2009, Klement 2010). Similar abundant substructure has been detected in the M31 halo (Ibata et al. 2001a, Ferguson et al. 2002). Last but not least, the SDSS imaging data have enabled a large number of new discoveries of dwarf galaxy companions to the Milky Way, with luminosities as small as $10^{-7}$ of the Milky Way luminosity (for an up-to-date review, see Willman 2010).

Annu. Rev. Astro. Astrophys. 2012.50:251-304. Downloaded from www.annualreviews.org
by California Institute of Technology on 01/21/14. For personal use only.

Annu. Rev. Astro. Astrophys. 2012.50:251-304. Downloaded from www.annualreviews.org
by California Institute of Technology on 01/21/14. For personal use only.

These substructures exhibit various degrees of contrast with respect to the background counts, metallicity, and kinematic distributions of the smooth halo. Bell et al. (2010) used a novel method for investigating differences in age and metallicity between different halo substructures: the ratios of counts of BHB stars to main-sequence turnoff stars. Using SDSS data across a quarter of the sky, they found large variations of this ratio, with some halo features almost completely devoid of BHB stars. The Monoceros stream is a good example of substructure that simultaneously deviates from the background distributions in all three observables (see **Figure 19**). Originally interpreted as a ring around the Galaxy (Ibata et al. 2003, Yanny et al. 2003), it was later revealed as an inclined stream that rotates faster than the surrounding stars and has a metallicity distribution between those of disk and halo stars (Rocha-Pinto et al. 2003, Jurić et al. 2008, Ivezić et al. 2008a).

The discoveries of abundant substructure represent ample evidence that the Milky Way halo is a very complex structure that holds important clues for deciphering the processes that governed its formation and evolution. Yet, despite this menagerie of substructure, we still do not have a consensus answer for as simple a question as, “What fraction of halo stars was accreted from merged galaxies?” Of course, questions about the luminosity and metallicity distributions of the merged galaxies are even more open. A part of the problem is that, within the neighborhood of strong individual substructures, such as those listed above, it is hard to define the smooth background, and when strong substructure is absent, it is hard to find weaker features. Several approaches to quantifying the amount of halo substructure have been taken in recent years.

Three studies compared the spatial distribution of SDSS stars, with distances based on photometric parallax methods, to estimates of the smooth background, and they used variations (the root-mean-square deviation, rms scatter) of the measured density around that background as a quantitative measure of substructure. The Jurić et al. (2008) approach used their best-fit smooth models for the background estimate and ruled out significant “clumpiness” on spatial scales comparable to the pixel size of their maps (ranging from 25 pc to 500 pc). However, Bell et al. (2008) compared the spatial distribution of SDSS stars to that from simulations where the halo is composed entirely of disrupted satellites and found them to be similar for Galactocentric radii less than 40 kpc. They argued that no smooth model can describe the data and concluded that the stellar halo is dominated by substructure, with the rms scatter, relative to smooth models on spatial scales above 100 pc, of at least 40%. The Bell et al. study relied on SDSS observations of main-sequence stars and pushed the data all the way to its faint limit ($r$ : 22.5). Deason, Belokurov & Evans (2011) instead used BHB and blue-straggler stars from SDSS DR8 to study their distribution to a similar distance limit of 40 kpc but with much brighter stars. They reported for their smooth models that the rms scatter of the data around the maximum likelihood model typically ranges between 5% and 20%. They concluded that, “This indicates that the Milky Way stellar halo, or at least the component traced by the A-type stars in the SDSS DR8, is smooth and not dominated by unrelaxed substructure.” It should be kept in mind that this inference reflects the present situation, and may not apply to the situation at earlier times. Using RR Lyrae stars from SDSS Stripe 82, Sesar et al. (2010a) found that “At least 20% of halo stars within 30 kpc from the Galactic center can be statistically associated with substructure.” And further, that “. . .beyond a Galactocentric distance of ∼30 kpc, a larger fraction of the stars are associated with substructure” (see **Figure 20**).

The addition of kinematic data increases the contrast ratio relative to the smooth background when searching for substructure. Using data from the SEGUE spectroscopic survey, Schlaufman et al. (2009) have shown that metal-poor main-sequence turnoff stars within ∼20 kpc from the Sun exhibit clear evidence for radial-velocity clustering on very small spatial scales (dubbed “ECHOS” for Elements of Cold HalO Substructure; see **Figure 14*c,d***). They estimated that about 10% of the inner-halo turnoff stars belong to ECHOS, and inferred the existence of about 1,000 ECHOS

Annu. Rev. Astro. Astrophys. 2012.50:251-304. Downloaded from www.annualreviews.org
by California Institute of Technology on 01/21/14. For personal use only.

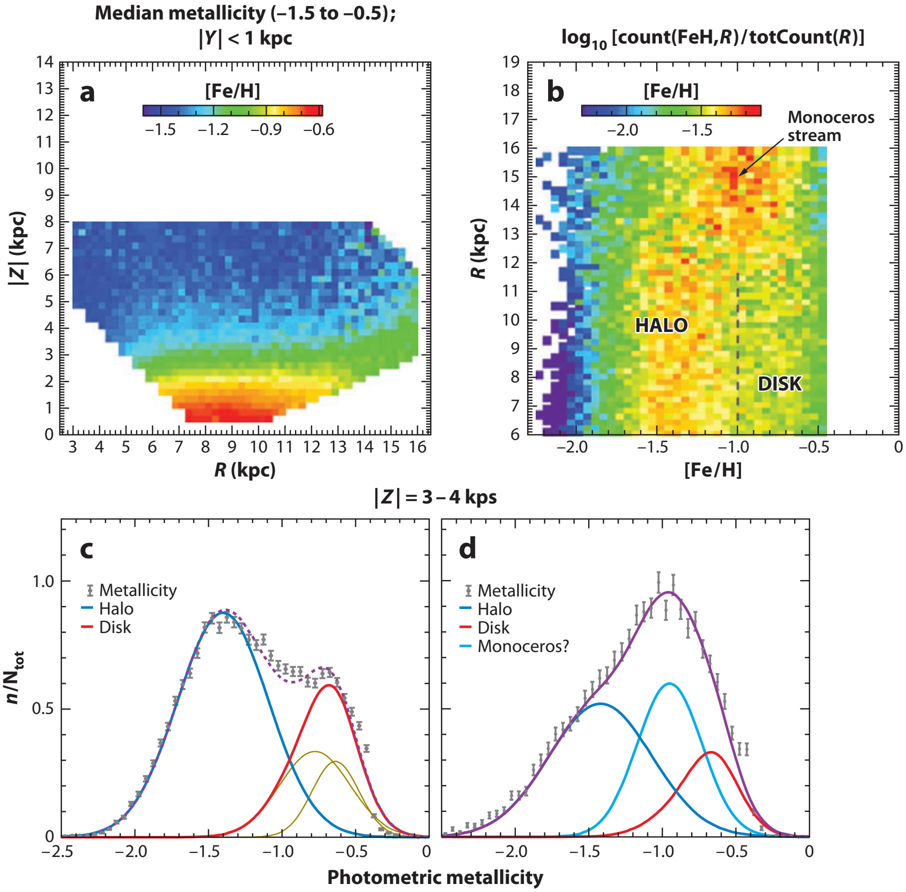

**Figure 19**

(*a*) Dependence of the median photometric metallicity for one million stars with $14.5 < r < 20$, $0.2 < g - r < 0.4$, and $|Y| < 1$ kpc in cylindrical Galactic coordinates $R$ and $|Z|$. This $Y$ range is selected to include the Monoceros stream, which represents an overdensity by a factor of ∼1.5 in a region around $R \sim 15$ kpc and $|Z| \sim 3$–4 kpc. As discernible from the map, this region has a larger median metallicity than expected for this $|Z|$ range based on extrapolation from smaller $R$. (*b*) Conditional metallicity probability distribution for a subsample of ∼111,000 stars with $3 < |Z|/\mathrm{kpc} < 4$. The strong overdensity at $R > 12$ kpc is the Monoceros stream. The bottom panels show the metallicity distribution (*gray symbols with error bars*) for (*c*) a subsample of ∼40,000 stars with $6 < R/\mathrm{kpc} < 9$ and (*d*) for ∼12,000 stars with $13 < R/\mathrm{kpc} < 16$. The lines represent empirical fits based on Gaussian decomposition from Ivezić et al. (2008a) (*blue lines* for halo component, and *red lines* for disk component; the latter is modeled as a sum of two Gaussians shown by the dark yellow lines). The light blue line in panel *d* is a 0.22-dex wide Gaussian centered on $[Fe/H] = -0.95$. It accounts for 33% of stars in the sample that presumably belong to the Monoceros stream. Reprinted from Ivezić et al. (2008a).

in the entire inner halo. Their "result suggests that the level of merger activity has been roughly constant over the past few gigayears and that there has been no accretion of single stellar systems more massive than a few percent of a Milky Way mass in that interval." Schlaufman et al. (2011) argue that the most likely progenitors of ECHOS are dwarf spheroidal galaxies. Typical values of metallicity ($[Fe/H] \sim -1$) and radial-velocity dispersion (∼20 km s$^{-1}$) for ECHOS imply a dwarf galaxy mass of about $10^9\ M_\odot$. Theoretical predictions that prominent halo substructures are likely

Annu. Rev. Astro. Astrophys. 2012.50:251-304. Downloaded from www.annualreviews.org
by California Institute of Technology on 01/21/14. For personal use only.

**Figure 20**

The distribution of RR Lyrae stars from the Sloan Digital Sky Survey Stripe 82 contrasted with an artist's concept of the disk plane. The color scheme displays the RR Lyrae number density multiplied by the cube of the Galactocentric radius (logarithmic scale, from *light blue* to *red*). Note the rich structure present. The white dots, outlined by white dashed lines, show the Sagittarius dwarf spheroidal ("Sgr dwarf") and its tidal streams, as modeled by the Law, Johnston & Majewski (2005) "spherical" model (the model stream overlaps with one of the detected clumps, Sgr; for discussion, see Sesar et al. 2010a). Adapted from Sesar et al. 2010a. An animated version is available from the *Annual Review of Astronomy and Astrophysics* Web site (**http://www.annualreviews.org;** courtesy of A. Mejia and B. Sesar).

to be metal-rich (Bullock & Johnston 2005, Font et al. 2008) are consistent with the typical ECHOS metallicity, as well as with the measurements reported for the Monoceros stream ($[Fe/H] = -1.0$, Ivezić et al. 2008a) and the trailing part of the Sagittarius tidal stream ($[Fe/H] = -1.2$, Sesar et al. 2010a).

Smith et al. (2009) used the full phase-space coordinates for a sample of some 1,700 SDSS subdwarfs and found evidence for four discrete overdensities localized in angular momentum space, which they dubbed Sloan Kinematic Overdensities (SKOs). One of them was identified earlier in the pioneering work by Helmi et al. (1999), and two new substructures contain stars that are localized in both kinematics and metallicity. One of them has metallicity lower than that of halo background by ~0.5 dex and appears to be related with an association of four globular clusters (NGC5466, NGC6934, NGC7089/M2, and NGC6205/M13), suggesting that they may have been part of the same accretion event. If so, then this implies that the progenitor must have been a large satellite, similar in size to Fornax.

Xue et al. (2011) analyzed kinematic data for a sample of over 4,000 BHB stars detected by the SDSS at distances of 5–40 kpc. Using a method developed for the analysis of data from the

Annu. Rev. Astro. Astrophys. 2012.50:251-304. Downloaded from www.annualreviews.org
by California Institute of Technology on 01/21/14. For personal use only.

Spaghetti project (Starkenburg et al. 2009), they found an excess of stars that are both close neighbors and have similar radial velocities, compared to a distribution expected for a random sample. Notably, the excess is larger for a subsample of stars at distances beyond 20 kpc than for the closer subsample. Analogous analysis of mock catalogs from simulations in which the stellar halo is composed entirely of disrupted satellite debris exhibits a similar, though somewhat less prominent, level of structure. In a separate study, also based on SDSS observations of BHB stars and using a similar analysis method, Cooper et al. (2011) analyzed a large number of state-of-the-art models for the stellar halo. They also found that, for the inner halo, the models predict stronger clustering than observed, suggesting the existence of a smooth component not currently included in their simulations.

In summary, these new studies consistently reveal that the inner region of the Milky Way's stellar halo, within 30 kpc or so, definitely exhibits substructure. Estimates of the fraction of stars that belong to substructures cluster around a few tens of percent. Observations of several luminous tracers of the outer region of the halo, such as RR Lyrae and BHB stars, suggest that the substructure becomes more prominent with increasing distance from the Galactic center, and that the fraction of stars belonging to substructures is higher than for the inner halo. The available data (still) cannot reliably exclude the possibility that practically all stars in the outer halo belong to substructures.

## 7. UNANSWERED QUESTIONS

It is not difficult to appreciate the progress that has been made when considering the state of the field and the open questions of only a decade ago. The metallicity distribution of the halo was found to possess a very low-metallicity tail, one that is correlated with kinematics and points to an existence of a separate outer-halo component. The density profile of the halo was shown to be more complex than originally thought, becoming steeper beyond ∼25 kpc and exhibiting significant substructure. Tens of dwarf galaxies and a number of new streams, some with clear dwarf galaxy progenitors, have been found, proving that the Sgr stream, though still remaining the largest, was in no way a qualitatively unique event. Finally, it has become clear that the thin and thick disks of the Milky Way are demonstrably distinct physical components, separable by their kinematics and $[\alpha/Fe]$ ratios, and mapped and measured in exquisite detail. Thus, we argue that the past decade of large surveys has successfully retired issues #1 through #4, as well as issue #6, mentioned in Section 3.

However, as usually happens, these breakthroughs have left us with new puzzles and questions to ponder over the decade to come. Here, we call attention to only a few.

1. What is the nature, and the formation mechanism, of the two chemically and kinematically separate disk populations? On the most basic level, is the thick disk a result of one or more merger events or is it a natural consequence of secular evolution and radial migration? If it is the latter, what explains the counter-rotating disks seen in some external galaxies?
2. If the thick disk was formed by mergers, how massive and numerous were they? What fraction of the thick disk material (if any) has been accreted, and what fraction came from heating of the material already settled into the thin disk (both gas and stars)? Is there even a single thick disk to speak of or are there multiple intertwined populations tracing their origin to individual merger events? Could this be the explanation of the metal-weak thick disk and the non-Gaussianity of $[Fe/H]$ and $[\alpha/Fe]$ distributions?
3. How do the properties of the bulge compare to those of the disk and the halo?
4. Will the inner/outer halo dichotomy be confirmed by in situ measurements? Currently, our inferences about the outer-halo population are largely drawn from local kinematically

selected samples. In situ measurements of the properties of halo stars at $r > 25$ kpc, using large and representative samples, may settle these controversies.

5. Assuming the outer halo is distinct from the inner halo, what are their origins and mechanisms of formation? What (if any) fraction of the outer halo has formed stars in situ, as opposed to having accreted them? What fraction of the inner halo traces its origin to merger events? What does this tell us about the merger history of the Galaxy?
6. Finally, what is the gravitational potential of the Milky Way's dark matter halo? Multiple lines of evidence currently point to its near sphericity, a result at odds with expectations for a typical dark matter halo (either prolate or oblate, with $q \sim 0.6$) from N-body simulations.

Annu. Rev. Astro. Astrophys. 2012.50:251-304. Downloaded from www.annualreviews.org
by California Institute of Technology on 01/21/14. For personal use only.

## 8. THE ROAD AHEAD

The past decade has seen fascinating observational progress in Milky Way studies. Nevertheless, the results discussed here will be greatly extended by several upcoming large-scale, ground-based projects, including the APOGEE, the Large Area Multi-Object Fibre Spectroscopic Telescope (LAMOST), SkyMapper, the Dark Energy Survey (DES), the Panoramic Survey Telescope & Rapid Response System (Pan-STARRS), and ultimately the LSST. These new surveys will extend the faint limit of the current surveys, such as the SDSS, by up to 5 mag. (Regretfully, due to space constraints we do not address IR surveys, such as WISE (Wright et al. 2010), GLIMPSE (Churchwell et al. 2009), VISTA (McPherson et al. 2006), and UKIDSS (Lawrence et al. 2007). These surveys will have a major impact on studies of the Galactic bulge and the dust-obscured regions of the Galactic plane.) In addition, the upcoming Gaia space mission will provide superb astrometric and photometric measurement accuracy for sources with $r < 20$ and will enable unprecedented science programs. We briefly describe these new surveys and some of the impact they are expected to have on Milky Way studies.

### 8.1. The Sloan Digital Sky Survey Apache Point Observatory Galaxy Evolution Experiment Survey

The SDSS-III APOGEE project will soon yield unprecedented insight into the chemical and kinematic properties of the main Galactic components, with a unique data set for studying the bulge (Allende Prieto et al. 2008, Rockosi et al. 2009, Schiavon & Majewski 2010, Eisenstein et al. 2011). The APOGEE project is a three-year high-resolution near-IR spectroscopic survey that targets over 200 field centers covering about 1,200 deg$^2$ of sky. The project utilizes a new 300-fiber-fed $H$-band (1.51- to 1.68-μm) spectrograph with a resolution of $R \sim 20{,}000$ and an expected signal-to-noise ratio of 100 per resolution element for stars with $H \sim 12$ (with the Astrophysical Research Consortium 2.5-m telescope used by the SDSS). The goal of the survey is to derive precision radial velocities ($\sigma < 1$ km s$^{-1}$) and abundances ($\sigma < 0.1$ dex) for about 100,000 stars that will be targeted using the 2MASS imaging survey (red giants will be observable all the way to the Galactic center). Abundances of 15 different elements, including Fe, C, N, O, $\alpha$-elements, odd-$Z$ elements, and iron-peak elements will be measured.

The APOGEE project is to be the first spectroscopic survey to pierce through the dust obscuration in the Galactic plane (extinction in the near-IR $H$ band is about six times smaller than in the optical $V$ band) and provide a large, uniform database of chemical abundances and radial velocities for stars across all of the known Galactic components. These data will provide a robust set of constraints against which chemodynamical models for the formation and evolution of the Galaxy can be tested. In particular, the APOGEE data set will provide powerful new constraints on the nature and influence of the Galactic bar and spiral arms, and it will conduct a legacy survey of Galactic open clusters to constrain the history of star formation and chemical enrichment of the Galactic disk (Frinchaboy et al. 2010).

### 8.2. The Large Area Multi-Object Fibre Spectroscopic Telescope Galactic Surveys

LAMOST is a 4-m class telescope with 4,000 optical fibers in the focal plane situated at the Xinglong Observatory in northeast China. This telescope, built by the National Astronomical Observatory of China, will carry out a spectroscopic survey of millions of Galactic stars over a five- or six-year period that is expected to start in 2012. The magnitude limit, wavelength range, and spectral resolution of the LAMOST Galactic structure surveys will be similar to that achieved by the SEGUE/SDSS.

The stellar science goals, grouped under the LAMOST Experiment for Galactic Understanding and Exploration (LEGUE) effort, are divided into three major parts: (*a*) the spheroid survey, (*b*) the Galactic anticenter survey, and (*c*) the Galactic disk and open clusters survey. The stellar surveys will receive about half of the available time, resulting in a sample of about 6 million bright disk stars, and at least 2 million fainter halo stars. These surveys will result in the largest homogeneous spectroscopic data sets for stars in the Milky Way, with several times more spectra than obtained by the SDSS and RAVE surveys combined.

Annu. Rev. Astro. Astrophys. 2012.50:251-304. Downloaded from www.annualreviews.org
by California Institute of Technology on 01/21/14. For personal use only.

### 8.3. SkyMapper, Pan-STARRS, and the Dark Energy Survey

There are three imminent optical surveys that will cover large swaths of the optical sky to faint limits and are destined to yield many significant discoveries. They are, in many ways, similar to the SDSS imaging survey (including the photometric systems), but they will extend it significantly in sky coverage, imaging depth, and temporal coverage.

**8.3.1. SkyMapper.** SkyMapper (Murphy et al. 2009) is a 1.35-m telescope with a 5.7-deg$^2$ field of view and a 0.27-Gigapixel camera. Its primary goal is to undertake the Southern Sky Survey: a six band, six-epoch (in each band) digital record of the entire southern sky. The survey aims to provide astrometry and photometry for objects with $8 < r < 23$. Each of the six epochs will use 110-s exposures that will be about 1 mag shallower than SDSS data; but when coadded, the data will reach the SDSS depth. The four red bandpasses (*griz*) are designed to be similar to the SDSS bandpasses. SkyMapper has two additional, distinctive UV filters: a Strömgren system-like *u*-band filter and a unique narrow *v*-band filter near 4,000 Å. These two filters bracket the Balmer jump in stellar spectra and are designed to efficiently identify metal-poor stars (Bessell et al. 2011). The advertised performance requirements include a photometric precision of 0.03 mag globally and astrometric precision (better than 50 mas) that will enable the measurement of proper motions accurate to about 4 mas yr$^{-1}$ over the five-year baseline of the survey.

The SkyMapper's Southern Sky Survey will extend many of the results based on the SDSS imaging survey to the Southern hemisphere, which is over 20,000 deg$^2$ of sky (Keller et al. 2007). The photometric parallax methods developed for SDSS data should be directly applicable to SkyMapper's data, and photometric metallicity methods should perform even better, thanks to the optimized UV bandpasses. The expected proper-motion accuracy is essentially the same as delivered by the SDSS-POSS proper-motion catalog, and thus it will be possible to extend many of the SDSS-based studies described here to essentially the entire sky.

Annu. Rev. Astro. Astrophys. 2012.50:251-304. Downloaded from www.annualreviews.org
by California Institute of Technology on 01/21/14. For personal use only.

**8.3.2. The panoramic survey telescope and rapid response system.** The Pan-STARRS project (Kaiser et al. 2010) is a wide-field, multifilter, multiepoch astronomical survey program. The program is currently based on a 1.8-m telescope with a 7-deg$^2$ field of view and a 1.4-Gigapixel camera (PS1), which began full science operations in 2010. The largest of the PS1 surveys is the $3\pi$ Survey, which is planned to cover the 30,000 deg$^2$ of sky visible from Hawaii ($\delta > -30°$) in five filters (the SDSS-like *griz* and *y* at $\sim$1 μm), with pairs of observations in each filter being taken at six different epochs.

PS1 will increase the SDSS sky coverage by a factor of two and will reach at least a magnitude deeper (with a second telescope, or perhaps all four that are envisioned in this program, the depth gain could be up to another magnitude). Both of these advantages will most likely yield new discoveries in the context of Milky Way studies. An additional magnitude of depth corresponds to 60% larger distance limit and could bridge the 25 kpc to 40 kpc range, where the transition between the inner and outer halo is probably taking place, with turnoff stars. In addition, the coverage of the Galactic plane will be much better than with the SDSS, and the *y*-band will be more apt at penetrating through the high ISM dust extinction at low Galactic latitudes. Unfortunately, the Pan-STARRS system does not include an UV band required for photometric metallicity estimates.

**8.3.3. The dark energy survey.** The DES will utilize a new 0.52-Gigapixel camera at the 4-m Blanco telescope (3.8-deg$^2$ field of view) to cover 5,000 square degrees of the Southern sky (Flaugher 2008). The survey will be completed during a 5-year period starting in 2012 and will include SDSS-like *griz* bandpasses and the *y*-band. Similar to the Pan-STARRS, the DES will not include an UV band. As its name implies, although Milky Way studies are not its primary goal, it will nevertheless provide valuable data.

Although the DES will cover "only" about 5,000 deg$^2$ of the Southern sky, it will reach about 1.5–2 mag deeper than the SkyMapper survey (and the SDSS). This depth gain, and corresponding improvement in the limiting distance by a factor of 2–2.5, is likely to bring significant new discoveries, especially in the context of the Galactic halo.

## 8.4. Gaia

Gaia is an ESA Cornerstone mission set for launch in 2013. Building on experience from HIPPARCOS, it will survey the sky to a magnitude limit of $r \sim 20$ (approximately, see below) and obtain astrometric and three-band photometric measurements for about 1 billion sources, as well as radial-velocity and chemical-composition measurements (using the 847–874-nm wavelength range) for 150 million stars with $r < 18$ (Perryman 2002, Wilkinson et al. 2005). The final data product, the Gaia Catalog, is expected to be published by 2020, although early data releases are planned.

Gaia's payload will include two telescopes sharing a common focal plane, with two 1.7° × 0.6° viewing fields separated by a highly stable angle of 106.5°. The focal plane includes a mosaic of 106 CCDs, with a total pixel count close to one billion. Due to the spacecrafts' rotation and precession, the entire sky will be scanned in TDI mode (time-delay-and-integrate, or drift scanning) about 70 times, on average, during 5 years of operations. Gaia will produce broad-band *G* magnitudes with sensitivity in the wavelength range of 330–1,020 nm (FWHM points at $\sim$400 nm and $\sim$850 nm). The spectral energy distribution of each source will be sampled by a spectrophotometric instrument providing low-resolution spectra in the blue (*BP*, effective wavelength $\sim$520 nm) and in the red (*RP*, effective wavelength $\sim$800 nm). In addition, the RVS instrument (radial-velocity spectrograph) will disperse the light in the range of 847–874 nm, for which it will include a dedicated filter.

## 8.5. Large Synoptic Survey Telescope

The LSST is the most ambitious currently planned wide-field ground-based optical system (Ivezić et al. 2008b). The current baseline design, with an 8.4-m primary mirror, a 9.6-deg$^2$ field of view, and a 3.2-Gigapixel camera, will allow about 20,000 square degrees of sky visible from Cerro Pachón in Northern Chile to be covered to a depth of $r \sim 27.5$ over the 10-year survey. About 1,000 observations (summed over the six bands, *ugrizy*) will be obtained during that period, enabling unprecedented time-domain studies. The LSST will obtain proper-motion measurements of comparable accuracy to those of Gaia at its faint limit (and $r \sim 20$) and smoothly extend the error versus magnitude curve deeper by about 5 mag (see **Figure 21**).

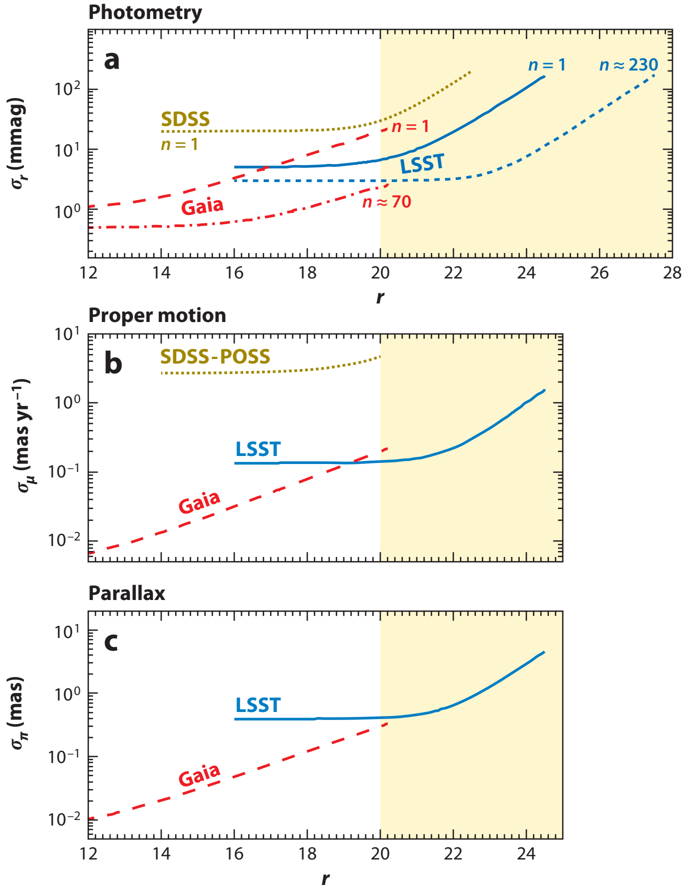

**Figure 21**

A comparison of the (*a*) photometric, (*b*) proper-motion, and (*c*) parallax errors for the Sloan Digital Sky Survey (SDSS, *dark yellow*), Gaia (*red*), and the Large Synoptic Survey Telescope (LSST, *blue*) as a function of apparent magnitude *r*, for a G2V star (L. Eyer, Ž. Ivezić, M. Jurić, R.L. Jones, D.G. Monet, et al., in preparation). (*a*) The curve marked "SDSS" corresponds to a single SDSS observation. The red long-dashed curve for Gaia shows a single-transit accuracy, whereas the dot-dashed curve shows the end-of-mission accuracy (assuming 70 transits). The blue curves correspond to the LSST; the solid curve shows a single-visit accuracy, whereas the short-dashed curve shows the accuracy for coadded data (assuming 230 visits in the *r*-band). (*b*) The curve marked "SDSS-POSS" shows the accuracy delivered by the proper-motion catalog of Munn et al. (2004).

Annu. Rev. Astro. Astrophys. 2012.50:251-304. Downloaded from www.annualreviews.org
by California Institute of Technology on 01/21/14. For personal use only.

The LSST project will produce a massive and exquisitely accurate photometric and astrometric data set for about 10 billion Milky Way stars. The coverage of the Galactic plane will yield data for numerous star-forming regions, and the $y$-band data will penetrate through the interstellar dust layer. With its $u$-band data, the LSST will enable studies of metallicity and kinematics using the same sample of stars out to a distance of ~40 kpc [~200 million F/G main-sequence stars brighter than $r = 23$; for a discussion see Ivezić et al. (2008a)] and the spatial distribution of halo turnoff stars will be traced out to ~100 kpc. No other existing or planned survey will provide such a massive and powerful data set to study the outer halo. The LSST, in its standard surveying mode, will be able to efficiently detect RR Lyrae stars and, hence, explore the extent and structure of the halo out to 400 kpc (see **Figure 22**). All together, the LSST will enable studies of the stellar distribution beyond the presumed edge of the Galactic halo, of their metallicity distribution throughout most of the halo, and of their kinematics beyond the thick disk/halo boundary (for more detailed discussion see the LSST Science Book; LSST Science Collaborations et al. 2009).

Annu. Rev. Astro. Astrophys. 2012.50:251-304. Downloaded from www.annualreviews.org
by California Institute of Technology on 01/21/14. For personal use only.

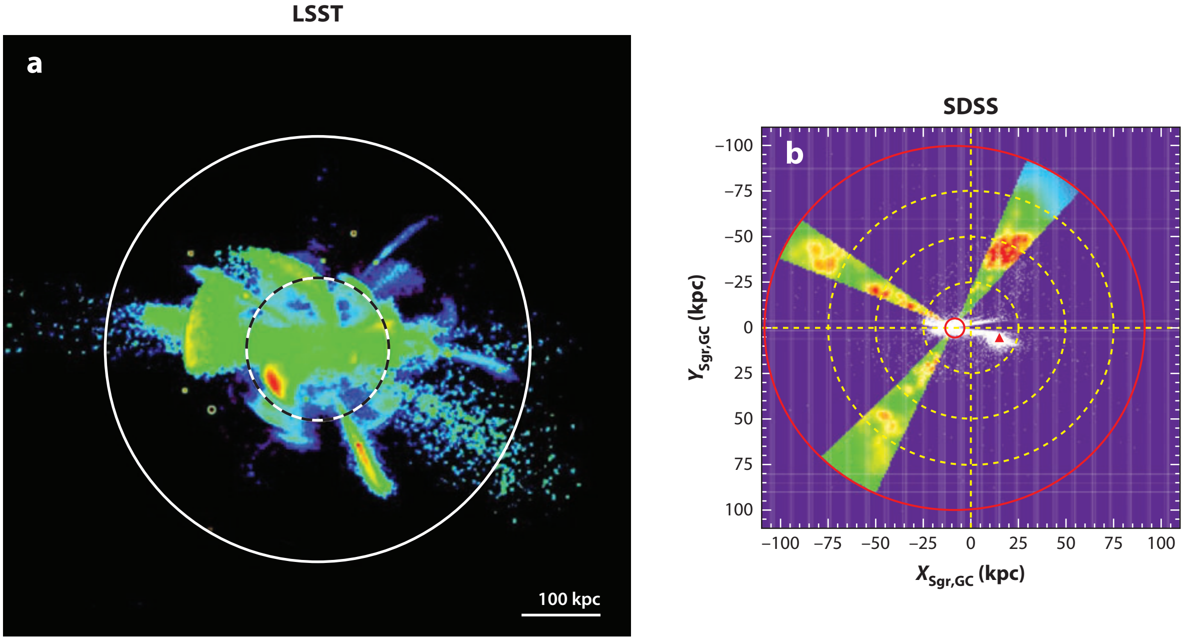

**Figure 22**

A simulation of (*a*) the outer regions of the Milky Way compared to (*b*) the current state-of-the-art data shown on the same spatial scale. The data panel (*b*) presents the number density multiplied by the cube of the Galactocentric radius (logarithmic scale with dynamic range of 1,000, from *blue* to *red*), for ~1,000 Sloan Digital Sky Survey (SDSS) RR Lyrae stars within 10° of the Sgr dwarf tidal stream plane (Ivezić et al. 2004). The same color coding was used to visualize the stellar number density for a Milky Way–type galaxy simulation (*a*) from Bullock & Johnston (2005), shown on the left. Set within an ΛCDM merger history, these simulations track the accretion and disruption of hundreds of dwarf galaxies into Milky Way–size halos. With the Large Synoptic Survey Telescope (LSST), RR Lyrae stars will be found beyond the presumed Milky Way tidal radius (~300 kpc, *white circle*), and the much more numerous main-sequence stars will trace the structure out to 100 kpc (*black-and-white dashed circle*) The latter distance range can at present only be probed using RR Lyrae stars and other rare nonmain-sequence stars.

### 8.6. The Synergy between Gaia and the Large Synoptic Survey Telescope

In the context of Gaia, the LSST can be thought of as its deep complement. A detailed comparison of LSST and Gaia performance is given in **Figure 21**. Gaia will provide an all-sky catalog with unsurpassed trigonometric parallax, proper-motion, and photometric measurements to $r \sim 20$, for about $10^9$ stars. The LSST will extend this map to $r \sim 27$ over half of the sky, detecting about $10^{10}$ stars. Because of Gaia's superb astrometric and photometric quality and the LSST's significantly deeper reach, the two surveys are highly complementary—Gaia will map the Milky Way's disk with unprecedented detail, and the LSST will extend this map all the way to the edge of the known halo and beyond.

A quantitative comparison of the distance-color coverage for main-sequence stars by Gaia and the LSST is shown in **Figure 23**. For example, stars just below the main-sequence turnoff, with

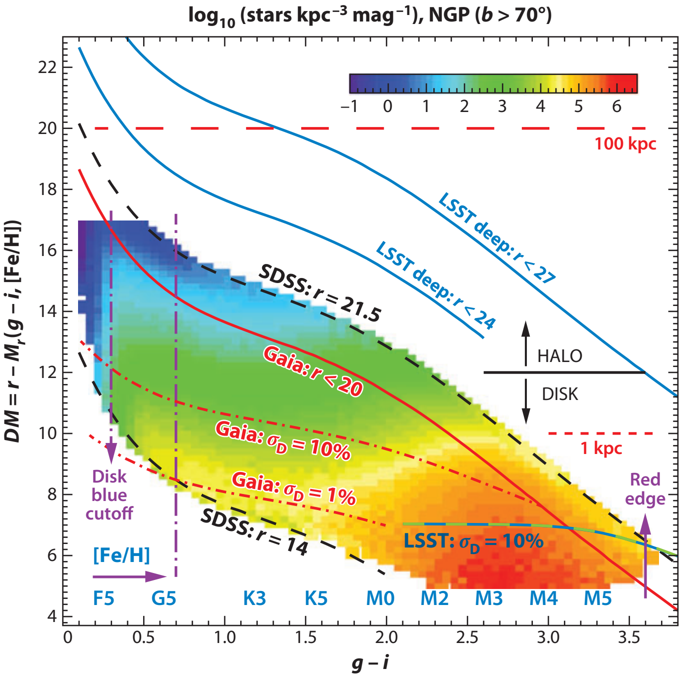

**Figure 23**

The volume number density (stars per cubed kiloparsec per magnitude, log scale according to the legend) of main-sequence stars with $14 < r < 21.5$ and $b > 70°$ as a function of their distance modulus and $g - i$ color [based on Sloan Digital Sky Survey (SDSS) data]. The absolute magnitudes are determined using the photometric parallax relation from Ivezić et al. (2008a). The MK spectral type is indicated above the $g - i$ axis. The two purple vertical arrows mark the turnoff color for disk stars and the red edge of the M-dwarf color distribution. The *[Fe/H]* label shows the color range ($g - i < 0.7$), where the photometric metallicity estimator from Ivezić et al. (2008a) performs best. The two diagonal dashed lines, marked $r = 14$ and $r = 21.5$, show the apparent magnitude limits for SDSS data. The colored diagonal solid lines mark the apparent magnitude limits for Gaia ($r < 20$), the Large Synoptic Survey Telescope (LSST)'s single-epoch data ($r < 24$, $10\sigma$), and the LSST's stacked data ($r < 27$, $10\sigma$). The blue and green dashed line in the lower right corner marks the distance limits for obtaining 10% accurate trigonometric distances using LSST data. The two red dot-dashed lines mark analogous limits for obtaining 1% and 10% accurate trigonometric distances using Gaia's data.

Annu. Rev. Astro. Astrophys. 2012.50:251-304. Downloaded from www.annualreviews.org
by California Institute of Technology on 01/21/14. For personal use only.

$M_r = 4.5$, will be detected by Gaia to a distance limit of ~10 kpc ($r < 20$), and to ~100 kpc with the LSST's single-epoch data ($r < 24.5$). For intrinsically faint stars, such as late M dwarfs, L/T dwarfs, and white dwarfs, the deeper limit of the LSST will enable detection and characterization of the halo populations. A star with $M_r = 15$ will be detectable to a distance limit of 100 pc with Gaia and ~800 pc with the LSST; hence, the LSST samples will be about 100 times larger. In addition, for a substantial fraction of red stars with $r > 20$, the LSST will provide trigonometric parallax measurements accurate to better than 10%. Hence, despite the unprecedented performance of Gaia for $r < 20$, the LSST will enable major discoveries with its deep $r > 20$ sky coverage. At the same time, and in addition to its own discoveries, Gaia will provide excellent astrometric and photometric calibration samples for the LSST. To conclude, "these are exciting times to study local galaxies" (Wyse 2006).

Annu. Rev. Astro. Astrophys. 2012.50:251-304. Downloaded from www.annualreviews.org
by California Institute of Technology on 01/21/14. For personal use only.

## DISCLOSURE STATEMENT

The authors are not aware of any affiliations, memberships, funding, or financial holdings that might be perceived as affecting the objectivity of this review.

## ACKNOWLEDGMENTS

Ž.I. acknowledges support by NSF grants AST 61-5991 and AST 07-07901, and by NSF grant AST 05-51161 to the LSST for design and development activity. T.C.B. acknowledges partial support from NSF grants PHY 02-16783 and PHY 08-2268: Physics Frontier Center/Joint Institute for Nuclear Astrophysics (JINA). M.J. is a Hubble Fellow.

## LITERATURE CITED

Aihara H, Allende Prieto C, An D, Anderson SF, Aubourg É, et al. 2011. *Ap. J. Suppl.* 193:29–46
Allende Prieto C, Beers TC, Wilhelm R, Newberg HJ, Rockosi CM, et al. 2006. *Ap. J.* 636:804–20
Allende Prieto C, Majewski SR, Schiavon R, Cunha K, Frinchaboy P, et al. 2008. *Astron. Nachr.* 329:1018–21
Bahcall JN, Soneira RM. 1980. *Ap. J. Suppl.* 44:73–110
Battaglia G, Helmi A, Morrison H, Harding P, Olszewski EW, et al. 2005. *MNRAS* 364:433–442
Beers TC, Carollo D, Ivezić Ž, An D, Chiba M, et al. 2012. *Ap. J.* 746:34–57
Beers TC, Chiba M, Yoshii Y, Platais I, Hanson RB, et al. 2000. *Astron. J.* 119:2866–81
Beers TC, Christlieb N. 2005. *Annu. Rev. Astron. Astrophys.* 43:531–80
Beers TC, Lee Y, Sivarani T, Allende Prieto C, Wilhelm R, et al. 2006. *Mem. Soc. Astron. Ital.* 77:1171
Beers TC, Preston GW, Shectman SA. 1992. *Astron. J.* 103:1987–2034
Bell EF, Xue XX, Rix HW, Ruhland C, Hogg DW. 2010. *Astron. J.* 140:1850–59
Bell EF, Zucker DB, Belokurov V, Sharma S, Johnston KV, et al. 2008. *Ap. J.* 680:295–311
Belokurov V, Evans NW, Bell EF, Irwin MJ, Hewett PC, et al. 2007a. *Ap. J. Lett.* 657:L89–92
Belokurov V, Evans NW, Irwin MJ, Lynden-Bell D, Yanny B, et al. 2007b. *Ap. J.* 658:337–44
Belokurov V, Zucker DB, Evans NW, Gilmore G, Vidrih S, et al. 2006a. *Ap. J. Lett.* 642:L137–40
Belokurov V, Zucker DB, Evans NW, Kleyna JT, Koposov S, et al. 2007c. *Ap. J.* 654:897–906
Belokurov V, Zucker DB, Evans NW, Wilkinson MI, Irwin MJ, et al. 2006b. *Ap. J. Lett.* 647:L111–14
Bensby T, Feltzing S, Lundström I. 2004. *Astron. Astrophys.* 421:969–76
Bessell M, Bloxham G, Schmidt B, Keller S, Tisserand P, Francis P. 2011. *Publ. Astron. Soc. Pac.* 123:789–98
Boeche C, Siebert A, Williams M, de Jong RS, Steinmetz M, et al. 2011. *Astron. J.* 142:193–213
Bonaca A, Jurić M, Ivezić Ž, Bizyaev D, Brewington H, et al. 2012. *Astron. J.* 143(5):105
Bond NA, Ivezić Ž, Sesar B, Jurić M, Munn JA, et al. 2010. *Ap. J.* 716:1–29
Bonifacio P, Centurion M, Molaro P. 1999. *MNRAS* 309:533–42
Bovy J, Rix HW, Hogg DW. 2012. *Ap. J.* 751:131

Brook CB, Gibson BK, Martel H, Kawata D. 2005. *Ap. J.* 630:298–308

Brook CB, Richard S, Kawata D, Martel H, Gibson BK. 2007. *Ap. J.* 658:60–64

Brown WR, Geller MJ, Kenyon SJ, Diaferio A. 2010. *Astron. J.* 139:59–67

Bullock JS, Dekel A, Kolatt TS, Kravtsov AV, Klypin AA, et al. 2001. *Ap. J.* 555:240–57

Bullock JS, Johnston KV. 2005. *Ap. J.* 635:931–49

Bullock JS, Kravtsov AV, Weinberg DH. 2001. *Ap. J.* 548:33–46

Burnett B, Binney J, Sharma S, Williams M, Zwitter T, et al. 2011. *Astron. Astrophys.* 532:A113

Cabrera-Lavers A, González-Fernández C, Garzón F, Hammersley PL, López-Corredoira M. 2008. *Astron. Astrophys.* 491:781–87

Carney BW, Laird JB, Latham DW, Aguilar LA. 1996. *Astron. J.* 112:668–92

Carollo D, Beers TC, Bovy J, Sivarani T, Norris JE, et al. 2012. *Ap. J.* 744:195–217

Carollo D, Beers TC, Chiba M, Norris JE, Freeman KC, et al. 2010. *Ap. J.* 712:692–727

Carollo D, Beers TC, Lee YS, Chiba M, Norris JE, et al. 2007. *Nature* 450:1020–25

Casetti-Dinescu DI, Girard TM, Korchagin VI, van Altena WF. 2011. *Ap. J.* 728:7–25

Chiba M, Beers TC. 2000. *Astron. J.* 119:2843–65

Churchwell E, Babler BL, Meade MR, Whitney BA, Benjamin R, et al. 2009. *Publ. Astron. Soc. Pac.* 121:213–30

Cioni MRL, Clementini G, Girardi L, Guandalini R, Gullieuszik M, et al. 2011. *Astron. Astrophys.* 527:A116–38

Clarkson W, Sahu K, Anderson J, Smith TE, Brown TM, et al. 2008. *Ap. J.* 684:1110–42

Clewley L, Kinman TD. 2006. *MNRAS* 371:L11–15

Cooper AP, Cole S, Frenk CS, Helmi A. 2011. *MNRAS* 417:2206–15

Covey KR, Ivezić Ž, Schlegel D, Finkbeiner D, Padmanabhan N, et al. 2007. *Astron. J.* 134:2398–417

Deason AJ, Belokurov V, Evans NW. 2011. *MNRAS* 416:2903–15

De Jong JTA, Yanny B, Rix H-W, Dolphin AE, Martin NF, et al. 2010. *Ap. J.* 714:663–74

De Lucia G, Helmi A. 2008. *MNRAS* 391:14–31

De Propris R, Harrison CD, Mares PJ. 2010. *Ap. J.* 719:1582–87

Dierickx M, Klement R, Rix HW, Liu C. 2010. *Ap. J. Lett.* 725:L186–90

Di Matteo P, Lehnert MD, Qu Y, van Driel W. 2011. *Astron. Astrophys.* 525:L3–7

Dong R, Gunn J, Knapp G, Rockosi C, Blanton M. 2011. *Astron. J.* 142:116–26

Duffau S, Zinn R, Vivas AK, Carraro G, Méndez RA, et al. 2006. *Ap. J. Lett.* 636:L97–100

Eggen OJ, Lynden-Bell D, Sandage AR. 1962. *Ap. J.* 136:748–66

Eisenstein DJ, Weinberg DH, Agol E, Aihara H, Allende Prieto C, et al. 2011. *Astron. J.* 142:72–96

Fellhauer M, Belokurov V, Evans NW, Wilkinson MI, Zucker DB, et al. 2006. *Ap. J.* 651:167–73

Feltzing S. 2006. *Mem. Soc. Astron. Ital.* 77:1103–10

Ferguson AMN, Irwin MJ, Ibata RA, Lewis GF, Tanvir NR. 2002. *Astron. J.* 124:1452–63

Flaugher B. 2008. In *A Decade of Dark Energy: Spring Symp.*, *Proc. Conf.*, *Baltimore*, *MD*, May 5–8, ed. N Pirzkal, H Ferguson. Baltimore, MD: Space Telesc. Sci. Inst. **http://www.stsci.edu/institute/conference/spring2008**

Font AS, Johnston KV, Ferguson AMN, Bullock JS, Robertson BE, et al. 2008. *Ap. J.* 673:215–25

Font AS, McCarthy IG, Crain RA, Theuns T, Schaye J, et al. 2011. *MNRAS* 416:2802–20

Frebel A, Christlieb N, Norris JE, Beers TC, Bessell MS, et al. 2006. *Ap. J.* 652:1585–603

Freeman K, Bland-Hawthorn J. 2002. *Annu. Rev. Astron. Astrophys.* 40:487–537

Freeman KC. 1987. *Annu. Rev. Astron. Astrophys.* 25:603–32

Frinchaboy P, Zasowski G, Jackson K, Johnson JA, Majewski SR, et al. 2010. In *Star Clusters in the Era of Large Surveys*, *Proc. Symp. 5 JENAM 2010*, ed. A Moitinho, J Alves, pp. 31–38. Heidelberg: Springer

Fuhrmann K. 2004. *Astron. Nachr.* 325:3–80

Fulbright JP, Wyse RFG, Ruchti GR, Gilmore GF, Grebel E, et al. 2010. *Ap. J. Lett.* 724:L104–8

Ghigna S, Moore B, Governato F, Lake G, Quinn T, Stadel J. 2000. *Ap. J.* 544:616–28

Gilmore G, Reid N. 1983. *MNRAS* 202:1025–47

Gilmore G, Wyse RFG, Kuijken K. 1989. *Annu. Rev. Astron. Astrophys.* 27:555–627

Gonzalez OA, Rejkuba M, Zoccali M, Hill V, Battaglia G, et al. 2011. *Astron. Astrophys.* 530:A54–66

Governato F, Mayer L, Wadsley J, Gardner JP, Willman B, et al. 2004. *Ap. J.* 607:688–96

Governato F, Willman B, Mayer L, Brooks A, Stinson G, et al. 2007. *MNRAS* 374:1479–94

Grillmair CJ. 2009. *Ap. J.* 693:1118–27

Annu. Rev. Astro. Astrophys. 2012.50:251-304. Downloaded from www.annualreviews.org
by California Institute of Technology on 01/21/14. For personal use only.

Grillmair CJ, Dionatos O. 2006. *Ap. J. Lett.* 643:L17–20

Harding P, Morrison HL, Olszewski EW, Arabadjis J, Mateo M, et al. 2001. *Astron. J.* 122:1397–419

Hartwick FDA. 1987. In *NATO ASIC Proc. 207: The Galaxy*, ed. G Gilmore, B Carswell, pp. 281–90. Dordrecht: Reidel

Helmi A. 2004. *Ap. J. Lett.* 610:L97–100

Helmi A. 2008. *Astron. Astrophys. Rev.* 15:145–88

Helmi A, White SDM. 1999. *MNRAS* 307:495–517

Helmi A, White SDM, de Zeeuw PT, Zhao H. 1999. *Nature* 402:53–55

Ibata R, Irwin M, Lewis G, Ferguson AMN, Tanvir N. 2001a. *Nature* 412:49–52

Ibata R, Lewis GF, Irwin M, Totten E, Quinn T. 2001b. *Ap. J.* 551:294–311

Ibata RA, Gilmore G, Irwin MJ. 1994. *Nature* 370:194–96

Ibata RA, Irwin MJ, Lewis GF, Ferguson AMN, Tanvir N. 2003. *MNRAS* 340:L21–27

Ivezić Ž, Goldston J, Finlator K, Knapp GR, Yanny B, et al. 2000. *Astron. J.* 120:963–77

Ivezić Ž, Lupton R, Schlegel D, Smolčić V, Johnston D, et al. 2004. In *Satellites and Tidal Streams*, *ASP Conf. Ser. 327*, ed. F Prada, D Martinez-Delgado, TJ Mahoney, p. 104. San Francisco: Astron. Soc. Pac.

Ivezić Ž, Sesar B, Jurić M, Bond N, Dalcanton J, et al. 2008a. *Ap. J.* 684:287–325

Ivezić Ž, Tyson JA, Acosta E, Allsman R, Anderson SF, et al. 2008b. *LSST: From Science Drivers to Reference Design and Anticipated Data Products.* Work. Pap., Dep. Astron., Univ. Wash. (arXiv:0805.2366)

Johnston KV, Bullock JS, Sharma S, Font A, Robertson BE, Leitner SN. 2008. *Ap. J.* 689:936–57

Johnston KV, Hernquist L, Bolte M. 1996. *Ap. J.* 465:278–87

Jurić M, Ivezić Ž, Brooks A, Lupton RH, Schlegel D, et al. 2008. *Ap. J.* 673:864–914

Kaiser N, Burgett W, Chambers K, Denneau L, Heasley J, et al. 2010. *Proc. SPIE* 7733:77330E

Keller SC, Murphy S, Prior S, Da Costa G, Schmidt B. 2008. *Ap. J.* 678:851–64

Keller SC, Schmidt BP, Bessell MS, Conroy PG, Francis P, et al. 2007. *Publ. Astron. Soc. Aust.* 24:1–12

Klement R, Rix H-W, Flynn C, Fuchs B, Beers TC, et al. 2009. *Ap. J.* 698:865–94

Klement RJ. 2010. *Astron. Astrophys. Rev.* 18:567–94

Kollmeier JA, Gould A, Shectman S, Thompson IB, Preston GW, et al. 2009. *Ap. J. Lett.* 705:L158–62

Law DR, Johnston KV, Majewski SR. 2005. *Ap. J.* 619:807–23

Lawrence A, Warren SJ, Almaini O, Edge AC, Hambly NC, et al. 2007. *MNRAS* 379:1599–617

Lee YS, Beers TC, Allende Prieto C, Lai DK, Rockosi CM, et al. 2011a. *Astron. J.* 141:90

Lee YS, Beers TC, An D, Ivezić Ž, Just A, et al. 2011b. *Ap. J.* 738:187–204

Lee YS, Beers TC, Sivarani T, Allende Prieto C, Koesterke L, et al. 2008a. *Astron. J.* 136:2022–49

Lee YS, Beers TC, Sivarani T, Johnson JA, An D, et al. 2008b. *Astron. J.* 136:2050–69

Loebman SR, Roškar R, Debattista VP, Ivezić Ž, Quinn TR, Wadsley J. 2011. *Ap. J.* 737:8–25

LSST Sci. Collab., Abell PA, Allison J, Anderson SF, Andrew JR, et al. 2009. *LSST Science Book*. Tucson, AZ: LSST (arXiv:0912.0201)

Majewski SR. 1992. *Ap. J. Suppl.* 78:87–152

Majewski SR. 1993. *Annu. Rev. Astron. Astrophys.* 31:575–638

Majewski SR. 2010. In *Stellar Populations—Planning for the Next Decade*, *IAU Symp. 262*, ed. G Bruzual, S Charlot, pp. 99–110. Cambridge UK: Cambridge Univ. Press

Majewski SR, Skrutskie MF, Weinberg MD, Ostheimer JC. 2003. *Ap. J.* 599:1082–115

Mayer L, Moore B, Quinn T, Governato F, Stadel J. 2002. *MNRAS* 336:119–30

McPherson AM, Born A, Sutherland W, Emerson J, Little B, et al. 2006. *Proc. SPIE* 6267:626707

Miceli A, Rest A, Stubbs CW, Hawley SL, Cook KH, et al. 2008. *Ap. J.* 678:865–87

Minchev I, Famaey B. 2010. *Ap. J.* 722:112–21

Minniti D, Zoccali M. 2008. In *Formation and Evolution of Galaxy Bulges*, *IAU Symp. 245*, ed. M Bureau, E Athanassoula, B Barbuy, pp. 323–32. Cambridge, UK: Cambridge Univ. Press

Monet DG, Levine SE, Canzian B, Ables HD, Bird AR, et al. 2003. *Astron. J.* 125:984–93

Moore B, Davis M. 1994. *MNRAS* 270:209–21

Morrison HL, Flynn C, Freeman KC. 1990. *Astron. J.* 100:1191–222

Munn JA, Monet DG, Levine SE, Canzian B, Pier JR, et al. 2004. *Astron. J.* 127:3034–42

Annu. Rev. Astro. Astrophys. 2012.50:251-304. Downloaded from www.annualreviews.org
by California Institute of Technology on 01/21/14. For personal use only.

Murphy S, Keller S, Schmidt B, Tisserand P, Bessell M, et al. 2009. In *The Eighth Pacific Rim Conference on Stellar Astrophysics: A Tribute to Kam Ching Leung*, ed. B Soonthornthum, S Komonjinda, KS Cheng, KC Leung, ASP Conf. Ser. Vol. 404, p. 356. San Francisco: ASP

Newberg HJ, Yanny B, Cole N, Beers TC, Re Fiorentin P, et al. 2007. *Ap. J.* 668:221–35

Newberg HJ, Yanny B, Grebel EK, Hennessy G, Ivezić Ž, et al. 2003. *Ap. J. Lett.* 596:L191–94

Newberg HJ, Yanny B, Rockosi C, Grebel EK, Rix HW, et al. 2002. *Ap. J.* 569:245–74

Nordström B, Mayor M, Andersen J, Holmberg J, Pont F, et al. 2004. *Astron. Astrophys.* 418:989–1019

Norris J. 1986. *Ap. J. Suppl.* 61:667–98

Norris J, Bessell MS, Pickles AJ. 1985. *Ap. J. Suppl.* 58:463–92

Norris JE, Ryan SG. 1991. *Ap. J.* 380:403–18

Perryman MAC. 2002. *Astron. Astrophys. Suppl. Ser.* 280:1–10

Perryman MAC, Lindegren L, Kovalevsky J, Hoeg E, Bastian U, et al. 1997. *Astron. Astrophys.* 323:L49–52

Pont F, Eyer L. 2004. *MNRAS* 351:487–504

Pourbaix D, Knapp GR, Szkody P, Ivezić Ž, Kleinman SJ, et al. 2005. *Astron. Astrophys.* 444:643–49

Preston GW, Shectman SA, Beers TC. 1991. *Ap. J.* 375:121–47

Prior SL, Da Costa GS, Keller SC, Murphy SJ. 2009. *Ap. J.* 691:306–19

Ramírez I, Allende Prieto C, Lambert DL. 2007. *Astron. Astrophys.* 465:271–89

Rangwala N, Williams TB. 2009. *Ap. J.* 702:414–24

Rangwala N, Williams TB, Stanek KZ. 2009. *Ap. J.* 691:1387–99

Rattenbury NJ, Mao S, Sumi T, Smith MC. 2007. *MNRAS* 378:1064–78

Reddy BE, Lambert DL, Allende Prieto C. 2006. *MNRAS* 367:1329–66

Rich RM. 2011. In *RR Lyrae Stars, Metal-Poor Stars, and the Galaxy*, ed. A McWilliam, pp. 264–85. Pasadena, CA: Obs. Carnegie Inst. Wash.

Robin AC, Marshall DJ, Schultheis M, Reyle C. 2012. *Astron. Astrophys.* 538:106–20

Robin AC, Reylé C, Derrière S, Picaud S. 2003. *Astron. Astrophys.* 409:523–40

Rocha-Pinto HJ, Flynn C, Scalo J, Hänninen J, Maciel WJ, Hensler G. 2004a. *Astron. Astrophys.* 423:517–35

Rocha-Pinto HJ, Majewski SR, Skrutskie MF, Crane JD. 2003. *Ap. J. Lett.* 594:L115–18

Rocha-Pinto HJ, Majewski SR, Skrutskie MF, Crane JD, Patterson RJ. 2004b. *Ap. J.* 615:732–37

Rockosi C, Beers TC, Majewski S, Schiavon R, Eisenstein D. 2009. In *Astro2010: The Astronomy and Astrophysics Decadal Survey, Science White Papers, No. 14*, Natl. Acad., Washington, D.C. **http://adsabs.harvard.edu/abs/2009astro2010S..14R**

Roškar R, Debattista VP, Quinn TR, Stinson GS, Wadsley J. 2008a. *Ap. J. Lett.* 684:L79–82

Roškar R, Debattista VP, Stinson GS, Quinn TR, Kaufmann T, Wadsley J. 2008b. *Ap. J. Lett.* 675:L65–68

Ruchti GR, Fulbright JP, Wyse RFG, Gilmore GF, Bienaymé O, et al. 2011. *Ap. J.* 737:9–33

Ryan SG, Lambert DL. 1995. *Astron. J.* 109:2068–80

Ryan SG, Norris JE. 1991. *Astron. J.* 101:1865–78

Saha A, Olszewski EW, Brondel B, Olsen K, Knezek P, et al. 2010. *Astron. J.* 140:1719–38

Sales LV, Helmi A, Abadi MG, Brook CB, Gómez FA, et al. 2009. *MNRAS* 400:L61–65

Schiavon RP, Majewski SR. 2010. In *Stellar Populations—Planning for the Next Decade, IAU Symp. 262*, ed. G Bruzual, S Charlot, pp. 428–29. Cambridge UK: Cambridge Univ. Press

Schlaufman KC, Rockosi CM, Allende Prieto C, Beers TC, Bizyaev D, et al. 2009. *Ap. J.* 703:2177–204

Schlaufman KC, Rockosi CM, Lee YS, Beers TC, Allende Prieto C. 2011. *Ap. J.* 734:49

Schönrich R. 2012. In *Assembling the Puzzle of the Milky Way, Le Grand-Bornand, France*, ed. C Reylé, A Robin, M Schultheis, 19:05003–10. Les Ulis, Fr.: EPJ Web of Conf., EDP Sci. **http://dx.doi.org/10.1051/epjconf/20121905003**

Schönrich R, Asplund M, Casagrande L. 2011. *MNRAS* 415:3807–23

Schönrich R, Binney J. 2009a. *MNRAS* 396:203–22

Schönrich R, Binney J. 2009b. *MNRAS* 399:1145–56

Schwarzschild M, Searle L, Howard R. 1955. *Ap. J.* 122:353–56

Searle L, Zinn R. 1978. *Ap. J.* 225:357–79

Sellwood JA, Binney JJ. 2002. *MNRAS* 336:785–96

Sesar B, Ivezić Ž, Grammer SH, Morgan DP, Becker AC, et al. 2010a. *Ap. J.* 708:717–41

Annu. Rev. Astro. Astrophys. 2012.50:251-304. Downloaded from www.annualreviews.org
by California Institute of Technology on 01/21/14. For personal use only.

Sesar B, Ivezić Ž, Jurić M. 2008. *Ap. J.* 689:1244–73
Sesar B, Ivezić Ž, Lupton RH, Jurić M, Gunn JE, et al. 2007. *Astron. J.* 134:2236–51
Sesar B, Jurić M, Ivezić Ž. 2011. *Ap. J.* 731:4–17
Sesar B, Svilković D, Ivezić Ž, Lupton RH, Munn JA, et al. 2006. *Astron. J.* 131:2801–25
Sesar B, Vivas AK, Duffau S, Ivezić Ž. 2010b. *Ap. J.* 717:133–39
Siebert A, Bienayme O, Binney J, Bland-Hawthorn J, Campbell R, et al. 2008. *MNRAS* 391:793–801
Siebert A, Williams MEK, Siviero A, Reid W, Boeche C, et al. 2011. *Astron. J.* 141:187
Sirko E, Goodman JJ, Knapp GR, Brinkmann J, Ivezić Ž, et al. 2004. *Astron. J.* 127:914–24
Skrutskie MF, Cutri RM, Stiening R, Weinberg MD, Schneider S, et al. 2006. *Astron. J.* 131:1163–83
Smith MC, Evans NW, Belokurov V, Hewett PC, Bramich DM, et al. 2009. *MNRAS* 399:1223–37
Smith MC, Wyn Evans N, An JH. 2009. *Ap. J.* 698:1110–16
Smolinski JP, Lee YS, Beers TC, An D, Bickerton SJ, et al. 2011. *Astron. J.* 141:89–118
Soderblom DR. 2010. *Annu. Rev. Astron. Astrophys.* 48:581–629
Sommer-Larsen J, Götz M, Portinari L. 2003. *Ap. J.* 596:47–66
Sommer-Larsen J, Zhen C. 1990. *MNRAS* 242:10–24
Springel V, Wang J, Vogelsberger M, Ludlow A, Jenkins A, et al. 2008. *MNRAS* 391:1685–711
Starkenburg E, Helmi A, Morrison HL, Harding P, van Woerden H, et al. 2009. *Ap. J.* 698:567–79
Steinmetz M, Navarro JF. 2002. *New Astron.* 7:155–60
Steinmetz M, Zwitter T, Siebert A, Watson FG, Freeman KC, et al. 2006. *Astron. J.* 132:1645–68
Twarog BA, Anthony-Twarog BJ. 1994. *Astron. J.* 107:1371–80
van der Kruit PC, Freeman KC. 2011. *Annu. Rev. Astron. Astrophys.* 49:301–71
Vivas AK, Jaffé YL, Zinn R, Winnick R, Duffau S, Mateu C. 2008. *Astron. J.* 136:1645–57
Vivas AK, Zinn R. 2006. *Astron. J.* 132:714–28
Vivas AK, Zinn R, Andrews P, Bailyn C, Baltay C, et al. 2001. *Ap. J. Lett.* 554:L33–36
Watkins LL, Evans NW, Belokurov V, Smith MC, Hewett PC, et al. 2009. *MNRAS* 398:1757–70
West AA, Hawley SL, Bochanski JJ, Covey KR, Reid IN, et al. 2008. *Astron. J.* 135:785–95
Westerlund BE. 1990. *Astron. Astrophys. Rev.* 2:29–78
Wetterer CJ, McGraw JT. 1996. *Astron. J.* 112:1046–53
Wilkinson MI, Vallenari A, Turon C, Munari U, Katz D, et al. 2005. *MNRAS* 359:1306–35
Willman B. 2010. *Adv. Astron.* 10:285454–65
Wilson ML, Helmi A, Morrison HL, Breddels MA, Bienaymé O, et al. 2011. *MNRAS* 413:2235–41
Wright EL, Eisenhardt PRM, Mainzer AK, Ressler ME, Cutri RM, et al. 2010. *Astron. J.* 140:1868–81
Wyse RFG. 2006. *Mem. Soc. Astron. Ital.* 77:1036–48
Xue XX, Rix HW, Yanny B, Beers TC, Bell EF, et al. 2011. *Ap. J.* 738:79–91
Xue XX, Rix HW, Zhao G, Re Fiorentin P, Naab T, et al. 2008. *Ap. J.* 684:1143–58
Yanny B, Newberg HJ, Grebel EK, Kent S, Odenkirchen M, et al. 2003. *Ap. J.* 588:824–41
Yanny B, Newberg HJ, Kent S, Laurent-Muehleisen SA, Pier JR, et al. 2000. *Ap. J.* 540:825–41
Yanny B, Rockos C, Newberg HJ, Knapp GR, Adelman-McCarthy JK, et al. 2009. *Astron. J.* 137:4377–99
Yoachim P, Dalcanton JJ. 2006. *Astron. J.* 131:226–49
Yoachim P, Dalcanton JJ. 2008. *Ap. J.* 682:1004–19
York DG, Adelman J, Anderson JE Jr, Anderson SF, Annis J, et al. 2000. *Astron. J.* 120:1579–87
Yoshii Y. 1982. *Publ. Astron. Soc. Jpn.* 34:365–79
Zwitter T, Matijevič G, Breddels MA, Smith MC, Helmi A, et al. 2010. *Astron. Astrophys.* 522:A54–69

Annu. Rev. Astro. Astrophys. 2012.50:251-304. Downloaded from www.annualreviews.org
by California Institute of Technology on 01/21/14. For personal use only.

Annual Review of
Astronomy and
Astrophysics

Volume 50, 2012

# Contents

Annu. Rev. Astro. Astrophys. 2012.50:251-304. Downloaded from www.annualreviews.org
by California Institute of Technology on 01/21/14. For personal use only.

## Indexes

## Errata

An online log of corrections to *Annual Review of Astronomy and Astrophysics* articles may be found at http://astro.annualreviews.org/errata.shtml

Annu. Rev. Astro. Astrophys. 2012.50:251-304. Downloaded from www.annualreviews.org
by California Institute of Technology on 01/21/14. For personal use only.